MicroRNAs in alternative and classic activation of macrophages

Dissertation

Zur Erlangung des akademischen Grades

d o c t o r r e r u m n a t u r a l i u m

(Dr. rer. nat.)

im Fach Biologie

eingereicht an der

Lebenswissenschaftlichen Fakultät

der Humboldt-Universität zu Berlin

von

Diplom-Biologe Wilhelm Bertrams

Präsident der Humboldt-Universität zu Berlin:
Prof. Dr. Jan-Hendrik Olbertz

Dekan der Lebenswissenschaftlichen Fakultät
Prof. Dr. Richard Lucius

Gutachter/innen: 1. Prof. Dr. Richard Lucius

2. Prof. Dr. Bernd Schmeck

3. Prof. Dr. Nils Blüthgen

Tag der mündlichen Prüfung: 11.12.2014

Nihil admiRari

Table of Contents

Abstract

Macrophage polarization is a key feature of innate immunity that gives rise to a plethora of macrophage subtypes. Broadly, pro-inflammatory (classic, M1) and anti-inflammatory (alternative, M2) activation patterns have been described in the past. The polarization process is enabled by inherent macrophage versatility, and it is subject to tight regulation. Failure of this surveillance can lead to inappropriate polarization that can potentiate a skewed immune response and thus aggravate a disease. Due to this complex nature of activation, macrophages are at the core of a number of diseases as various as cancer and allergy. The precise analysis of macrophage subtype manifestation necessitates a global investigation of parameters, e.g. mRNA or microRNA (miRNA) profiling, since individual markers considered in isolation hold little information about the subtype in question.

In this thesis, I aim to point out some features of macrophage polarization in the pathogenesis of allergic asthma. The chosen approach started with the establishment of subtype-characteristic mRNA and miRNA profiles of prototypical *in vitro* polarized human macrophages. In a second step, the miRNA patterns were used in an attempt to interpret the polarization status of isolated lung macrophage phenotypes from a murine model of asthma.

At the outset, *in vitro* polarization of human blood-derived macrophages was performed. Classic activation was achieved by administration of IFNγ and LPS, while IL4 and IL13 induced alternative activation. Cellular signal transduction patterns and bactericidal capacity were tested to assess polarization efficiency. Subsequently, polarized macrophages were isolated cytometrically by positive selection for subtype-specific surface markers (classic activation: CD80; alternative activation: CD23). Global mRNA and miRNA profiling of the purified populations established a broad data base for subsequent investigation. The magnitude of response on the transcriptional level appeared to be much greater in classic macrophages as compared to alternative macrophages. In classic macrophages, hallmark genes such as TNFα, IL6 and IL1β were induced, whereas in alternative macrophages, an up-regulation of CD209 and PPARγ could be observed. Prominent miRNAs that were up-regulated in classic macrophages included hsa-miR-187-3p, hsa-miR-155-5p and hsa-miR-146a-5p. In contrast, hsa-miR-193b-3p and hsa-miR-511-5p were induced in alternative macrophages. In-depth *in silico* correlation of the mRNA and miRNA expression patterns was carried out in cooperation with Dr. Annalisa Marsico (MPI for Molecular Genetics, Berlin). On the basis of these data, putative mRNA/miRNA interaction partners were identified and experimentally validated in a luciferase-based reporter assay. In this setting, affirmative

candidates included hsa-miR-187-3p as a regulator of SH2B2 and the pair of hsa-miR-187-3p and hsa-miR-155-5p as cooperative regulators of LAMP2. While the precise function of the scaffold molecule SH2B2 in macrophages is currently unknown, LAMP2 is closely associated with lysosomal organization and activity and therefore centrally involved in macrophage biology. Under physiologic conditions, hsa-miR-187-3p was able to down-regulate SH2B2 transcript. However, no impact of either hsa-miR-187-3p or hsa-miR-155-5p, or a combination of both, on LAMP2 mRNA or protein could be observed.

While they revealed no functional interaction, the gathered systemic mRNA and miRNA data constitute a potential tool to assess the polarization status of *in vivo* macrophages in the context of a disease. Allergic asthma is one of the most severe forms of allergic diseases of the airways, and it poses a substantial socio-economic burden. Long neglected, macrophages have recently been credited with a central role in several forms of asthma, since they seem to determine disease progression by means of their polarization status.

In this study, the miRNA profiles of murine lung macrophages from the bronchoalveolar lavage fluid and from digested lung tissue were established. These profiles were employed in a comparative analysis of healthy mice and mice suffering from acute Ovalbumin-induced eosinophilic airway inflammation. It was hypothesized that the pattern of miRNA expression might yield clues as to the polarization status of inflammation-associated macrophages when assessed on the basis of the prototypical human *in vitro* data. Individual miRNAs that were regulated in response to Ovalbumin were identified, e.g. mmu-miR-21a-5p and mmu-miR-155-5p (up-regulated), as well as mmu-miR-126-3p and mmu-miR-146a-5p (down-regulated).

Although the gathered murine miRNA data could only in part be compared to the human reference samples due to a limited intersection of the significantly regulated candidates, they still suggest a mixed macrophage phenotype in eosinophilic airway inflammation, as they show characteristics of both M1- and M2-associated miRNA patterns. This was represeneted most prominently in the concomitant reciprocal expression of mmu-miR-155-5p (up-regulated) and mmu-miR-146a-5p (down-regulated).

Keywords: macrophage, polarization, microRNA, asthma

Zusammenfassung

Die Polarisierung von Makrophagen ist ein zentraler Mechanismus der angeborenen Immunität, der in einer Vielzahl verschiedener Makrophagen-Subtypen resultiert. Vereinfachend sind in der Vergangenheit pro-inflammatorische (klassische, M1) und anti-inflammatorische (alternative, M2) Aktivierungsmuster beschrieben worden. Die Polarisierung ist Ausdruck der Vielseitigkeit von Makrophagen und verdeutlicht die Notwendigkeit, diese Vielseitigkeit zu regulieren. Ein Versagen dieser Kontrolle kann dazu führen, dass Makrophagen durch fehlgeleitete Polarisierung eine gestörte Immunantwort verstärken und somit einen Krankheitsverlauf negativ beeinflussen können. Damit sind Makrophagen grundlegend an so diversen Krankheitsbildern wie Krebs und Allergie beteiligt. Eine genaue Analyse der Ausprägung von Makrophagen Subtypen erfordert ein globales Erfassen von Parametern, wie z.B. von mRNA oder microRNA (miRNA) Expressionsmustern, da die isolierte Betrachtung von einzelnen Markern wenig Aussagekraft über den betrachteten Subtyp enthält.

In der vorliegenden Studie beabsichtige ich, die Makrophagen-Polarisierung in der Pathogenese von allergischem Asthma darzulegen. Am Beginn des hierzu gewählten Vorgehens stand die Etablierung von Subtyp–charakteristischen mRNA und miRNA Expressionsprofilen *in vitro* polarisierter, humaner blutstämmiger Makrophagen. In einem zweiten Schritt wurde überprüft, ob sich die miRNA Expressionsdaten eignen, um den Polarisierungsstatus isolierter Lungenmakrophagen in einem Mausmodell des Asthmas zu ermitteln.

Initial wurden humane blutstämmige Makrophagen *in vitro* durch Gabe von IFNγ und LPS (M1) bzw. IL4 und IL13 (M2) polarisiert. Zur Beurteilung der Polarisierungseffizienz wurden zelluläre Signaltransduktionsmuster und die bakterizide Kapazität untersucht. In der Folge wurden polarisierte Makrophagen mit Hilfe von spezifischen Oberflächenmarkern (M1: CD80, M2: CD23) zytometrisch isoliert, und es wurden globale mRNA und miRNA Profile erstellt. In M1 Makrophagen war die transkriptionelle Antwort auf den Stimulus deutlich umfassender als in M2 Makrophagen. Charakteristische Gene, wie z.B. TNFα, IL6 und IL1β, waren in M1 Makrophagen induziert, während in M2 Makrophagen eine verstärkte Expression von CD209 und PPARγ beobachtet werden konnte. Unter den maßgeblich heraufregulierten miRNAs befanden sich hsa-miR-187-3p, hsa-miR-155-5p und hsa-miR-146a-5p (M1) bzw. hsa-miR-193b-3p und hsa-miR-511-5p (M2). Eine *in silico* Korrelation der mRNA und miRNA Expressionsmuster wurde im Rahmen einer Kooperation von Dr. Annalisa Marsico durchgeführt (MPI für Molekulare Genetik, Berlin). Diese Daten lieferten die Grundlage für eine Identifizierung hypothetischer mRNA/miRNA Interaktionspartner, die

anschließend in einem Luciferase-basierten Reportermodell überprüft wurden. Bestätigte Kandidaten waren u.a. hsa-miR-187-3p als Regulator von SH2B2 und hsa-miR-187-3p sowie hsa-miR-155-5p als kooperative Regulatoren von LAMP2. Während die genaue Funktion des Scaffold Moleküls SH2B2 in Makrophagen noch unbekannt ist, ist LAMP2 mit Aufbau und Aktivität des Lysosoms assoziiert und damit wesentlich in die Makrophagenbiologie eingebunden. Es konnte gezeigt werden, dass hsa-miR-187-3p unter physiologischen Bedingungen in der Lage ist, SH2B2 auf Transkriptebene herunter zu regulieren. Auf der anderen Seite konnte weder ein Einfluß von hsa-miR-187-3p oder hsa-miR-155-5p, noch einer Kombination von beiden, auf LAMP2 mRNA oder Protein beobachtet werden.

Obwohl kein funktioneller Zusammenhang gezeigt werden konnte, sind die erhobenen systemischen mRNA und miRNA Daten potentiell von Wert, um den Polarisierungsstatus von primären Makrophagen im Kontext einer Krankheit zu bestimmen. Allergisches Asthma ist eine ernstzunehmende Atemwegserkrankung mit schweren sozio-ökonomischen Implikationen. Makrophagen wurde erst in jüngerer Vergangenheit eine zentrale Rolle in verschiedenen Formen von Asthma zugesprochen, die durch ihren Polarisierungsstatus bestimmt wird.

In der vorliegenden Studie wurden die miRNA Profile von murinen Lungenmakrophagen erhoben, die aus der bronchoalveolären Lavage und aus verdautem Lungengewebe gewonnen wurden. Diese Profile wurden in einer vergleichenden Analyse von gesunden Mäusen und Mäusen mit akuter Ovalbumin-induzierter eosinophiler Atemwegsentzündung eingesetzt. Es wurde postuliert, dass das miRNA Expressionsprofil Hinweise auf den Polarisierungsstatus Entzündungs-assoziierter Makrophagen beinhalten könnte, wenn es in Anlehnung an die prototypischen humanen *in vitro* Daten analysiert wird. Einzelne in der Immunantwort auf Ovalbumin regulierte miRNAs waren z.B. mmu-miR-21a-5p und mmu-miR-155-5p (herauf reguliert), sowie mmu-miR-126-3p und mmu-miR-146a-5p (herunter reguliert).

Obwohl die erhobenen murinen miRNA Daten aufgrund einer geringen gemeinsamen Schnittmenge nur teilweise mit den humanen Referenzproben vergleichbar waren, kann dennoch ein gemischter Makrophagen-Subtyp postuliert werden, da sowohl M1 als auch M2 assoziierte miRNA-Muster gefunden werden konnten. Dies zeigte sich vor allem in der gleichzeitigen reziproken Regulation von mmu-miR-155-5p (herauf reguliert) und mmu-miR-146a-5p (herunter reguliert).

Schlagworte: Makrophagen, Polarisierung, microRNA, Asthma

List of Abbreviations

°C	degree Celsius
µ	micro
A	Ampère
aa	amino acid
AGO	argonaute
AHR	airway hyper-responsiveness
AM	alveolar macrophage
APS	ammonium persulfate
BAL	bronchoalveolar lavage
BALF	BAL fluid
BDM	blood-derived macrophage
bp	base pair
BSA	bovine serum albumin
CD	cluster of differentiation
cDNA	complementary DNA
CFU	colony forming unit
CSF1	colony-stimulating factor 1
CSF1R	colony-stimulating factor 1 receptor
Ct	threshold cycle
DAMP	danger associated molecular pattern
DC	dendritic cell
DNA	deoxyribonucleic acid
DNase	deoxyribonuclease
dNTP	deoxyribonucleoside triphosphate
ds	double stranded
e.g.	*exempli gratia*
ECL	enhanced chemoluminescence
EDTA	ethylenediaminetetraacetic acid
et al.	*et alii*
FACS	fluorescence-activated cell sorting
FCS	fetal calf serum
FITC	fluorescein isothiocyanate
g	acceleration of gravity
g	gram
GAPDH	glyceraldehyde 3-phosphate dehydrogenase
h	hour
HDM	house dust mite
HRP	horseradish peroxidase
HSC	hematopoietic stem cell
i.p.	intraperitoneal
i.v.	intravenous
IFN	interferon

Ig	immunoglobulin
IKK	IκB Kinase
IL	interleukin
IM	interstitial macrophage
JAK	Janus-associated tyrosin kinase
kDa	kilodalton
l	liter
LB	lysogeny broth
LPS	lipopolysaccharide
m	milli
MACS	magnetic activated cell sorting
MAPK	mitogen-activated protein kinase
min	minute
miRNA	microRNA
mRNA	messenger RNA
MOI	multiplicity of infection
NCBI	National Center for Biotechnology Information
NFκB	nuclear Factor kappa B
NP-40	Nonidet P-40
O.D.	optical density
OVA	ovalbumin
PAA	polyacrylamide
PAMP	pathogen-associated molecular pattern
PCA	principal component analysis
p.i.	post infection
PBMC	peripheral blood mononuclear cell
PBS	phosphate buffered saline
PCR	polymerase chain reaction
PE	phycoerythrin
PFA	paraformaldehyde
pH	*potentia hydrogenii*
PI	propidium iodide
RdRP	RNA dependent RNA polymerase
rh	recombinant human
RIN	RNA integrity index
RISC	RNA-induced silencing complex
RLC	RISC loading complex
RNA	ribonucleic acid
RNAi	RNA interference
RNase	ribonuclease
rpm	rounds per minute
RPMI	Rosswell Park Memorial Institute
rRNA	ribosomal RNA
RT	reverse transcription

s	second
s	Svedberg
SD	standard deviation
SDS	sodium dodecyl sulfate
SDS-PAGE	sodium dodecyl sulfate polyacrylamide gel electrophoresis
ss	single stranded
STAT	signal transducer and activator of transcription
stRNA	small temporal RNA
TAM	tumor associated macrophage
Taq	*Thermus Aquaticus*
TEMED	tetramethylethylendiamine
T_H	T helper cell
TLDA	Taqman Low Density Array
TLR	Toll like receptor
tncRNA	tiny non-coding RNA
TNF	tumor necrosis factor
T_{reg}	regulatory T cell
TRIS	tris(hydroxymethyl)aminomethane
U	unit
UTR	untranslated region
V	Volt
vs.	*versus*
WB	Western Blot
WT	wildtype

Index of Figures and Tables

List of Figures

List of Tables

1 Introduction

1.1 The macrophage as a central cell type of the innate immune system

1.1.1 Innate immune cell lineages

The human immune system is composed of an innate and an adaptive branch. Innate immunity is the body´s first line of defence against pathogens and other insults from the environment. Besides chemically and physically protective surfaces, such as mucosa, and humoral proteins, e.g. the complement system, it includes a cellular constituent. Cells of the innate immune system stem from a universal progenitor cell, the hematopoietic stem cell (HSC) [1]. The HSC is generated in the bone marrow and migrates between bone marrow, blood and peripheral tissues [2]. It gives rise to the hematopoietic tree (Fig. 1-1), which is bifurcated into a myeloid and a lymphoid branch. While the lymphoid axis of the hematopoietic tree spawns lymphocytes (B-cells, T-cells), the myeloid axis generates granulocytes (neutrophils, eosinophils, basophils) and monocytes, which are all effector cells of innate immunity. Monocytes are precursor cells and establish the mononuclear phagocyte pool upon maturation via multiple, not yet fully understood lineages. Circulating monocytes in the blood constitute the pool from which resident macrophages are in part recruited. Upon entering the tissue, monocytes adopt a characteristic morphology and differentiate into functional organ-specific macrophages.

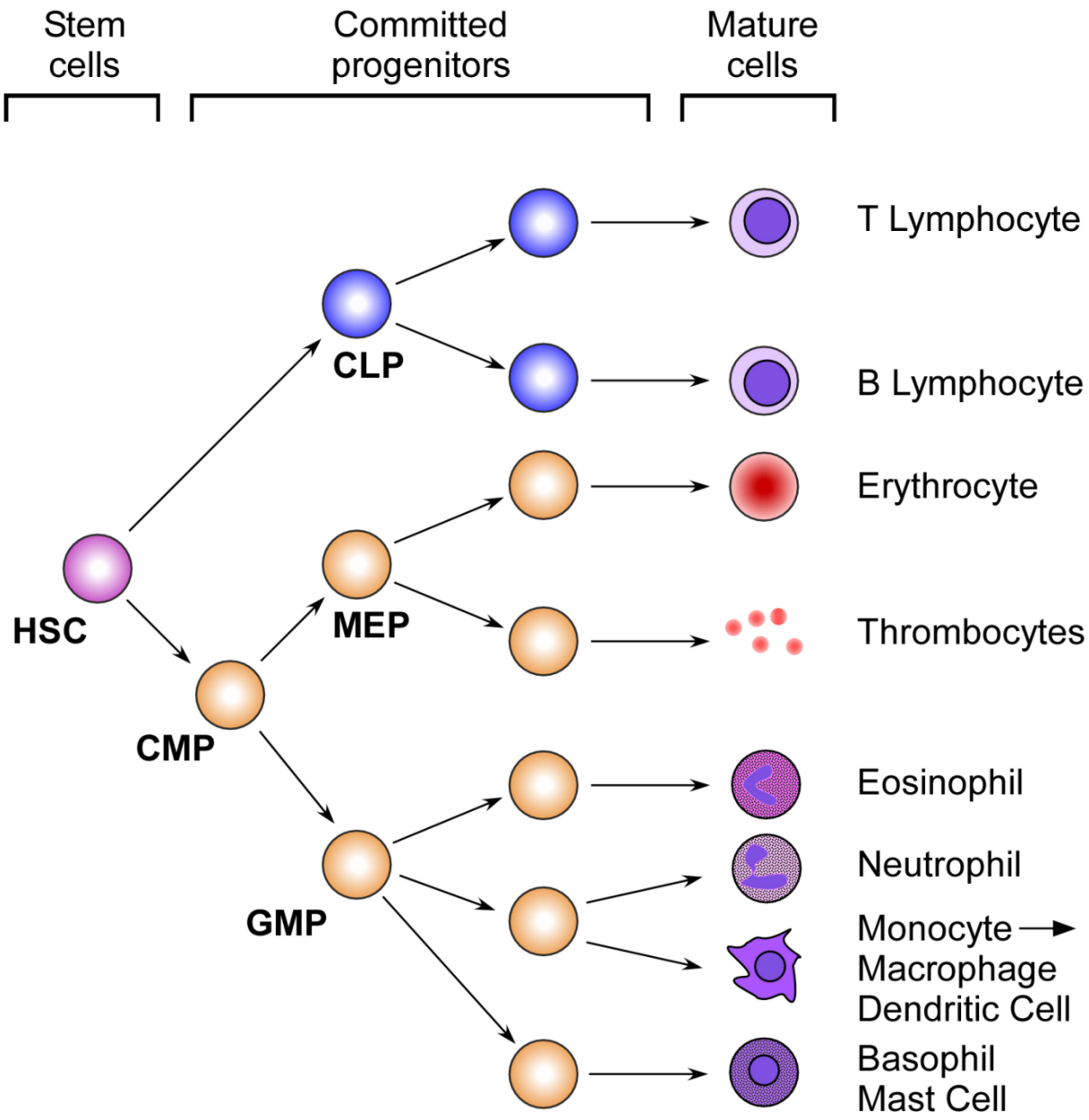

Figure 1-1: The hematopoietic tree. The canonical lineage maturation of HSC-derived myeloid cells is separated into a lymphoid and a myeloid branch that originate from the respective progenitor cell. HSC: hematopoietic stem cell; CMP: common myeloid progenitor; GMP: granulocyte-macrophage progenitor; MEP: megakaryocyte-erythroid progenitor; CLP: common lymphoid progenitor. (Adapted from D. Metcalf, Immunity, 2007)

1.1.2 Mononuclear phagocyte heterogeneity

In humans, circulating monocytes in the blood have been broadly classified into three subgroups by their most prominent surface molecules, CD14 and CD16. Classical monocytes are defined as $CD14^{++}CD16^{-}$, intermediate monocytes as $CD14^{++}CD16^{+}$ and non-classical

monocytes as $CD14^{+}CD16^{++}$. This nomenclature was officially proposed to replace misleading denomination such as "inflammatory monocyte", because the heterogeneity and migratory fate of monocytes *in vivo* do not necessarily match *in vitro* observations [3]. Until now, there is no evidence that the fate of a maturing monocyte is defined by its CD14/CD16 lineage. Instead, the diversity of mature subtypes is suggested to result of the plasticity that is inherent to all mononuclear phagocytes [4]. Whether a mononuclear phagocyte is classified as a dendritic cell (DC) or a macrophage largely depends on surface marker decoration and tissue localization; yet there is still considerable debate over the guidelines to differentiate between macrophages and dendritic cells. It has been proposed to define macrophages as cells that descend from blood-borne monocytes. In contrast, dendritic cells are suggested to stem from their own dedicated precursor cell [5].

In mice, monocytes are classified into two major subgroups, being $CCR2^{+}CX3CR1^{+}Ly\text{-}6C^{hi}$ and $CCR2^{-}CX3CR1^{++}Ly\text{-}6C^{lo}$ [6]. Murine $Ly\text{-}6C^{hi}$ monocytes have been described to resemble human $CD14^{++}$ monocytes, whereas $Ly\text{-}6C^{lo}$ monocytes appear to share features with human $CD14^{dim}CD16^{+}$ cells [7]. Furthermore, murine monocyte subtype manifestation appears to be in part caused by differential microRNA expression [8].

Besides these canonical monocyte lineages, a common bone marrow progenitor for monocytes, some macrophage subsets and resident spleen dendritic cells has been described to originate from the HSC in mice. It has been named macrophage and dendritic cell progenitor (MDP) [9]. It is on the one hand committed to the generation of a common DC precursor (CDP) that gives rise to classical and plasmacytoid dendritic cells. On the other hand, it directly spawns monocytes. These two paths have been described as strictly separated [10]. Thus, a murine monocyte-independent DC lineage seems to exist.

Another study conducted in mice recently revealed an alternative, bone marrow-independent lineage from which macrophages can arise [11]. This lineage originates from the embryonic yolk sac. These macrophages have been found in an attempt to elucidate why some tissue-resident macrophages remain unaffected by bone marrow transplantation. The exact contribution of HSCs and yolk sac to the adult´s macrophage pool remains unknown. In humans, such a lineage awaits identification [12].

The macrophage, its versatility and plasticity being of particular interest in the present study, will be focused on hereafter.

1.2 Regulation of macrophage function in the immune defense

Macrophages, populating the various organs of the body in their manifold subtypes, serve as sentinels of the immune system. Their diversity manifests in subtypes such as Kupffer cells in the liver or alveolar macrophages in the lung, to name only two. The key cytokine that is involved in monocyte production, recruitment and maturation is the macrophage colony-stimulating factor M-CSF (CSF-1) [13]. M-CSF is produced by endothelial and by local tissue cells and acts on monocytes and macrophages via the CSF-1 receptor tyrosine kinase (CSF-1R) [14]. In homeostasis, the M-CSF stimulus ensures a stable macrophage count and distribution throughout the body. In contrast to the monocytes that permanently replenish the resident macrophage sentinel population in good health, there is amplified recruitment to sites of acute or chronic inflammation. This process requires elaborate cell-to-cell communication in order to orchestrate a coordinated immune response, which is achieved by ligand-receptor interaction.

1.2.1 Macrophage receptor signaling

Like many tissue cells, cells from the immune system are equipped with invariable surface and intracellular receptors that detect patterns common to pathogens (pathogen associated molecular patterns, PAMPs) or to sterile threats (danger associated molecular patterns, DAMPs). The most prominent PAMP receptor type is the germ-line encoded Toll like receptor (TLR) family. Originally discovered to determine dorsoventral polarity in *Drosophila melanogaster* in 1985, it was later associated with host defence in Drosophila and also in mammals [15]. Thirteen mammalian TLR genes have been identified so far, 10 of which are functionally expressed in humans [16]. They recognize a plethora of different PAMPs, such as lipopolysaccharide (LPS) from gram-negative bacteria (via TLR4), peptidoglycan from gram-positive bacteria (via TLR2), the bacterial motility protein flagellin (via TLR5), nucleic acids of bacterial or viral origin, such as unmethylated CpG motifs (via TLR9), double-stranded RNA (via TLR3) and single-stranded RNA (via TLR7).

All TLRs share a cytoplasmic Toll/interleukin-1 receptor (TIR) domain, a transmembrane domain and leucine rich repeat motifs (LRRs) on the extracellular/intravesicular side. These LRRs are responsible for PAMP detection. Upon PAMP binding, TLRs dimerize, bringing their cytoplasmic TIR domains into close spatial proximity. This process creates the binding sites necessary for adapter molecule binding. Association of myeloid differentiation primary

response protein 88 (MyD88) or TIR-domain-containing adapter-inducing interferon-β (TRIF) to the dimerized TIR domains triggers a signalling cascade, involving mitogen activated protein kinases (MAPK), nuclear factor kappa B (NFκB) and interferon regulatory factors (IRF), which eventually leads to the activation of pro-inflammatory genes that establish an unspecific immune reaction against the detected threat.

LPS is a structure of three subunits, the hydrophobic region (lipid A), a core oligosaccharide and a distal oligosaccharide [17]. TLR4, the LPS receptor, requires co-factors for dimerization and subsequent intracellular signalling. Myeloid differentiation factor 2 (MD2), an auxiliary protein, and CD14, a surface molecule with no intracellular domain, both assist in TLR4 homodimer formation. LPS can be detected only if it is bound to a soluble LPS-binding protein (LBP) [18]. Altogether, this multimeric structure triggers a pro-inflammatory signalling cascade via the dimerized TIR domains of TLR4 and MyD88, which bears a C-terminal TIR domain that engages in homotypic interaction with TLR4 [1, 19]. At the N-terminus, MyD88 possesses a death domain, which is required to recruit Interleukin-1 receptor-associated kinase 4 (IRAK4). By its kinase activity, IRAK4 phosphorylates IRAK1, which in turn associates with TNF receptor associated factor 6 (TRAF6). Subsequent downstream signalling events via TAB2 lead to the activation of transforming growth factor-β (TGFβ) activated kinase 1 (TAK1) by lysine 63 (k63)-linked ubiquitin [20, 21]. TAK1 is able to trigger two distinct signalling pathways [22]. One is the NFκB pathway, which is initiated by activation of the IκB kinase complex (IKKα,β,γ) [23, 24]. IKK phosphorylates the inhibitor of kappa B alpha (IκBα), which inhibits NFκB entry into the nucleus in steady state. IκBα is degraded upon phosphorylation. This enables NFκB to shuttle into the nucleus and participate in the initiation of pro-inflammatory gene transcription [23]. The other pathway which TAK1 is able to initiate is the MAPK cascade, culminating in the MAP kinase kinase 6 (MKK6)-mediated phosphorylation and activation of p38 kinase and c-Jun N-terminal kinase (JNK) [22]. Both factors also participate in inflammatory gene transcription by phosphorylating transcriptional regulators.

Further receptors that are present on cells of the innate immune system recognize autologous messenger molecules such as interleukins and interferons, both of which belong to the cytokine family. As cytokines are produced by cells of the innate and adaptive immune system alike, they represent a means of crosstalk between innate and adaptive immunity. Cytokines that are typically produced by cells of the adaptive immune system are e.g. Interleukin-4 (IL4), Interleukin-13 (IL13) by T_H2 cells and Interferon-γ (IFNγ) by T_H1 cells. IL4 is

recognized via the dimeric type I receptor, consisting of the IL4Rα chain and a common gamma chain (IL4Rα/γc), or the dimeric type II IL4Rα/IL13Rα1 receptor, while IL13 is sensed exclusively by the type II receptor [25]. Macrophages, unlike most other cells, express both the type I and the type II receptor. Even though IL4 and IL13 work in a very similar way and even share the IL4Rα receptor chain, they have some non-redundant functions which can at least in part be explained by receptor sensitivity, which is higher for IL4 [26]. Receptor binding leads to Janus kinase 1 and 3 (JAK1/3) activation and subsequently to signal transducer and activator of transcription 6 (STAT6) phosphorylation. Upon phosphorylation, STAT6 dimerizes and enters the nucleus, where it serves as an activator of transcription [26]. The gene products, e.g., peroxisome proliferator-activated receptor gamma (PPARγ) and krueppel like factor 4 (KLF4), participate in insulin metabolism and immunomodulation.

Unlike these interleukins, IFNγ signalling gives rise to a distinctly pro-inflammatory gene transcription. Upon binding to the IFNγ receptor (IFNGR), a dimer consisting of the IFNγR1 and IFNγR2 chain, JAK1 and JAK2 are activated by tyrosine residue phosphorylation [27]. The transcription factor STAT1 is recruited to these phospho-tyrosines, and subsequently, JAK1 and JAK2 mediate STAT1 phosphorylation and dimerization. As a homodimer, STAT1 can translocate into the nucleus and initiate the transcription of pro-inflammatory mediators, such as CCL2, CCL5 and CXCL10 [28].

A key feature of macrophages is the phagocytosis of cellular debris or pathogens, mediated by different receptors: Surface receptors such as the IgG receptor (FcγRI) mediate engulfment of non-self structures opsonized with antibodies. Scavenger receptor CD163 is involved in the clearance of free haemoglobin. The mannose receptor CD206 is responsible for glycoprotein disposal and also recognition of glycostructures on pathogens. Phagocytosis thus serves as both a disposal system for debris and as a mechanism of defence. The ingested material is engulfed by a vesicle, the phagosome. Neutralization of the potentially harmful phagosome content is achieved by fusion to a lysosome, yielding a phagolysosome. Lysosomes are vesicles that contain toxic compounds such as reactive oxygen species and nitric oxide, or lytic enzymes such as elastase and cathepsins [1]. Since these enzymes require a pH between 4 and 5, the phagolysosome is actively acidified by an ATP-dependent proton pump [29], which further supports pathogen incapacitation. In order to fully activate the phagolysosomal machinery, macrophages require an IFNγ stimulus from T_H1 cells [30]. After chemical pathogen breakdown, remaining fragments are displayed on IFNγ-induced major

histocompatibility complex type II (MHC II) surface molecules, which raises the MHC II affinity to T cells equipped with a matching T cell receptor.

1.2.2 Macrophage activation by the adaptive immune system

Macrophages participate in the induction and maintenance of the adaptive immune response and also require its stimuli for subtype manifestation. The initiation of an adaptive immune response necessitates the presentation of antigen to the memory and effector cells of the immune system. The cells that ingest, process and present antigen are the antigen presenting cells (APCs), which are mostly mononuclear phagocytes. They sample antigen and present antigen fragments on their type II MHC surface molecules. Upon activation by antigen encounter, macrophages mount a local and unspecific immune response. Secretion of lipid mediators such as leukotrienes and prostaglandins induce an inflammatory state. The release of cytokines like TNFα, IL1β, IL8 and CCL2 promotes further recruitment of leukocytes, such as neutrophils and additional monocytes, to the affected tissue. Resident dendritic cells take up antigen material at the site of an infection and migrate to the T cell zones of proximal lymphoid organs via lymphatic vessels and activate $CD4^+$ T helper cells equipped with a compatible T cell receptor. By this match, T cells pass a positive selection process and are clonally expanded, a process that makes them available in great numbers to fight the source of the antigen they were selected for. A portion of these T cells leaves the lymph node and enters the blood stream. At the site of infection, T cells cross the endothelial barrier by a selectin- and integrin-mediated process. Activated $CD4^+$ T helper cells can develop into $CD4^+$ Type 1 (T_H1) or Type 2 (T_H2) helper cells, depending on the microenvironment they encounter in the tissue. At the inflamed site, these T helper cells mediate further activation and maintenance of other immune cells, such as macrophages. T_H1 cells produce IFNγ, while T_H2 cells produce IL4, IL5 and IL13. These cytokines reinforce the respective T cell activation status while inhibiting the opposite one. Furthermore, these cytokines shape the macrophage activation status by paracrine stimulation.

1.2.3 Macrophage polarization

Macrophages can be activated in a variety of different ways, and the T_H1 and T_H2 cell subtypes have a profound impact on directing and maintaining macrophage activation. T_H1 cells bind to macrophages that carry intracellular pathogens such as *Listeria* and *Leishmania*

in vesicular compartments. These macrophages interact with T_H1 cells via CD80-CD28, CD40-CD40L and MHCII-T cell receptor interaction and release of IL12 [1]. Subsequent IFNγ release by T_H1 cells activates macrophages in a pro-inflammatory way, a process that has been termed M1 polarization [31], thus rendering them capable of fighting intracellular pathogens.

In contrast, the T_H2 response is elicited in response to allergens or parasites such as helminths and can also be mounted in response to a weak antigen that is not sufficiently immunogenic to trigger a T_H1 response. T_H2 cells can activate macrophages by secretion of IL4 and IL13. Unlike activation by IFNγ, IL4 and IL13 trigger an alternative activation of macrophages, which has been termed M2a polarization. This macrophage subtype is associated with allergy and T_H2 inflammation [32]. In addition to the M2a subtype, further distinct polarization states have been described to be inducible *in vitro*, referred to as M2b and M2c. The focus herein will lie on M2a-stimulated macrophages, which will henceforth be denominated M2, as the M2a/b/c nomenclature has been discouraged (see below).

In vivo, the M1 and the M2 states represent two extremes of a broad spectrum of phenotypes that a macrophage can adopt [33]. Macrophages both require and promote a certain microenvironment, and their transient phenotype is a product of this delicate interplay. The pro-inflammatory microenvironment that arises at the site of an ongoing infection is primarily established by macrophages and leads to immune cell recruitment from the blood into the tissue and to the subsequent formation of the pro-inflammatory M1 macrophage subtype. The M1 macrophage actively participates in killing invading pathogens and infected cells by phagocytosis and lysis. The highly aggressive properties of this subtype need to be tightly controlled in order to prevent an excessive and inappropriate response to the present threat that might become deleterious to the host. Upon clearance of the infection, the cytokine microenvironment gradually shifts from pro-inflammatory to immunomodulatory, leading to a change of macrophage behavior. Phagocytosis of apoptotic cells primes macrophages to release anti-inflammatory mediators such as IL10 and TGFβ [34, 35]. This newly arising immunoregulatory subtype has long been considered to be inactive, but it has increasingly become clear that even though many pro-inflammatory functions are switched off, these so-called M2c macrophages show a defined pattern of activity that helps restoring the physiological state of the inflamed site. Their contribution to angiogenesis, wound repair and extracellular matrix restoration is crucial for the re-establishment of homeostasis. The effector cell that is required for these processes is the myofibroblast whose activation is triggered and

maintained by M2 macrophage-derived TGFβ and platelet-derived growth factor (PDGF). Furthermore, M2 macrophages can directly contribute to tissue rebuilding by phagocytosis of cellular debris [36]. It has recently been emphasized that the term "alternatively activated" should be used for T_H2-associated macrophages only, while "immunoregulatory" and "wound healing" macrophages are also entities of their own, respectively [37]. This differentiation is reflected in the M2a/b/c nomenclature as it was proposed in 2004 [32]. However, it has since become clear that this discrete attempt of categorization still overly simplifies the versatile nature of macrophage biology, which should rather be represented as a continuum of states [38, 39].

Other than in the wake of an M1-dominated inflammation, M2 macrophages can also arise as the primary macrophage response of the immune system, e.g. during parasite infection. It has been shown that the T_H2 response that is initiated as a response to a parasite is able to trigger local macrophage proliferation, induced by the T_H2 hallmark cytokine IL4. Unlike M1 macrophages that are thought to accumulate at the site of infection by elevated monocyte recruitment, IL4-induced M2 macrophages have been shown to expand *in situ* [40]. This observation discourages the hypothesis of an existing specific M2 monocyte precursor in the blood, again stressing the assumption that the plasticity of macrophages lies in their inherent versatility, not in lineage commitment. It is still unclear, though, how monocyte differentiation and recruitment is altered in the course and aftermath of inflammation to re-establish the tissue´s pre-inflammatory cell count and activation status [41].

Due to its modulatory properties, the M2 subtype can be found at the root of various diseases that are characterized by a skewed or suppressed immune response, such as cancer and allergy. Cancerous tissue usually carries a high load of macrophages that are polarized toward the M2 phenotype by tumor-derived substances such as CCL2, M-CSF/CSF1, TGFβ and IL10 [42]. Even though these M2-like tumor-associated macrophages (TAMs) contribute to vascularization and immunologic tolerance of the tumor tissue, they have therapeutic potential. Efforts to re-polarize these TAMs toward the more aggressive M1 subtype via the NFκB axis led to shrinking of the tumor size in a mouse model of IKKβ activity [43]. Similar results were obtained in a study using human TAMs purified from ovarian cancer ascites. Their M2-like phenotype could be reversed *in vitro* by IFNγ administration, and the resulting M1-like phenotype showed increased tumoricidal properties [44].

1.3 The lung as a model organ for macrophage-associated pathogenesis

The lung is a lobular organ which is located in the thoracic cavity. In humans, it is ventilated through the bifurcated trachea that allows airflow to and from the left and the right lung compartment. The tracheal branches form the *bronchus principalis dexter* and *sinister*, which progressively ramify and ultimately give rise to the alveoli, the effectors of gas exchange. They deplete CO_2 from the the blood and re-oxygenate it. The right lung is composed of three lobes, the *lobus superior*, the *lobus inferior* and the *lobus medius*. With a volume of approximately 1500 cm^3, it is larger than the left lung, which misses the *lobus medius* and has a total volume of 1400 cm^3. The lung is passively ventilated by the diaphragm and various accessory muscles, e.g. the *musculi scaleni*. The airflow to the individual lung compartments can be directed by the selective constriction and dilatation of the bronchi by smooth muscle cells. Expiration normally occurs by muscle relaxation that leads to shrinking of the lung. It can also be forced by activation of auxiliary muscles, e.g the *musculi intercostales interni*. The disturbance of the coordinated breathing process heightens the risk of airflow obstruction and may lead to labored breathing.

1.3.1 Experimental eosinophilic airway inflammation as a model for asthma

Asthma is a widespread chronic, non-communicable disease with increasing worldwide prevalence and significant socio-economic consequences. It is characterized by reversible airflow obstruction, airway-hyperresponsiveness, airway inflammation, mucus hypersecretion, and subepithelial fibrosis [45]. Clinically, at least two asthma phenotypes have been identified, namely allergic (extrinsic, atopic) and non-allergic (intrinsic, non-atopic) asthma [46]. Allergic asthma arises from an inappropriate immune reaction against harmless airborne antigen, e.g. birch pollen, which is initiated and maintained by antigen sampling dendritic cells [47]. Immunologically, several asthma phenotypes have been described, e.g. eosinophilic, neutrophilic and paucigranulocytic asthma. These types vary in severity, persistence and steroid sensitivity [48]. Especially in eosinophilic asthma, symptoms are caused in part by cytokines from the T_H2 axis of the adaptive immune system, including IL4 and IL13 [49, 50]. While they poise airway smooth muscle cells for hypercontractility and thereby contribute to air flow obstruction [51], they also induce an M2 skew of airway associated macrophages. The involvement of macrophage subtypes in the pathogenesis of asthma is still poorly understood [52].

Experimental allergic airway inflammation mimicking eosinophilic asthma can be induced in e.g. mice or rats by sensitizing the animal to a non-self antigen (e.g. ovalbumin, OVA, coupled to the adjuvant $Al(OH)_3$) and subsequent challenge with nebulized OVA applied intratracheally by normal breath intake [53]. Another way of asthma induction is exposure to house dust mite extract (HDM) [54]. Besides lung function assessment, airway inflammation outcome can be monitored by determining cells and cytokines in the bronchoalveolar lavage (BAL) and lung tissue [55].

1.3.2 Macrophages of the lung and their putative role in asthma

The lung, constantly exposed to air flow, needs tight surveillance by the immune system. In the airways, alveolar macrophages defend the body against air-borne pathogens. These macrophages are recruited from the pool of interstitial (parenchymal) macrophages, which reside in the lung tissue [56]. The inital classification of these two populations as distinct was solidified by transcriptome studies that highlighted differential gene expression by comparison [57]. Furthermore, interstitial macrophages can inhibit dendritic cell maturation and migration, whereas alveolar macrophages cannot [58]. Long neglected as an important contributor to asthma pathogenesis [50], macrophages have been found to be a crucial part in the asthma-related imbalance of the immune system. In a rat model of asthma, adoptively transferred naive alveolar macrophages were shown to alleviate asthma symptoms in OVA-sensitized and -challenged animals that were depleted of their residual macrophages. It was hypothesized that the protective effect of macrophages is eliminated in the course of OVA sensitization [59]. At least in part, the effect of macrophages on asthma can be attributed to IL17. Macrophages, and not T_H17 cells, have been identified as the primary IL17 producers in asthma. This cytokine was reported to be involved in leukocyte infiltration, neutrophil recruitment and -expansion and initiation of allergic inflammation. Its neutralization by antibodies or macrophage depletion reduced IL4, IL5, IL13 and IL17 levels in bronchoalveolar lavage fluid (BALF) [60]. In another study in rats, alveolar macrophages were cultured *ex vivo* and then re-administered. Re-instillation of *ex vivo* cultured cells caused elevated levels of IL12 and IFNγ in the BAL, which are both cytokines of the T_H1 axis. Thus, withdrawal of the T_H2 environment which the macrophages are exposed to in the asthmatic lung seems to deprogram their asthmatic M2 skew. In these animals, asthma was attenuated [61], feeding the hypothesis that the M2 polarization state of macrophages promotes asthma. Of note, the association of M2-like macrophages with asthma is complicated by the

observation that M1 macrophages can promote disease progression in severe cases of asthma by being refractory to glucocorticosteroids [49, 62]. Due to the interactions of macrophage versatility and asthma heterogeneity, clarification of their mutual dependency has yet to be achieved [52].

1.4 Non-coding RNAs have emerged as regulators of cellular processes

The field of RNA biology is rapidly expanding. In addition to the classically known protein-coding messenger RNAs (mRNA), the non-coding transfer RNAs (tRNA) and ribosomal RNAs (rRNAs), further RNA species exist which have active regulatory capacities. The impact of these RNAs on the immune system with its manifold aspects as outlined above has only begun to be revealed. In the following, the central discoveries that have led to the current understanding of certain non-coding RNA functions will be highlighted.

1.4.1 The initial discovery of RNA interference

The concept of antisense-mediated gene silencing as a tool for genetic engineering in eukaryotes was first introduced in 1984. It was shown that transgenic RNA sequences that bear Watson/Crick complementarity to the herpes simplex thymidine kinase mRNA can inhibit the expression of this kinase in a model using mouse L cells [63]. The mechanism relied on a flipped full-length thymidine kinase transgene that was hypothesized to inhibit expression by duplex formation with the mRNA. Long antisense transcripts have also been described as natural regulators of gene expression in eukaryotes, but only little evidence could be gathered to prove that they are functional [64]. Accordingly, experimental introduction of full-length antisense RNA often entails specificity and efficacy issues [64, 65]. Furthermore, the detailed molecular background of antisense suppression was unresolved [64]. In 1993, new light was shed on the mechanisms behind natural antisense-mediated gene silencing by a study in *Caenorhabditis elegans*.

Established as a model organism for genetic research by Sydney Brenner in 1974 [66], this nematode worm has certain peculiarities that make it ideally suited for use as a genetic tool, such as eutely (a constant number of somatic cells), ease of handling and transparency. In 1993, it was discovered that the *lin-4* gene encodes a short RNA with incomplete antisense complementarity to the *lin-14* mRNA in *C. elegans* [67]. The authors suggested a RNA – RNA interaction that negatively regulates translation of *lin-14* mRNA, thereby reducing lin-

14 protein levels. Since *lin-4* played a role in developmental timing, it was included in the group of small temporal RNAs (stRNAs). Natural antisense mechanisms that inhibit translation by interference with ribosomes at the transcript 5´UTR were already known to exist and to require broad sequence complementarity with the target [68, 69]. In the case of *lin-4*, the authors proposed a novel mechanism of direct translational inhibition that takes place at the transcript 3´UTR and therefore was unlikely to involve ribosome binding. They furthermore hypothesized that *lin-14* was probably not the only gene whose expression is controlled by a small RNA that binds in the 3´UTR. Indeed, Dougherty and Parks listed the *lin-4/lin-14* interaction as one of a few known natural antisense suppression mechanisms in eukaryotes [70]. They suspected it to be part of a cellular surveillance system that keeps aberrant or pathogenic RNAs in check via sense and antisense suppression. The obvious paradox that could not be solved yet was how a few antisense RNA molecules could confer efficient downregulation of a stoichiometrically over-represented target. In an attempt to explain the mechanism of antisense suppression, Dougherty and Parks introduced the idea of a RNA-dependent RNA polymerase (RdRP) that uses the sense or antisense transgene RNA as a template. It would, in their model, synthesize short RNA molecules which then bind and tag the endogenous transcript for degradation.

In 1998, new light was shed on that matter. Fire et *al.* performed an experiment that turned out to revolutionize the field of genetic engineering. They discovered that dsRNA injection of *unc-22* sense and antisense sequences into *C. elegans* specifically interfered with the expression of unc-22 protein [71]. As Dougherty and Parks, they noted that due to its relative paucity, the injected dsRNA could not be responsible for the strong down-regulation of protein they observed without the help of an additional boosting mechanism. In order to emphasize that what they had found was not a classical antisense phenomenon, they termed the mechanism RNA interference (RNAi). For their pioneering work in the field of RNAi, Fire and Mello were awarded the Nobel Prize in Physiology or Medicine in 2006. Variations of dsRNA administration to *C. elegans* turned out to be equally effective, e.g. soaking the worms in solution containing dsRNA, or feeding them dsRNA-expressing *E. Coli* [72].

In the years following the initial discovery, RNAi was hypothesized to ensure genome stability *in vivo* [73] and to take part in the antiviral response [74]. The exact mechanism behind the RNAi phenomenon was still a mystery, though. Tuschl *et al.* confirmed that RNAi requires double stranded RNA (as suggested by Fire *et al.* in 1998) and pointed out the sequence specificity of RNAi in a cell free system derived from syncytial blastoderm *Drosophila* embryos [75]. They furthermore observed that the relative inability of single

strand RNA to inhibit gene expression was not due to its inherent instability, because capped ssRNA failed to induce RNAi, whereas uncapped dsRNA inhibited gene expression. It was not until two years after the initial discovery that Zamore *et al*., using the same cell free *Drosophila* system, finally proposed a mechanism for RNAi (Fig. 1-2).

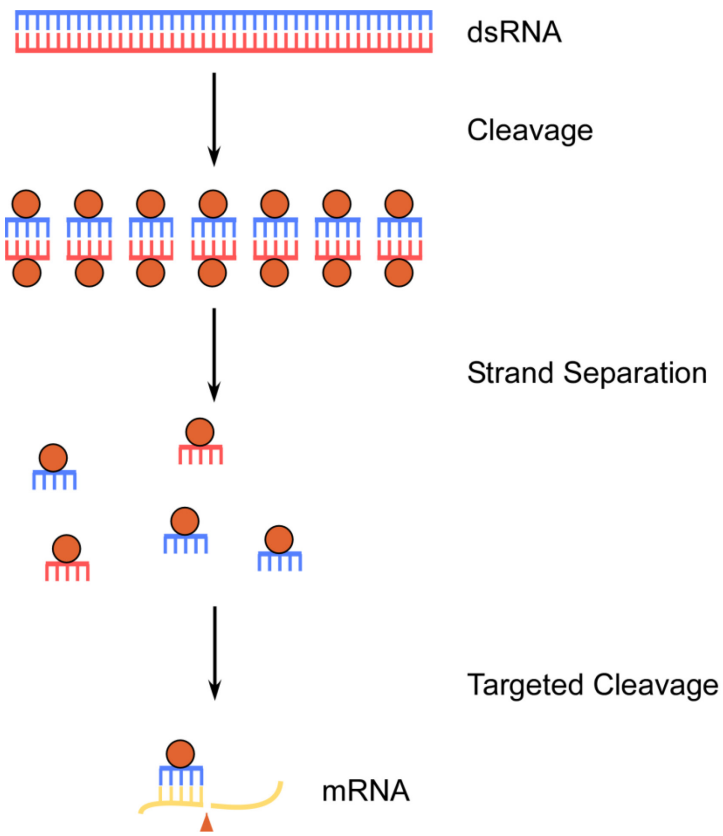

Figure 1-2: A proposed mechanism for RNAi. Long dsRNA molecules are cleaved into fragments and undergo strand separation. They subsequently bind mRNA and mediate directed cleavage by recruitment of endonucleases. Circles = RNAi-specific proteins; Triangles = nucleases; dsRNA = double-stranded RNA (adapted from P. Zamore, Cell, 2000)

Here, RNAi was described as an ATP-dependent mechanism that cleaves dsRNA into 21 to 23 nucleotide fragments. It was also noted that the target mRNA was digested at 21 to 23 nucleotide intervals, even though an interpretation of this observation was still lacking [76]. The model partially explained how a small amount of exogenous dsRNA could silence a vastly dominating mRNA. If every 21 to 23 nucleotide fragment was an active unit capable of RNAi, this would greatly enhance their regulatory potential. One year later, in 2001, the group of Fire proposed a refined model of RNAi in *C. elegans* (Fig. 1-3) [77]. In addition to the

concept of cleavage by the endoribonuclease Dicer (DCR-1), they proposed re-use of the short RNA molecules and generation of secondary silencing RNAs by an RNA dependent RNA polymerase (RdRP) to explain the potency of RNAi. Furthermore, they implemented two accessory dsRNA binding proteins into their model that were indispensable for RNAi, rde-1 and rde-4, which had already been considered by Zamore *et al*. They called the effector oligomers small interfering RNAs (siRNAs), which were integrated into a protein complex with nucleolytic capacities, the RNA-induced silencing complex (RISC) [78]. As they and others noted, the model they had proposed was not generally applicable to all species, since mammals seem to lack an RNA-dependent RNA polymerase [79].

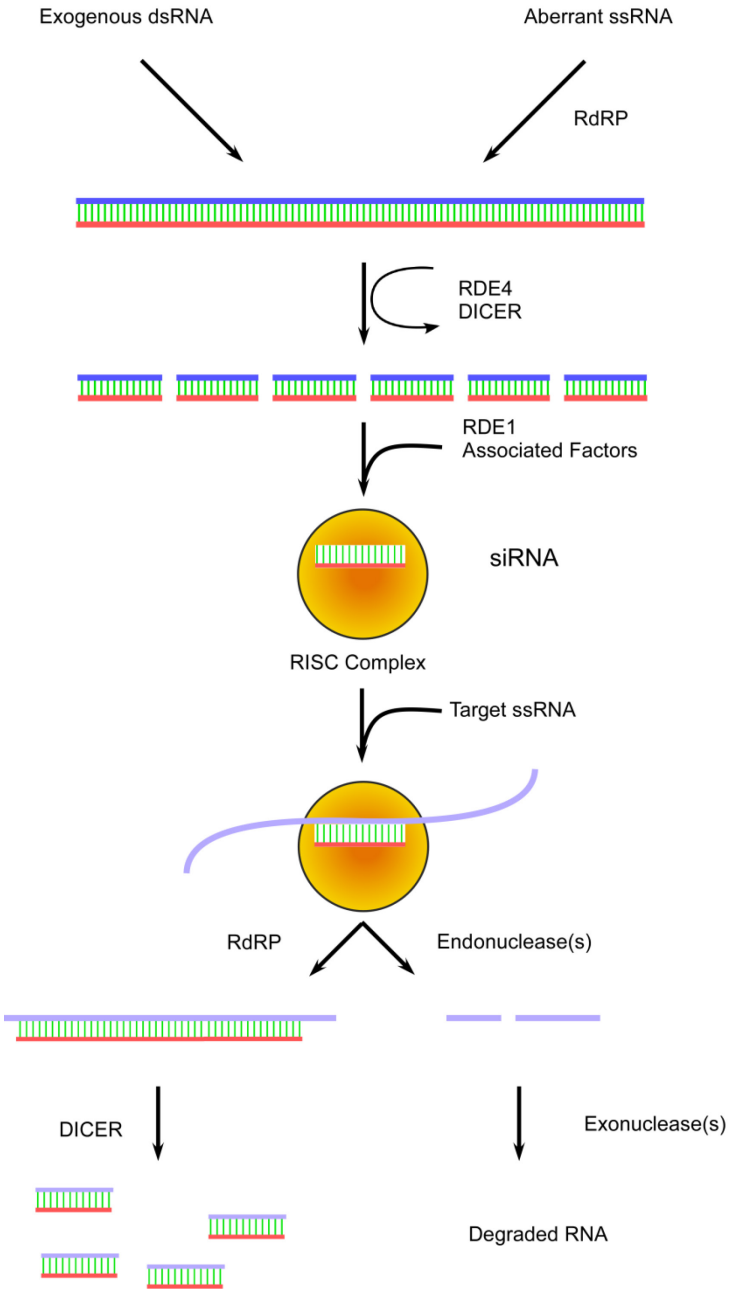

Figure 1-3: A refined model for RNAi. The model introduces the RISC complex that assists binding of the siRNA and the target RNA and subsequent cleavage, as well as the concept of physical amplification by RdRP. The generation of multiple catalytic units was hypothesized to explain in part the potency of RNAi. RdRP = RNA dependent RNA Polymerase; RDE = RNAi-deficient (accessory dsRNA binding protein); RISC = RNA-induced silencing complex (Adapted from T. Sijen, Cell, 2001).

The question was raised whether RNAi was a mechanism that was restricted to pathogen response and control of transposable elements, or whether it was also an active regulator of physiologically expressed genes [65]. In the following years, it became clear that there are at least three endogenous subtypes of small RNAs with regulatory function in *C. elegans* that differ in terms of origin, maturation processes and complementarity to target sequences [80].

Endogenous siRNAs were described to result from Dicer-mediated cleavage of a long double stranded RNA precursor. They were reported to be ~22 nucleotides in size, and to be fully complementary to their target. Furthermore, they stem from the antisense strand of protein coding regions in the genome. This is in contrast to a second class of regulatory RNAs, the tiny non-coding RNAs (tncRNAs), which were described to be transcribed from non-coding genomic sequences. The term tncRNA was established by Victor Ambros in 2003 in an attempt to classify endogenous RNAs with a regulatory function in *C. elegans* [80].
A third class, the microRNAs (miRNAs), are generated by cleavage of a ~70 nucleotide single-stranded hairpin precursor RNA [81]. This prompted Ambros to suggest that the main difference between miRNAs and endogenous siRNAs lies in their biogenesis and in their mode of action (imperfect complementarity in the case of miRNA and tncRNA vs. perfect complementarity in the case of endogenous siRNA). The term "microRNA" (miRNA) was coined in 2001 by consent of three different groups [82-84]. In contrast to siRNAs that always lead to target RNA degradation, it was observed that miRNAs can also act as translational repressors, leaving the target transcript intact [85]. The machinery behind its biogenesis was thought to be different from siRNA. Dicer, the endonuclease giving rise to siRNAs by cleaving double stranded precursors, was suggested to generate miRNAs by digesting stem-loop precursors. Due to these new insights, the *lin-4* RNA described in 1993 was classified as a miRNA in retrospect.

1.4.2 microRNAs are a subclass of non-coding RNAs

1.4.2.1 microRNA biogenesis and function

miRNAs are encoded in the genome, either as independent miRNA genes or as parts of an annotated gene. In the former case, transcription directly gives rise to a repetitive hairpin structure, which is the pri-miRNA. It measures up to several thousand nucleotides in length and possesses typical mRNA features, such as a 5′ cap sequence and a 3′ poly-A-tail. This pri-miRNA is further processed by the nuclear microprocessor complex, consisting of the double-stranded RNA-binding protein DiGeorge syndrome critical region gene 8 (DGCR8) and the type III RNAse Drosha [86], yielding ~70-nucleotide pre-miRNA hairpin structures (Fig. 1-4). Canonical intron-derived miRNAs are excised from the primary transcript by DGCR8 and Drosha prior to splicing. Additional cropping and trimming gives rise to the pre-miRNA hairpin. Non-canonical intronic miRNAs stem from spliced introns that undergo debranching and trimming of single-strand overhangs. Unlike the canonical pathways, this

non-canonical procedure does not require the DGCR8/Drosha microprocessor complex. Irrespective of their canonical or non-canonical origin, an active shuttle mechanism exports the pre-miRNA into the cytosol upon complexation with RanGTP and Exportin 5. Here, another type III RNAse, Dicer, cleaves the miRNA precursor into 22-nucleotide double-stranded RNA fragments. This process requires the assembly of the argonaute proteins AGO 1–4, the RNA – binding protein TRBP and Dicer itself [87]. Once cleaved, one strand of RNA (the guide strand) remains bound to the AGO proteins, while the other strand (the passenger strand) is in the majority of cases degraded. In some cases, accumulation of passenger strand was shown to be indicative of later occurring guide strand up-regulation [88]. The strand bias is thought to be determined by the thermodynamic stability of the RNA duplex. Unlike in *Drosophila melanogaster* or *Caenorhabditis elegans*, where different AGO proteins discriminate between miRNA duplexes with perfect or imperfect complementarity and bind selectively, no such sorting mechanism is suggested in humans [87].

Dicer, TRBP and the argonaute proteins form a loading complex (RLC, risc loading complex) that incorporates the mature miRNA into the miRNA-induced silencing complex (miRISC), consisting of AGO and GW182 family proteins. The miRISC guides the miRNA to the target mRNA, where binding occurs predominantly in the 3´UTR. The region determining complementarity is a stretch of nucleotide 2-7 at the miRNA 5´ end, the seed region. A match of miRNA and mRNA in this region has been shown to be necessary and sufficient for translational regulation. GW182 proteins were suggested to recruit deadenylating complexes to the miRISC, thereby achieving mRNA deadenylation and destabilization [89]. The modification of target mRNA by miRNA-mediated deadenylation has been described as the predominant mode of action by which miRNAs achieve down-regulation of protein, since initial deadenylation was presumed to precede translational inhibition. Progressive deadenylation plus a decreased amount of protective ribosomes on the mRNA then confer mRNA destabilization and reduced protein synthesis [90]. Target destabilization can also be conferred by endonucleolytic cleavage, exerted by the AGO2 protein. While this mechanism is common in plants, it is only of minor importance in the mammalian system [91]. A third way of neutralizing transcript is binding and sequestration of mRNA, which renders it inaccessible to ribosomes, thereby leaving it intact but translationally silenced [91]. These mRNA-miRNA duplexes have been shown to accumulate in designated foci within the cytoplasm, termed processing bodies (P-bodies) [92]. In rare cases, miRNAs can enhance translation by alleviating repression, as has been described for the impact of miR-10a on

ribosomal protein mRNA [93], or by displacing destabilizing mediators, such as tristetraprolin (ZFP36) [94].

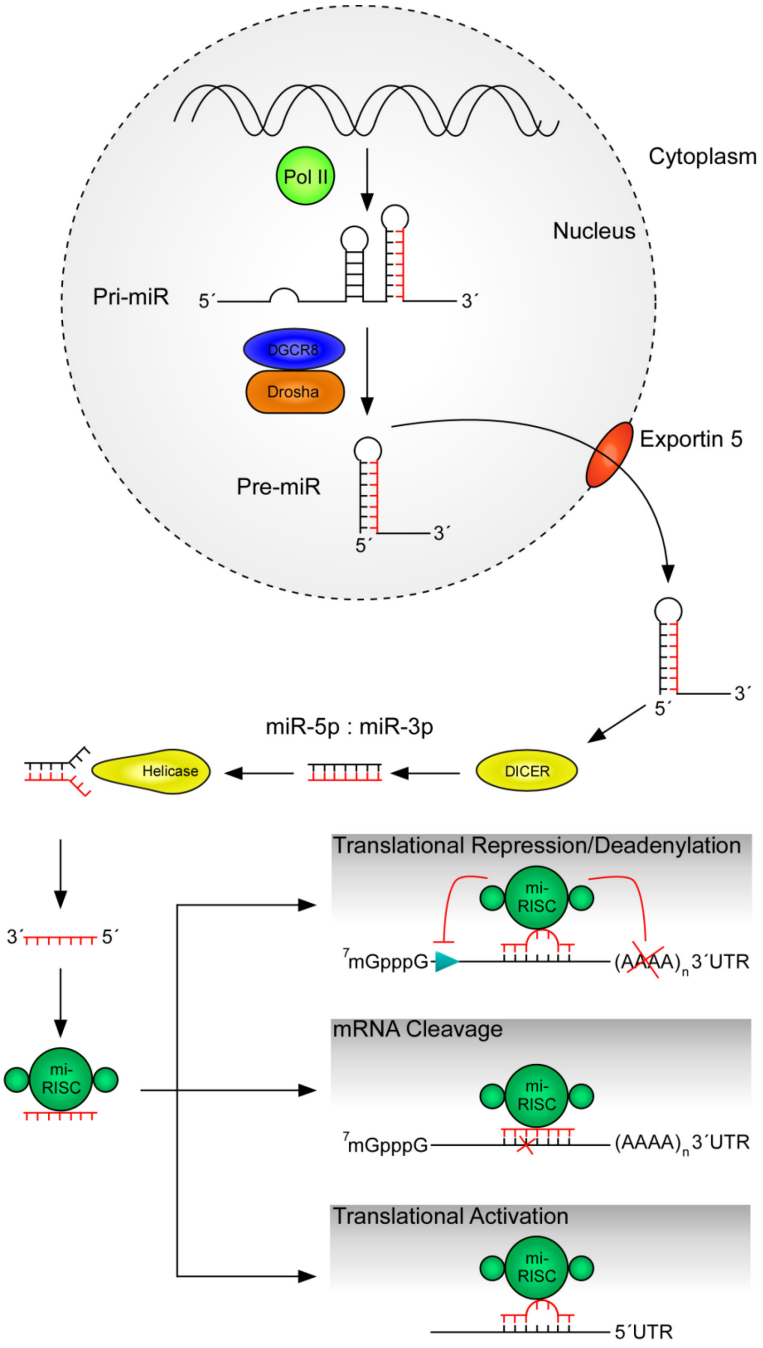

Figure 1-4: miRNA biogenesis and function. The long primary pri-miR transcript is cleaved by the RNAse Drosha, yielding a pre-miR of ~70 nucleotides in length, which is exported into the cytoplasm. There, it undergoes further cleavage by DICER. The resulting 22 nucleotide double strand is opened, and either the 5p or the 3p single strand is loaded into the miRISC. This complex can then mediate translational repression, mRNA cleavage, and in rare cases translational activation. DGCR8: DiGeorge syndrome critical region gene 8; miRISC: microRNA-induced silencing complex. (Adapted from Iorio, EMBO Mol Med, 2012 and Shyu, EMBO, 2008).

The clinical relevance of miRNAs lies in their potential as biomarkers. They were successfully isolated from various body fluids, such as plasma/serum, urine or saliva [95]. This minimally invasive sampling method significantly facilitates diagnosis. The challenge remains, though, to link a certain miRNA pattern found in a patient with a specific disease diagnosis and prognosis. Some forms of cancer have been characterized by one or more de-regulated miRNAs [96]. Since their aberrant expression implies their involvement in disease manifestation, efforts have been made to target these "oncomiRs" [95] by anti-miRNAs [97, 98].

Selective interference with the miRNA setup of a given cell can be basically achieved by two methods, ectopic overexpression or ectopic silencing. The introduction of a miRNA precursor (pre-miR) leads to an abundance of this miRNA in the cell. Conversely, introduction of a reverse complement, the anti-miRNA (anti-miR), confers downregulation of the target by antisense suppression. Of note, the global perturbation that occurs in the wake of introduction of an artificial RNA into a cell due to saturation and competition effects of the processing machinery has been shown to be both detectable and significant [99].

1.4.2.2 microRNA nomenclature

The miRNA nomenclature follows a standardized pattern that allows quick identification of a miRNA´s key properties. The name hsa-miR-146a-5p, e.g., contains information about the species ("hsa", *homo sapiens*), it identifies the molecule as a mature miRNA (capitalization in "miR"), it assigns a number to address the family ("146") and a letter to indicate the specific member of that family ("a"). The appendix "5p" reveals that the miRNA comes from the 5´arm of the mir-146a hairpin (lack of capitalization in "mir" denotes the precursor). Depending on the specific miRNA, the 3p or 5p variant may be the guide strand or the passenger strand. Originally, the miRNA passenger strand was labeled with an asterisk ("hsa-miR-146a*") to highlight its minor importance. This biased nomenclature has been revoked in favor of the 3p and 5p annotation, because asterisk-labeled miRNAs have been found to be of relevance in some cases, e.g. hsa-miR-19* [100], which has been consequently re-named into hsa-miR19-5p. A systematic nomenclature of miRNAs can be retrieved from the miRBase database [101].

1.4.2.3 microRNA target prediction requires elaborate bioinformatics

The likelihood of a miRNA-mRNA interaction can be computed to a certain extent. Publicly available databases and algorithms (TargetScan, miRBase, miRanda) combine information about e.g. sequence conservation across species and thermodynamic stability of the putative miRNA/mRNA duplex and provide a numeric score that is indicative of interaction probability [101]. Due to the underlying biological complexity of mRNA-miRNA interaction, every target prediction needs to be validated experimentally, since all algorithms produce a certain amount of false positive or false negative results.

1.4.2.4 microRNAs can be targeted to alleviate experimental asthma

Several miRNAs are up-regulated in models of experimental asthma, in both immune cells and cells of the airways. In T cells, miR-21 is among the most prominently expressed. It is speculated that this miRNA acts on the T_H1/T_H2 balance by targeting IL-12p35. This would drive the immune response toward the T_H2 axis, maybe contributing to the exaggerated T_H2 response seen in many asthma subtypes. Accordingly, miR-$21^{-/-}$ mice were shown to have increased levels of T_H1 cytokines, reduced levels of T_H2 cytokines and less eosinophilia in their lungs after OVA allergen challenge [102]. Another miRNA that has been described as induced in experimental asthma is miR-126, which was found to be up-regulated in the airway wall tissue in response to house dust mite extract in a TLR4/MyD88 dependent manner. The T_H2 response elicited by HDM was shown to be ablated by antagonizing miR-126, a mechanism that essentially relies on GATA3 down-regulation [103]. While these miRNAs are experimentally validated to influence asthma pathogenesis, other potential candidates are proposed on the basis of prediction [104]. More research is needed to establish a conclusive network of interaction that incorporates cellular and molecular components of asthma development and progression.

1.5 Aims of this study

The goal of this study was to understand the molecular basis of miRNA regulation in macrophage polarization, and to translate this knowledge into the context of eosinophilic airway inflammation. To this end, the mRNA and miRNA profiles of the prototypical human macrophage polarization types were assessed. The exploration of possible mRNA/miRNA

interactions was hypothesized to yield clues as to the impact of miRNA regulation on macrophage polarization. Furthermore, the global miRNA profiles were envisaged to provide generally applicable patterns that can be used to determine the polarization status of macrophages isolated from *in vivo* material. In this study, murine eosinophilic airway inflammation was used as an experimental disease model, and lung macrophages were isolated to determine their polarization status on the basis of their miRNA pattern.

2 Materials and Methods

2.1 Materials

2.1.1 Instruments and equipment

7300 Real Time PCR System	Life Technologies (Carlsbad, USA)
7900 HT Real Time PCR System	Life Technologies
autoMACS Pro Separator	Miltenyi Biotech (Bergisch-Gladbach, Germany)
Axio Vert.A1 Fluorescence Microscope	Zeiss (Oberkochen, Germany)
AxioCam MRm	Zeiss
Bioanalyzer 2100	Agilent (Böblingen, Germany)
Biomate3 Photometer	Thermo Fisher Scientific (Karlsruhe, Germany)
Cell Counting Chamber TC10	Bio-Rad (München, Germany)
Centrifuge 5424R	Eppendorf (Wesseling-Berzdorf, Germany)
FACS Aria III Cell Sorter	BD Biosciences (Heidelberg, Germany)
FACS Calibur Flow Cytometer	BD Biosciences
Gentle MACS Homogenizer	Miltenyi Biotech
HERACELL 240i CO_2 Incubator	Thermo Fisher Scientific
Heraeus Multifuge X3R	Thermo Fisher Scientific
Lumat LB9501 Luminescene Reader	Berthold Technologies (Bad Wildbad, Germany)
Master Nebulizer	Pari (Midlothian, USA)
Mini Protean Electrophoresis Chamber	Bio-Rad
Mini Protean Tetra System	Bio-Rad
Nanodrop	Peqlab Biotechnologie (Erlangen, Germany)
Neubauer –Improved Counting Chamber	Marienfeld (Lauda-Königshofen, Germany)
MaxQ 6000 Incubated Stackable Shaker	Thermo Fisher Scientific
Odyssey Infrared Imager	Li-cor Biosciences (Bad Homburg, Germany)
PEQPOWER 300V Power Supply	Peqlab Biotechnologie
PEQSTAR 2X Gradient Thermo Cycler	Peqlab Biotechnologie
Pipetman	Gilson (Middleton, USA)
Pipets	Gilson
Precision Scale SI-234	Denver Instrument (Göttingen, Germany)
Qubit Fluorometer 2.0	Life Technologies
Quadro MACS Magnetic Stand	Miltenyi Biotech
Surgical Preparation Set	Fine Science Tools (Heidelberg)
TC10 Automated Cell Counter	Bio-Rad
Thermomixer Comfort	Eppendorf
UV Transilluminator	Biostep (Jahnsdorf, Germany)
ViiA™ 7 Real Time PCR System	Life Technologies
Vortex-Genie 2	Scientific Industries (Bohemia, USA)

2.1.2 Consumables and plasticware

0.5 ml, 1.5 ml and 2 ml Reaction Tubes	Greiner (Frickenhausen, Germany)
1 ml Norm-Ject Syringe	Henke Sass Wolf (Tuttlingen, Germany)
10 µl, 20 µl, 100 µl, 200µl and 1000µl Pipet Tips	Gilson
15 ml and 50 ml Reaction Tubes	Greiner
18G Vasofix Safety Permanent Venous Catheter	B.Braun (Melsungen, Germany)
30 µm MACS pre Separation Filter	Miltenyi Biotech
5 ml, 10 ml and 25 ml Serological Pipets	Greiner
12 Well Cell Culture Plate	Greiner
BCYE Agar Plates	Oxoid (Hampshire, UK)
BD Microlance 3 20G	BD Biosciences
GentleMACS C Tubes	Miltenyi Biotech
MACS LS Columns	Miltenyi Biotech
Petri Dish 10 cm	Greiner
RNA Nano Chip	Agilent
Serum Pipets	Greiner
T75 Tissue Culture Flask	Sarstedt (Nümbrecht, Germany)
Taqman Low Density Array Card A v.2.0 human	Life Technologies
Taqman Low Density Array Card A v.2.0 rodent	Life Technologies
Ultra Low Attachment 6-Well Plates	Corning (Corning, USA)
Ultra Low Attachment Petri Dish 10 cm	Corning
Ultra Low Attachment T75 culture flask	Corning

2.1.3 Oligonucleotides

2.1.3.1 Cloning primers

Table 2-1: Cloning primers for insert amplification and restriction site integration. Restriction sites for NotI (GCGGCCGC) and XhoI (CTCGAG) are underlined.

Target 3´UTR	Accession Number, Position	Sequence (5´-3´)
DYRK2	NM_006482.2, 5688-5908	fw: GTTTTCTCGAGCGGTAAAGGTTTTAATATTGCC rv: GTTTTGCGGCCGCCACAGTTGCAGCATATTACAGTC
KLF4	NM_004235.4, 2020-2112	fw: GTTTTCTCGAGAAGAGGCATTTTTAAATCCCAG rv: GTTTTGCGGCCGCTCATCGGGAAGACAGTGTG
LAMP2	NM_002294.2, 4663-4740	fw: GTTTTCTCGAGGGATTCATTTTCATTGGTGG rv: GTTTTGCGGCCGCTAATGCTGATCAGGAGGTGG
MRC1	NM_002438.3, 4491-5180	fw: GTTTTCTCGAGCTAGTACCTCAATGCGATTCTG rv: GTGCGGCCGCGACCTTGTCTTTAATGTTTATTTCAC

PPARγ	NM_138712.3, 1682-1748	fw: GTTTTCTCGAGCAGAGAGTCCTGAGCCACTG rv: GTTTTGCGGCCGCTCAGATTTTCCCTCAGAATAGTG
PTK9	NM_001242397.1, 2758-2838	fw: GTTCTCGAGCTGTACCATCTATGTGCAATTATACTC rv: GTTTGCGGCCGCTCACATCTATATTCTGGAATGTCC
SH2B2	NM_020979.3, 2048-2137	fw: GTTTCTCGAGTGGAGAACCAGTACTCCTTCTACTAG rv: GTTGCGGCCGCGCTTTTAATAACATCGTGTCTTCAC
TREM2	NM_018965.3, 798-1053	fw: GAAAACTCGAGAGGAAGATGATGGGAGGAAAAG rv: GAAAGCGGCCGCTCCAGCTAAATATGACAGTCTTGG

All cloning primers were designed with Primer3plus and custom-made by Metabion (Martinsried, Germany).

2.1.3.2 qPCR primers

SYBR Green

Table 2-2: Custom oligonucleotides for mRNA target detection

Target	Sequence (5´-3´)
LAMP2 (isotype A)	fw: CCCTGGGAAGTTCTTATATGTGC rv: GAAGTTGTCGTCATCTGCACTG
RPS18	fw: CTTTGCCATCACTGCCATTA rv: ACACGTTCCACCTCATCCTC
SH2B2	fw: GCTGACCTTCAACTTCCAGG rv: GAACCACAGATGCTGTACGTG
TNFα	fw: GCTGCACTTTGGAGTGATCG rv: TCACTCGGGGTTCGAGAAGA

All SYBR Green primers were designed with Primer3plus and custom-made by Metabion (Martinsried, Germany).

Taqman Probes

Table 2-3: Commercial Taqman Probes for miRNA detection

Probe	Mature miRNA Sequence (5´-3´)
hsa-miR34c-5p	AGGCAGUGUAGUUAGCUGAUUGC
hsa-miR146a-5p	UGAGAACUGAAUUCCAUGGGUU
hsa-miR-146b-5p	UGAGAACUGAAUUCCAUAGGCU
hsa-miR155-5p	UUAAUGCUAAUCGUGAUAGGGGU
hsa-miR187-3p	UCGUGUCUUGUGUUGCAGCCGG
hsa-miR-193b-3p	AACUGGCCCUCAAAGUCCCGCU

hsa-miR-511-5p	GUGUCUUUUGCUCUGCAGUCA
RNU48	GAUGACCCCAGGUAACUCUGAGUGUGUCGCUGAUGCCAUCACCGCAGCG CUCUGACC
mmu-miR-21a-5p	UAGCUUAUCAGACUGAUGUUGA
mmu-miR-126-3p	UCGUACCGUGAGUAAUAAUGCG
mmu-miR-146a-5p	UGAGAACUGAAUUCCAUGGGUU
snoRNA202	GCUGUACUGACUUGAUGAAAGUACUUUUGAACCCUUUUCCAUCUGAUG

All Taqman Probes were provided by Life Technologies.

2.1.4 Plasmids

psiCheck2 Vector (Fig. 2-1) Promega (Mannheim, Germany)

2.1.5 Synthetic miRNAs

Table 2-4: pre-miR sequences

miRNA	**Mature miRNA sequence (5´-3´)**
hsa-miR-155-5p-5p	UUAAUGCUAAUCGUGAUAGGGGU
hsa-miR-187-3p-3p	UCGUGUCUUGUGUUGCAGCCGG

2.1.6 Antibodies

2.1.6.1 Flow Cytometry

Murine

Table 2-5: Antibody panel for cytometric sorting of murine macrophages

Specificity	**Clone**	**Isotype**	**Fluorochrome**	**Isotype Control Clone**	**Company**
CD45	30-F11	Rat IgG2b κ	FITC	RTK4530	Biolegend
SiglecF	E50-2440	Rat IgG2b κ	PE	eB149/10H5	BD
Gr-1	RB6-8C5	Rat IgG2b κ	PerCP-Cy5.5	RTK4530	BD
CD11b	M1/70	Rat IgG2b κ	Pacific Blue	RTK4530	Biolegend
CD11c	N418	Hamster IgG	APC-Cy7	HTK888	Biolegend

Human

Table 2-6: Antibody panel for cytometric analysis of human monocytes/macrophages

Specificity	Clone	Isotype	Fluorochrome	Company
CD14	M5E2	Mouse IgG2a κ	FITC	BD
CD23	EBVCS2	Mouse IgG1 κ	APC	eBioscience
CD80	3H5	Mouse IgG1 κ	PE	BD

2.1.6.2 Magnetic beads

Table 2-7: Magnetic microbeads for cell enrichment by positive selection

Specificity	Company
CD14 human	Miltenyi Biotech
APC	Miltenyi Biotech

2.1.6.3 Western Blot

Table 2-8: Primary Western Blot antibodies

Specificity	Source	Exp. Band Size (kDA)	Company
Phospho-STAT6	Rabbit	110	Cell Signalling
Phospho-ERK	Mouse	42/44	Santa Cruz Biotechnology
p38α	Rabbit	38	Santa Cruz Biotechnology
Phospho-p38	Mouse	38	Santa Cruz Biotechnology
Phospho-SAPK/JNK	Rabbit	46/54	Cell Signalling
IκBα	Rabbit	35-41	Santa Cruz Biotechnology
LAMP2	Mouse	105-110	Abcam
Actin	Goat	43	Santa Cruz Biotechnology

Table 2-9: Secondary Western Blot antibodies

Specificity	Source	Conjugate	Company
Rabbit IgG	Goat	Cy5.5	Rockland Immunochemicals
Mouse IgG	Goat	Cy5.5	Rockland Immunochemicals
Goat IgG	Donkey	IRDye800	Rockland Immunochemicals
Mouse IgG	Goat	HRP	Santa Cruz Biotechnology

2.1.6.4 Immunofluorescence

Table 2-10: Immunofluorescence antibodies

Specificity	Source	Conjugate	Company
LAMP2	Mouse	-	Abcam
Mouse IgG	Goat	AlexaFluor 555	Invitrogen

2.1.7 Bacterial Strains

Legionella pneumophila (Corby)	provided by the Robert Koch Institut (Berlin, Germany)
Supercompetent E. Coli DH5a	New England Biolabs (Ipswich, USA)

2.1.8 Enzymes

Collagenase D (0.242 U/mg)	Roche (Basel, Switzerland)
DNAse I (3000 Kunitz Units/mg)	Serva (Heidelberg, Germany)
NotI (10.000 U/ml)	New England Biolabs (Ipswich, USA)
Taq DNA Polymerase (5000 U/ml)	New England Biolabs
T4 DNA Ligase (400.000 U/ml)	New England Biolabs
XhoI (20.000 U/ml)	New England Biolabs

2.1.9 Stimulants and Cytokines

Lipopolysaccharide (LPS), Salmonella minnesota R595	Enzo Life Science (Lörrach, Germany)
rhInterferon-γ (E. Coli)	Promocell (Heidelberg, Germany)
rhInterleukin-13 (E. Coli)	Promocell
rhInterleukin-4 (E. Coli)	Promocell

2.1.10 Analytical Chemicals, Reagents and Kits

Acrylamide (Rotiphoresis Gel 30, 37.5:1)	Roth (Karlsruhe, Germany)
Actinomycin D	Biovision (Milpitas, USA)
Agarose NEEO Ultra Quality	Roth
Albumin Fraction V	Roth
Aluminum Hydroxide ($Al(OH)_3$)	Thermo Scientific
Ampicillin Sodium Salt	Sigma Aldrich (St. Louis, USA)
Ammonium Persulfate (APS)	Roth
Bacto Agar	BD Biosciences
Purified Bovine Serum Albumin 100X	New England Biolabs
Bromphenol Blue	Sigma
Complete Mini Protease Inhibitor Cocktail	Roche
4,6-Diamin-2-Phenylindol (DAPI)	ATT Bioquest (Sunnyvale, USA)
Dulbeccos´s Modified Eagle Medium (DMEM)	Gibco
Dulbecco´s Phosphate Buffered Saline (PBS)	PAA Laboratories (Pasching, Austria)
Ethylene Diamine Tetra-Acetic Acid (EDTA)	Roth (Karlsruhe, Germany)
Fetal Calf Serum (FCS)	PAA Laboratories
Firefly Luciferase Assay System	Promega
Gentamicin	Gibco
GlutaMAX	Gibco
Glycoblue	Life Technologies
High Capacity Reverse Transcription Kit	Applied Biosystems
Heparin	Ratiopharm (Ulm, Germany)
Human Serum off-the-clot, Type AB	Lonza (Basel, Switzerland)
Isol RNA Lysis Reagent	5Prime (Hamburg, Germany)
Ketamin	Inresa (Freiburg, Germany)
LB Agar	BD Biosciences
LB Broth	BD Biosciences
LSM 1077 Lymphocyte Separation Medium	PAA Laboratories
Lysis Buffer	Promega
Milk Powder	Roth
Mouse Fc Block	BD Biosciences
Mowiol 4-88	Roth
NEBuffer 3	New England Biolabs
Nonidet P40 BioChemica (Substitute)	AppliChem (Darmstadt, Germany)
Nuclease-Free Water	Ambion
Nucleo Spin Extract II Kit	Macherey Nagel (Düren, Germany)
Nucleo Spin Plasmid	Macherey Nagel
NucleoSpin Gel and PCR Cleanup Kit	Macherey Nagel
Odyssey Blocking Buffer	Li-Cor
Optimem Transfection Medium	Gibco/Life Technologies

Ovalbumin (grade VI)	Sigma Aldrich
PonceauS	Sigma Aldrich
Purified BSA	New England Biolabs
Qubit Molecular Probes	Invitrogen
Renilla Luciferase Assay System	Promega
RNA 6000 Nano Reagents	Agilent
Rompun	Bayer (Leverkusen, Germany)
Roti-Aqua-PCI	Roth
RPMI 1640	Gibco (Darmstadt, Germany)
Saponin	Roth
SOC Medium	Thermo Fisher Scientific
Sodium Dodecyl Sulfate (SDS)	Roth
Sodium Orthovanadate	Sigma Aldrich
SYBR Green Master Mix	Life Technologies
T4 Ligase Buffer	New England Biolabs
Taqman 2X Universal PCR Master Mix No AmpErase UNG	Life Technologies
Taqman microRNA Reverse Transcription Kit	Life Technologies
Tertraethylmethylenediamine (TEMED)	Roth
Thermopol Reaction Buffer 10X	New England Biolabs
Tris(hydroxymethyl)aminomethane (TRIS)	Roth
Triton X100	Roth
Trypsin-EDTA 0.05 % (1X)	Gibco
Trypticase Soy Agar	BD Biosciences
Tween 20	Roth
Xylencyanol	Roth
Yeast Extract	BD Biosciences

2.1.11 Chemicals

β-Mercaptoethanol	Sigma Aldrich
Chloroform	Roth
Ethanol	Roth
Ethidium Bromide	Invitrogen
Glycerol	Roth
Isopropanol	Roth
Methanol	Roth
Paraformaldehyde	Roth
Sodium Acetate	Roth
Sodium Azide	Roth
Sodium Chloride	Roth

2.1.12 Buffers and Solutions

BAL Lavage Solution	2 mM EDTA in PBS
FACS Wash Buffer	1 % v/v FCS 0.02 % w/v NaN_3 in PBS
HEK293 Culture Medium	1 % v/v GlutaMAX 10 % v/v FCS in DMEM
MACS Buffer	0.5 % v/v FCS 0.2 mM EDTA in PBS
Macrophage Culture Medium	1 % v/v GlutaMAX 1 % v/v human off-the-clot AB Serum in RPMI1640
Laemmli Buffer	13.15 % v/v Stacking Buffer 21.05 % v/v 10 % SDS 10.5 % v/v Glycerol 5.75 % v/v 1 % Bromphenol Blue
LB Agar	3.5 % w/v LB Agar in aqua dest.
LB Medium	2 % w/v LB Broth in aqua dest.
Lung Tissue Digestion Buffer	2 mg/ml Collagenase D (> 0.15 U/mg) 0.5 mg/ml DNAseI (>3000 Kunitz Units/mg) in PBS
Phosphoprotein Wash Buffer	2.5 mM Na_3VO_4 125 mM NaF 18.75 mM $Na_4P_2O_7$ in PBS

RPMI 1640 complete medium	1 % v/v L-GlutaMAX 1 % v/v Penicillin/Streptomycin 1 % v/v FCS
THP-1 Culture Medium	10 % v/v Fetal Calf Serum in RPMI 1640
Trypticase Soy Agar	4 % w/v Trypticase Soy Agar in aqua dest.
Western Blot Lysis Buffer	50 mM Tris-HCl pH 7.4 1 % v/v Nonidet P40 Complete Protease Inhibitor tablet in aqua dest.
Western Blot Running Buffer (5X)	123 mM Tris Base 950 mM Glycine 17 mM SDS in aqua dest.
Western Blot Resolving Buffer pH 8.8	1.5 M Tris Base in aqua dest.
Western Blot Stacking Buffer pH 6.8	490 mM Tris Base in aqua dest.
Western Blot Resolving Gel 10 %	132 mM Tris Base 350 mM PAA 170 mM Glycerol 3.5 mM SDS 2.2 mM APS 6.7 mM TEMED in aqua dest.
Western Blot Stacking Gel 5 %	87.5 mM Tris Base 174 mM PAA 3.5 mM SDS 2.2 mM APS 6.7 mM TEMED in aqua dest.
Western Blot Transfer Buffer (10X)	248 mM Tris Base 1.9 M Glycine in aqua dest.

Western Blot Transfer Buffer (1X)	8 % v/v 10X Transfer Buffer 20 % v/v Methanol in aqua dest.

2.1.13 PCR and RT Solutions

	Volume per Sample [µl]
High Capacity Reverse Transcription	4.2 H_2O 0.8 dNTP (100 mM) 2 Transcripton Buffer 10X 1 Multiscribe Enzyme 2 Random Hexamer Primer 10 RNA (500 ng – 1 µg)
Taqman microRNA Reverse Transcription (Singleplex)	4.16 H_2O 0.15 dNTP (100 mM) 1.5 Transcription Buffer 10X 1 Multiscribe Enzyme 3 RT Primer (5X) 5 RNA (1 – 10 ng)
Taqman microRNA Reverse Transcription (Multiplex)	1.01 H_2O 0.3 dNTP (100 mM) 1.5 Transcription Buffer 10X 3 Multiscribe Enzyme 6 RT Primerpool (0.05X per Primer) 3 RNA (350 ng – 1 µg)
Megaplex Reverse Transcription	0.2 H_2O 0.2 dNTP (100 mM) 0.8 Transcription Buffer 10X 0.9 $MgCl_2$ (25 mM) 1.5 Multiscribe Enzyme 0.1 RNAse Inhibitor (20 U/µl) 3 RNA (1 – 350 ng for PreAmplification; 350 ng – 1 µg for TLDA)
Pre-Amplification	6.25 H_2O 12.5 Taqman PreAmp Master Mix 2X Taqman Probe 0.2X 2.5 µl Megaplex RT Product
Taqman Low Density Array (TLDA)	450 Taqman 2X Universal PCR Master Mix 444 Nuclease free Water 6 Megaplex RT Product

qPCR (Taqman)	7.5 H_2O 1 Taqman Probe 20X 10 Taqman 2X Universal PCR Master Mix 1.5 RT Product
qPCR (SYBR Green)	8.1 H_2O 0.2 forward/reverser Primer (10 µM) 10 SYBR Green 2X 1.5 RT Product

2.1.14 Ligation and Restriction Solutions

	Volume per reaction [µl]
Insert Amplification	28 H_2O 10 Taq Reaction Buffer 1 dNTP (10 mM) 1 forward/reverse Primer (10 µM) 0.25 µl Taq Polymerase (5 U/µl) 10 cDNA (10 ng/µl)
Insert Digestion	45 Amplification Product 6 Buffer 3 6 BSA (100 µg/ml) 1 XhoI 1 NotI
Vector Linearization	34.1 H2O 6 psiCheck2 Vector (8 µg) 5 Buffer 3 5 BSA (100 µg/ml) 1 XhoI 1 NotI
Insert-Vector Ligation	8.5 H_2O 1.5 T4 Ligation Buffer 1 T4 Ligase 2 linearized Vector (15 ng) 2 restricted Insert (15 ng)

2.1.15 Mice strains

BALB/c	Harlan Laboratories (Indianapolis, USA)

2.1.16 Software

Adobe Photoshop CS5	Adobe Systems (San Jose, USA)
Canvas X	ACD Systems (Victoria, Canada)
FlowJo v. 7.6.5	TreeStar (Ashland, USA)
GENtle	M. Manske (University of Cologne, Germany)
GraphPad Prism	GraphPad Software (San Diego, USA)
LabImage 1D	Kapelan BioImaging (Leipzig, Germany)
Microsoft Office 2010	Microsoft (Redmond, USA)
NEB Cutter	New England Biolabs
Oligo Melting Temperature Calculator	Weizman Institute (Rehovot, Israel)
Primer3plus [105]	
R [106]	

2.1.17 External Services

Commercial

Metabion (Martinsried, Germany)
MFT Services (Tübingen, Germany)
Sequence Laboratories (Göttingen, Germany)
Flow Cytometry Core Facility (Marburg, Germany)

Cooperative

Department of Clinical Chemistry (Philipps University Marburg, Germany)
Max Planck Institute for Molecular Genetics (Berlin, Germany)

2.2 Methods

2.2.1 Cell culture

2.2.1.1 Preparation and cultivation of primary human monocytes

Monocytes were isolated from donor buffy coats provided by the German Red Cross. All donors gave informed written consent for use of their blood samples for scientific purposes. The blood sample was diluted 1:2 with PBS and stacked onto a cushion of Pancoll solution. Centrifugation for 25 minutes at 800 x g yielded a distinct leukocyte layer. Leukocytes were aspirated, resuspended in ambient temperature PBS and washed twice. The pellet was taken up in MACS Buffer. An appropriate amount of cells was incubated with anti-CD14 magnetic microbeads for 20 minutes at 4 °C. Labeled cells were magnetically retained in a MACS LS column and eluted after depletion of unlabeled leukocytes. Eluted cells were >90 % $CD14^+$ monocytes as routinely determined by FACS analysis. 7 x 10^5 cells/ml were left to adhere for two hours to ultra-low attachment plates in RPMI medium without supplements. After 2 h, adhesion of cells was validated by microscopy, and 1 % of human AB serum was added. Monocytes were then incubated for 6 days at 37°C and 5 % CO_2, and maturation to macrophages was confirmed by microscopy.

2.2.1.2 Macrophage polarization

On day 6 of culture, cells were polarized to M1 by administration of IFNγ (20 ng/ml) and LPS (100 ng/ml), to M2 by administration of Interleukin 4 and Interleukin 13 (20 ng/ml each) or left unpolarized (M0). After 18 h, cells were detached from the flask by carefully rinsing them with warm PBS. Polarization was verified by FACS analysis. M1 macrophages were >80% $CD80^+$ and M2 macrophages were ~40 % $CD23^+$, whereas M0 macrophages were devoid of either marker. In order to obtain an enriched population of $CD23^+$ M2 polarized macrophages, M2 cells were sorted for CD23 by autoMACS, yielding a purity of $CD23^+$ M2 macrophages of > 80 %.

2.2.1.3 THP-1 cell culture

The human monocytic leukemia THP-1 cell line was cultured in THP-1 culture medium at a density of 2 x 10^5 to 1 x 10^6 cells per ml. Cells were split regularly to maintain the appropriate density. Cells were discarded upon exceeding the 20^{th} passage, and the culture was re-

launched from a frozen stock aliquot. THP-1 cells were used for short-term mRNA decay studies upon actinomycin D administration (section 2.2.1.8)

2.2.1.4 HEK293 cell culture

Human embryonic kidney cells were cultured in HEK293 culture medium at 70-90 % confluency and split regularly to maintain the appropriate density. Cells were discarded upon exceeding the 15th passage, and the culture was re-launched from a frozen stock aliquot. Prior to usage, cells were detached from the culture flasks by incubation with trypsin-EDTA 0.05 % (1X). Subsequently, cells were transfected with miRNA precursors and the psiCheck2 vector, and the luciferase-based reporter assay was performed (section 2.2.3)

2.2.1.5 Automated Magnetic Activated Cell Sorting (autoMACS)

M2 polarized cells were incubated with anti-CD23-APC FACS antibody as described (section 2.2.6.1). Anti-APC microbeads were added in a second step to magnetically label CD23$^+$ cells. After 25 minutes at 4 °C, cells were washed in MACS Buffer. CD23$^+$ cells were positively selected by autoMACS to ensure a quick and gentle enrichment of CD23$^+$ M2 macrophages with minimal disturbance of the mRNA and microRNA profile. Purity of the CD23$^+$ population was afterwards determined by FACS analysis.

2.2.1.6 Determination of macrophage bactericidal capacity

2.2.1.6.1 Infection of polarized macrophages with *Legionella pneumophila*

Legionella pneumophila Corby was grown on BCYE agar plates for 3 days at 37 °C and 5 % CO_2. On day three, bacteria were scraped from the plate and resuspended in PBS^{++} to an OD_{600} of 0.1, which equals 2 x 10^8 bacteria/ml. Final multiplicity of infection (MOI) was set as indicated in the respective experiments. Initial infection of fully polarized macrophages (section 2.2.1.2) was carried out for 1 h. If not stated otherwise, extracellular *Legionella* were then killed by administration of gentamicin (50 µg/ml). After 1 h, all supernatant was aspirated, and cells were washed three times in PBS. For the remainder of the experiment, cells were kept in macrophage culture medium.

2.2.1.6.2 Colony forming unit (CFU) assay

Macrophages were polarized as described (section 2.2.1.2), and the fully developed M0, M1 and M2 subtypes were infected with *Legionella pneumophila* at a MOI of one. At indicated time points, cells were lysed by rigorous pipetting in 0.1 % saponin. Cell lysis was confirmed by microscopy. Lysate was serially diluted in a range from 1:10 to 1:10.000 in H_2O and was streaked on BCYE agar plates. After three days of incubation at 37 °C and 5 % CO_2, individual colonies were counted and total bacterial load was calculated.

2.2.1.7 Transfection of monocytes/macrophages with synthetic microRNA

Blood-derived macrophages or monocytic THP-1 cells were transfected with double-stranded miRNA precursors. Transfection was achieved by cultivating the cells in medium containing siPort NeoFX and Optimem in a 1:15 ratio plus the respective miRNA precursors in a final concentration of 30 nM. After 6 h, the transfection medium was replaced with growth medium, and cells were incubated for an additional 24 h or 48 h, respectively. Overexpression of a given miRNA was verified by qPCR.

2.2.1.8 Transcriptional inhibition by actinomycin D application

Monocytic THP-1 cells were transfected with miRNA precursors as described (section 2.2.1.7). Efficiency of miRNA transfection was routinely monitored by qPCR. After 18 h, the cytostatic actinomycin D was added to the culture at a final concentration of 10 µM, and RNA samples were taken at 0 min, 15 min, 30 min and 45 min. These samples were probed for miRNA-enhanced target mRNA degradation by qPCR.

2.2.2 Investigation of the global RNA profile

2.2.2.1 Isolation of total RNA from cells

Pelleted cells were lysed in Isol RNA Lysis Reagent and RNA was isolated according to the supplier's protocol. Centrifugation steps were carried out at 4 °C. All other steps were performed at ambient temperature if not stated otherwise. Samples were mixed with chloroform and vigorously shaken. After three minutes of incubation, samples were

centrifuged at 11.000 x g. The aqueous phase was collected and RNA pellets were obtained by isopropanol precipitation at 11.000 x g, assisted by glycoblue. RNA was washed twice with ethanol at 7.000 x g and air-dried pellets were resuspended in nuclease-free water. Potential RNA secondary structures were dissolved by incubating at 58 °C for 7 minutes. All RNA experimentation hereafter was carried out on ice. The RNA concentration was determined by Nanodrop or Qubit Fluorometer if higher sensitivity was required.

2.2.2.2 RNA integrity validation by capillary gel electrophoresis

Integrity of RNA was verified on a Bioanalyzer 2100, according the manufacturer´s protocol. Briefly, RNA 6000 Nano gel matrix was filtered at 1.500 x g for 10 minutes in a spin filter. 1 µl of fluorescent RNA 6000 Nano dye concentrate was added to 65 µl of filtered gel matrix, and the solution was vortexed. Gel-dye mix was applied to a RNA Nano Chip via the fill port and dispersed into all wells and the capillary system with the provided plunger. Afterwards, 5 µl of RNA 6000 Nano marker was added to all sample wells and to the dedicated ladder well. Finally, RNA samples and ladder were added to the appropriate wells, the chip was vortexed and subjected to analysis. Samples were sequentially driven into the capillary system by voltage. In the process, the stained RNA was resolved as a function of size and detected upon sensor passage. The fluorescence signal was recorded as a function of the elapsed time. The ratio of intact 18s and 28s rRNA was used to calculate a RNA integrity number (RIN). RINs of > 8 were considered indicative of sufficient RNA quality.

2.2.2.3 microRNA analysis by Taqman Low Density Array (TLDA, human)

500 ng of RNA from M0, M1 and M2 macrophages from 3 different donors were reversely transcribed into cDNA using the Taqman microRNA reverse transcription protocol with human megaplex primers v. 2.0 (Table 2-11).

Table 2-11: Megaplex reverse transcription thermo protocol

Stage	Duration	Temperature
Cycle (40x)	2 min	16 °C
	1 min	42 °C
	1 sec	50 °C
Hold	5 min	85 °C
Hold	∞	4 °C

100 µl of cDNA-containg TLDA reaction mix (section 2.1.13) were loaded into each of eight fill ports of a Taqman Low Density Array Card. (Set A, v. 2.0, human). Each fill port is connected to two parallel lanes of 24 serially linked wells with a 1 µl reaction volume, yielding a total of 384 wells. The individual wells are pre-loaded with Taqman miRNA amplification primers (see Appendix for plate layout). The reaction mix was distributed into all 384 wells by centrifugation (2 x 1 min at 330 x g). The plates were sealed, and miRNAs were detected on a 7900HT Fast Real-Time System (Table 2-12).

Table 2-12: Taqman Low Density Array thermo protocol

Stage	Duration	Temperature
Hold	2 min	50 °C
Hold	10 min	95 °C
Cycle (40x)	15 sec	95 °C
	1 min	60 °C

2.2.2.4 microRNA analysis by Taqman Low Density Array (TLDA, murine)

At least 350 ng of RNA from alveolar and interstitial macrophages from healthy and asthmatic mice were reversely transcribed into cDNA using the Taqman microRNA reverse transcription protocol with rodent megaplex primers v. 2.0 (Table 2-11). 100 µl of cDNA-containing reaction mix (2.1.13) were loaded into each of eight fill ports of a Taqman Low Density Array Card. (Set A, v. 2.0, rodent). Each fill port is connected to two parallel lanes of 24 serially linked wells with a 1 µl reaction volume, yielding a total of 384 wells. The individual wells are pre-loaded with Taqman miRNA amplification primers (Appendix). The reaction mix was distributed into all 384 wells by centrifugation (2 x 1 min at 330 x g).The plates were sealed, and miRNAs were detected on a ViiA7 Real Time system (Table 2-12).

2.2.2.5 mRNA analysis by Illumina HT12 Beadchip MicroArray

Transcriptome analysis was carried out by MFT Services (Tübingen, Germany). 1 µg of RNA as used for TLDA was taken up in nuclease-free water at a concentration of >50 ng/µl and sent to MFT Services for further processing. In short, RNA serves as a template to generate full-length cDNA. After second strand synthesis, *in vitro* transcription by a T7 RNA Polymerase yields labelled cRNA in multiple copies. This amplified and labelled cRNA is then used for direct hybridization with the Illumina HT12 BeadChip, which is equipped with 47.231 individual probes for whole genome analysis including splice variants and isoforms.

2.2.2.6 microRNA and mRNA detection by quantitative real time PCR

Quantitative real time PCR was performed with cDNA from miRNA or mRNA reverse transcription according to the following protocol (Table 2-13).

Table 2-13: Quantitative real time PCR thermo protocol

Stage	Duration	Temperature
Hold	2 min	50 °C
Hold	10 min	95 °C
Cycle (40x)	15 sec	95 °C
	1 min	60 °C

2.2.2.6.1 microRNA quantification

For relative quantification of individual miRNAs, 50 ng of total RNA were reverse transcribed using the Taqman microRNA reverse transcription kit and specific primers for miRNA and endogenous control according to the depicted protocol (Table 2-14). cDNA was subjected to Taqman RT-PCR on a 7300 or ViiA7 Real-Time PCR System. The signal of each individual miRNA was normalized to the small noncoding RNA RNU48 (human) oder sno202 (mouse). Fold-induction was calculated using the $2^{-\Delta\Delta ct}$ method.

Table 2-14: miRNA reverse transcription thermo protocol

Stage	Duration	Temperature
Hold	30 min	16° C
Hold	30 min	42 °C
Hold	5 min	85 °C
Hold	∞	4 °C

Weakly expressed miRNAs with a threshold cycle of 33 or higher in TLDA were pre-amplified according to the manufacturer´s protocol in order to robustly detect them in the individual validation assay. This additional precycling step (Table 2-15) was performed after reverse transcription, using the same Taqman probes that were employed in the subsequent qPCR reaction.

Table 2-15: Preamplification thermo protocol

Stage	Duration	Temperature
Hold	10 min	95 °C
Hold	2 min	55 °C
Hold	2 min	72 °C
Cycle (12x)	15 sec	95 °C
	4 min	60 °C
Hold	10 min	99.9 °C
Hold	∞	4 °C

The quantitative real time PCR for miRNA detection was performed with RNA quantities as indicated in section 2.1.13.

2.2.2.6.2 mRNA quantification

Total RNA was subjected to reverse transcription using the High Capacity reverse transcription kit (Table 2-16). For relative quantification of individual mRNAs, 500 ng of total RNA were reversely transcribed using provided random hexamer primers. cDNA was subjected to RT-PCR on a 7300 or ViiA7 Real-Time PCR System using the SYBR Green detection method. The signal of individual mRNAs was normalized to the ribosomal protein S18 mRNA (RPS18). The quantitative real time PCR for mRNA detection was performed with RNA quantities as indicated in section 2.1.13.

Table 2-16: High capacity reverse transcription thermo protocol

Stage	Duration	Temperature
Hold	10 min	25 °C
Hold	2 h	37 °C
Hold	5 min	85 °C

2.2.3 Functional microRNA evaluation by luciferase-based reporter constructs

2.2.3.1 Construction of reporter vectors

For the luciferase reporter assay, the listed 3'UTR fragments (Table 2-1) were amplified using the indicated primers. Each forward primer carried a XhoI restriction site (CTCGAG), while each reverse primer carried a NotI restriction site (GCGGCCGC), as highlighted. The absence of XhoI and NotI restriction sites in the sequence of interest was verified by NEBcutter. The 3´UTR fragments were amplified from M0 cDNA. PCR components were removed by column purification (NucleoSpin Extract II Kit), and 45 µl of cleaned PCR product were

digested with NotI and XhoI in supplied NEBuffer 3 for 1 h at 37 °C. Restriction enzymes were deactivated at 65 °C for 20 minutes. Digested fragments were isolated by gel electrophoresis, excised under UV light and extracted from the gel slices by column purification (NucleoSpin Gel and PCR Cleanup Kit). The psiCheck2 plasmid (Fig. 2-1) was linearized and purified accordingly (NucleoSpin Plasmid Kit). For ligation, 30 ng of insert and 15 ng of NotI- and XhoI-treated vector were incubated for 1 h at 37 °C with T4 Ligase at a final volume of 15 µl.

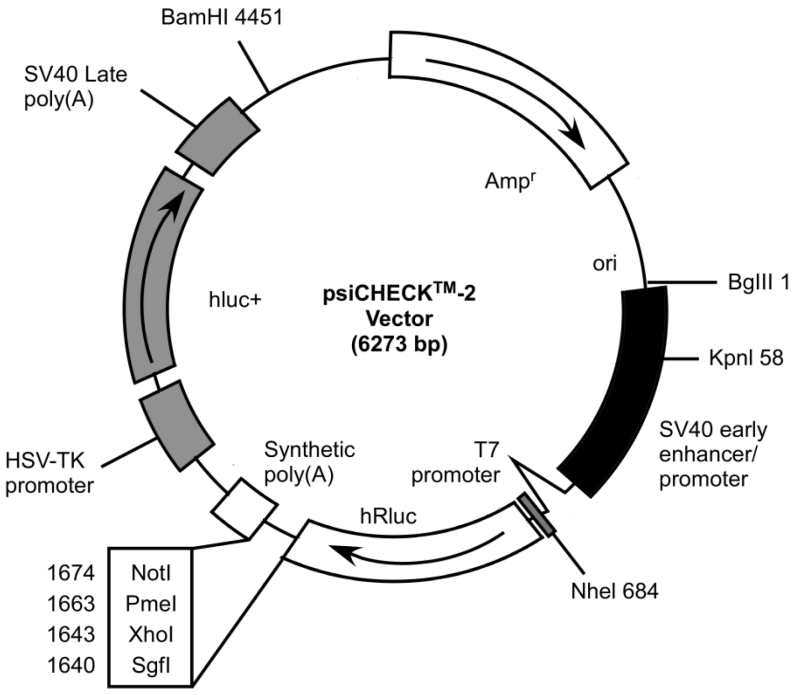

Figure 2-1: The psiCheck2 plasmid. The vector is equipped with a sequence encoding for firefly luciferase (hluc+) and for *Renilla reniformis* luciferase (hRluc). The hRluc sequence carries a multiple cloning site that was used for integration of the respective miRNA target sequences. For selection purposes, the vector also carries an ampicillin resistance gene (Amp^r). Vector design by Promega.

2.2.3.2 Vector amplification by transformation of *Escherichia coli*

30 µl of supercompetent DH5α *E. Coli* were incubated on ice for 30 minutes with 1.5 µl of ligation product. Transformation was performed by heat shock at 42 °C for 30 seconds. Bacteria were put back on ice for 5 minutes and recovered in SOC medium for 1 h at 37 °C with shaking. 70 µl of suspension were plated on pre-warmed trypticase soy broth agar plates containing 100 µg/ml ampicillin. After overnight incubation, single colonies were tested by colony PCR. For this purpose, a universal forward primer binding in the vector backbone at

approximately 30 bp upstream of the cloning site was combined with the respective insert-specific reverse primers as listed in Table 2-1. Positive clones were grown overnight in LB medium containing 100 µg/ml ampicillin at 37 °C. Plasmids were isolated by miniprep and 700 ng of each construct was sequenced (Sequence Laboratories GmbH) to verify correct insert integration. Validated clones were stored at -80 °C in 20 % glycerol.

2.2.3.3 Quantification of microRNA efficiency by bioluminescence

HEK293 cells were grown in DMEM containing 10 % FCS and 1 % Glutamine. 1 x 10^5 subconfluent cells were reverse transfected with NeoFX siPORT. Cells were simultaneously transfected with 300 ng of psiCheck2 plasmid carrying respective inserts and 50 nM of miRNA precursor, according to the manufacturer's protocol. Precursors used in this study were pre-hsa-miR-187-3p, pre-hsa-miR-155-5p and pre-hsa-miR-34c-5p. In case of presence of both a hsa-miR-187-3p and a hsa-miR-155-5p site in the cloned fragment, pre-hsa-miR-187-3p and pre-hsa-miR-155-5p were co-transfected at 25 nM each. Cells were taken up in 80 µl of lysis buffer 72 h after transfection. Cell lysate was diluted 1:10 in ice-cold water, and 80 µl of *Renilla* luciferase or firefly luciferase substrate was added to 20 µl of lysate dilution. After a brief incubation, luminescence was measured using a Lumat LB9501 reader. Relative luminescence units (RLU) were calculated by normalizing the *Renilla* luciferase signal to the firefly luciferase signal. Specificity of each individual miRNA precursor was determined by control transfection with a non-specific scramble miRNA.

2.2.4 Semiquantitative protein analysis by Western Blot

After indicated treatment, cells were washed twice with phosphoprotein wash buffer and lysed in western blot lysis buffer. Debris was removed by centrifugation at 10.000 x g for 10 minutes at 4° C. The protein concentration was determined by Bradford assay. Optical density was measured in a spectrophotometer at a wavelength of 595 nm, and the protein concentration was calculated. Samples were taken up at a 1:2 ratio in Laemmli buffer and denatured for 5 minutes at 95 °C. For protein separation, 10 % SDS gels were used, and 80 µg of protein were loaded per lane. A marker lane was included for reference. 80 V were applied for the focusing of proteins in the stacking gel and increased to 120 V upon transmigration into the resolving gel.

Transfer of protein to a nitrocellulose membrane was performed by tank blot for 1 h at 100 V. After blotting, protein integrity and transfer efficiency was validated by Ponceau S staining. In preparation for antibody staining, the membrane was blocked for 1 h at ambient temperature with Odyssey blocking solution. Primary antibody was added as indicated (Table 2-8) at a 1:1000 dilution and incubated over-night on the membrane at 4° C on a tumbling shaker. Unbound antibody was cleared by washing, and an appropriate fluorochrome-conjugated secondary antibody (Table 2-9) was added for 1 h at ambient temperature. After removal of excess antibody, protein signal was detected on a Licor Odyssey fluorescence scanner.
When required, quantification of signal was performed by densitometric analysis, using the LabImage 1D software.

2.2.5 Visualization of intracellular proteins by immunofluorescence

Macrophages were transfected with synthetic miRNA precursors as described (section 2.2.1.7). To allow microscopy of transfected cells, cells were seeded on glass cover slips. After 12 h, cells were M1-polarized or left unpolarized. Cells were fixed in 4 % PFA and permeabilized with 1 % TritonX100. After blocking of unspecific binding sites with 5 % goat serum in PBS + 1 % BSA, the primary antibody was added at a 1:500 dilution and incubated for 1 h at ambient temperature. After removal of excess antibody, the secondary antibody was given at a dilution of 1:5000 and incubated over night at 4 °C. After washing, cells were incubated with DAPI to counterstain nuclei, and cover slips were mounted with Mowiol. Pictures were taken with a AxioCam MRm on a Axio Vert.A1 Fluorescence Microscope.

2.2.6 Flow Cytometry

2.2.6.1 Cytometric analysis of human monocytes and macrophages

Freshly purified monocytes were resuspended in FACS blocking buffer and incubated with anti-CD14 FITC antibody at a 1:100 dilution for 20 min. at 4 °C. Polarized and unpolarized macrophages were labeled with anti-CD-80 PE and anti-CD23-APC antibodies accordingly (Table 2-6). To ensure specificity of binding, antibodies against surface markers restricted to polarized macrophages were applied to unpolarized macrophages. After washing with FACS washing buffer, cells were subjected to cytometric analysis on a BD FACSCalibur flow cytometer. The data were analyzed using FlowJo v. 7.6.5.

2.2.6.2 Fluorescence activated cell sorting (FACS) of murine lung macrophages

2.2.6.2.1 Antibody labelling of murine macrophages

Prior to staining, cells were filtered through a 30 µm MACS pre-separation filter. For antibody staining, a solution of 1 x 10^6 cells per 100 µl MACS buffer was created, and 1µl of Mouse Fc Block per 100 µl was added. Cells were then stained with 1 µl of antibody per 100 µl solution in the dark at 4 °C for 25 min (Table 2-5). Single fluorochrome stains and appropriate isotype controls were included.

2.2.6.2.2 Cytometric isolation of murine macrophages

All FACS experiments were performed at the flow cytometry core facility Marburg. Cells were subjected to sorting at a concentration of up to 2 x 10^7/ml on a FACS Aria III cell sorter. Cells were sorted at a maximal rate of 3000 events/second through a 85 µm nozzle into a vessel pre-coated with FCS. After sorting, cells were immediately centrifuged at 500 x g and 4 °C for 10 minutes, lysed with Isol RNA Lysis Reagent and frozen at -20 °C.

2.2.7 The murine model of eosinophilic airway inflammation

The mice used for this project were purchased from Harlan Laboratories and kept under standardized conditions. A 12 hours dark/light rhythm, an ambient temperature of 20-24 °C and an air humidity of 50-60 % were maintained. Mice were housed in individually ventilated Type II L cages (IVC) providing food and water *ad libitum*. For all experiments, 9 weeks old female BALB/c mice were used. All studies were approved by the appropriate authorities according to German legal requirements (Tierversuchsantrag V54-19c 20-15 (1) MR 20/13 Nr. 21/2010)

2.2.7.1 Induction of experimental allergic airway inflammation

Sensitization of mice to allergen was achieved by intraperitoneal (i.p.) administration of OVA-$Al(OH)_3$ compound on day 0, 14 and 21. Each time, 10 µg OVA and 2.8 mg $Al(OH)_3$ were given per mouse in a PBS solution. For the induction of asthma, 5 ml of a 1 % (w/v) OVA/PBS solution were vaporized with a Master Nebulizer over a period of 20 min. Mice were subjected to simultaneous group aerosol challenge on day 26, 27 and 28. Induction of

experimental allergic airway inflammation was routinely performed by the Department of Clinical Chemistry, Philipps University Marburg.

2.2.7.2 Preparation of murine alveolar and interstitial macrophages

Mice with acute eosinophilic airway inflammation and healthy control animals were sacrificed at 48 h past last challenge by i.p. injection of 7.6 mg Ketamine/1.1 mg Rompun/200 IU Heparin per animal. After median sternotomy, mice were tracheotomised with a permanent venous catheter, and bronchoalveolar lavage was performed. Two times 500 µl and four times 800 µl of BAL lavage solution were injected into the lung and re-aspirated carefully with a 1 ml syringe. Equal inflation and deflation of lung lobes was monitored to ensure coverage of all lung compartments. The BAL fluid was kept on ice. The aorta abdominalis and vena cava were severed, and the left atrium was punctured to allow drainage of blood from the lung. Lungs were perfused by cannulation of the right heart ventricle and pulsed application of 20 ml PBS until the lung was white. The lung was excised, minced in digestion buffer and incubated for 45 min at 37 °C and orbital shaking at 160 rpm. Further homogenization was achieved by forceful pulsed swirling of the homogenate using gentleMACS C tubes in a gentleMACS tissue homogenizer. Digestion was stopped by adding RPMI1640 complete medium. Cells were washed twice in complete medium at ambient temperature. If necessary, an erythrocyte lysis was performed by resuspending the cells in ultrapure water for 30 seconds. Lysis was stopped by addition of 15 ml PBS. Cells were then resuspended in ice-cold MACS buffer and incubated on ice for 15 min in preparation of antibody staining.

2.2.7.3 Validation of lung eosinophilia in allergic mice

Mice were sacrificed 48 h past challenge with aerosolized OVA. The extent of lung eosinophilia was monitored by quantification of eosinophils in the BAL fluid of healthy and asthmatic mice by FACS during the sorting procedure (section 2.2.6.2).

2.2.8 Statistical analyses of conventional experimental data

For comparison of two data columns, the two-tailed Student´s t Test was employed. For all tests, Gaussian distribution was assumed, and the confidence interval was set to 95 %.

2.2.8.1 Statistical analysis of high-throughput data

The data gained from Taqman low density arrays and Illumina HT12 BeadChip arrays required extensive correlation studies and statistical correction for large sample sizes. These advanced analyses were carried out by Dr. Annalisa Marsico, assisted by Dr. Brian Caffrey, Max Planck Institute for Molecular Genetics, Berlin.

The analysis of all 9 Illumina HT12 Beadchip Arrays was carried out with the *lumi* R Bioconductor Package, which is especially designed to process Illumina microarray data. After background correction, the variance stabilization and normalization procedure from the *vsn* R package was applied. This simultaneous normalization of intensities and variance stabilization transformation corrects for the fact that the variance of array replicates is not independent from the mean signal intensity, but increases at higher intensities. Differentially expressed genes were identified by means of a moderate t-test (R limma package), including Benjamin-Hochberg Correction for multiple testing. Genes with an adjusted p-value < 0.1 and a linear fold change > 1.5 were considered differentially expressed.

For interpretation of the TLDA analyses, the HTqPCR R package was used. All miRNAs with little or no variation among samples were removed prior to testing for differential expression. For each miRNA, the inter-quantile range among samples (IQR) was calculated, and miRNAs with an expression level of IQR < 1.2 were not considered for further analysis. The ΔΔCt model was used for quantification of differential expression. Statistical significance of miRNA differential expression was assessed by means of a moderate t-test. By converting the Ct values to a logarithmic scale ($\log_2$ transformation), miRNAs with a $|\Delta\Delta Ct| > 1$ (fold change of 2) and a p-value < 0.1 were considered differentially expressed.

In order to identify functional miRNA targets and reduce as much as possible the number of false positives an adjusted ranking score for prediction of microRNA and mRNA interaction was employed. The adjusted score was computed using the formula

$$SCORE_{adj} = A + bB + cC + d(1 - D) + eE + f_1F_1 + f_2F_2 + ... + f_n F_n$$

This formula integrates the following parameters:

- miRSVR (miRanda) prediction score (A) [107]
- positive target prediction by both miRanda and TargetScan [108] (B)
- conservation across species (C)
- Todorovski distance of miRNA and mRNA expression data (D)
- Published experimental validation (E)
- Number of miRNA binding sites in the mRNA 3´UTR (F_n)

Each factor is weighted by a negative coefficient (b, c, d, e, f_n).

Expression values of mRNA and miRNA are given as log_2 of linear expression data. This transformation corrects for high absolute standard deviation of highly expressed targets, and it allows treating the data set as Gaussian, which is a prerequisite for the Student´s t-test.

2.2.8.2 Principal Component Analysis

Prerequisites

In order to visually represent the global sample variation within the mRNA and miRNA array experiments, a principal component analysis (PCA) was performed.

Log_2-transformed expression data of genes or dCt values of miRNAs that were determined to be subject to significant regulation after treatment were provided by in-depths bioinformatic analyses (section 2.2.8.1). Prior to extraction of the first principal components of each dataset, a test on sampling adequacy was performed to ensure eligibility of the data for subsequent analyses. The Kaiser Meyer Olkin (KMO) Criterion was calculated on the basis of each data matrix, here exemplarily termed “transcriptome”. The “paf” command was retrieved from the R package *rela*.

paf(transcriptome)$KMO

The KMO is an index value between 0 and 1 for measuring the suitability of the attributes to be involved in PCA, higher values being better. The KMO takes into account the inter-sample

correlation and is computed on the basis of a correlation matrix. A value > 0.8 indicates low partial correlation between the samples, while a value > 0.6 is considered acceptable [109]. Such uncorrelated or weakly correlated samples are a prerequisite for PCA.

Furthermore, the following R command was used to run a measure of sampling adequacy (MSA):

paf(transcriptome)$MSA

While the KMO provides a single index number to characterize the dataset, the MSA returns an individual value for each sample that describes its eligibility for a factor analysis. Like the KMO, the MSA takes a value of 1 for uncorrelated values and declines as a reciprocal function of partial sample correlation. Value interpretation is analogous to the KMO (see above).

Principal Component Analysis

A principal component analysis reduces a high-dimensional dataset by summarizing variables and expressing them as a single composite numeric value, i.e. a principal component. Once the first principal component has been fit to the data, the following principal components are incrementally added to the first one at orthogonal axes along the directions of maximum variance in the data. Each principal component is an eigenvector of the covariance matrix that is computed on the basis of the original data. Once every eigenvector has been added, the orthogonal body of eigenvectors is rotated to optimize the fitting of all principal components to the variables in the dataset. The principal components with the highest explanatory power, i.e. representing the directions of maximum variation, can then be extracted to represent the original dataset with both reduced complexity and highest possible fidelity.

A principal component analysis was performed on the mRNA and miRNA array data using the “prcomp” R command. It z-transforms and rotates the data matrix and returns an object (“pca”) that contains the list of eigenvectors computed from the covariance matrix (i.e. the principal components).

pca ← prcomp(transcriptome, center = TRUE, scale= TRUE)

For a graphic representation, the first principal components (i.e. those with the highest explanatory power) were selected in order to achieve an explained variance > 95 %. The percentage of explained variance that was contributed by each principal component, i.e. the factor loading, was calculated as the ratio of the respective cumulative sum of variance (the standard deviation squared) and the sum of total variance.

var ← pca$sdev^2

cumsum ← cumsum(var)/sum(var)

The result identified the explanatory power of the first three principal components to be sufficient, as it amounted to > 95 % of total variance. A 3D cube was used for graphic representation. The “plot3d” and “spheres3d” commands were retrieved from the R package *rgl*.

plot3d(pca$rotation[,1:3], xlab = "x")

Color and shape were given to the data points by

spheres3d(pca$rotation[,1:3], radius=0.02, col=c("red", "red", "red", "blue", "blue", "blue", "darkgreen", "darkgreen", "darkgreen"))

3 Results

3.1 Monocyte isolation from donor samples

This study aimed at creating a comprehensive molecular background of macrophage polarization. As polarization profoundly influences macrophage biology and determines macrophage function in health and disease, a better understanding of the underlying mechanisms is needed. Here, the focus was set on exploring miRNA/mRNA co-dependency. In order to establish a concept of macrophage polarization that closely mimics the physiologic conditions, primary human monocytes were used instead of a cell line. These monocytes were isolated from donor buffy coats by positive magnetic selection for CD14. Prior to seeding, the purity of freshly isolated monocytes was routinely assessed by flow cytometry and reliably determined to be approximately 90 % of total cells as shown by CD14 staining (Fig. 3-1).

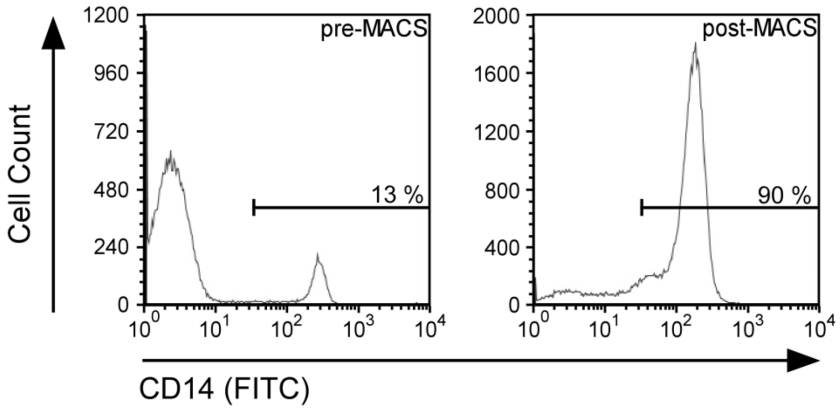

Figure 3-1: Purity of isolated monocytes by flow cytometry. Positive selection efficiency after magnetic activated cell sorting (MACS) was validated by subjecting isolated $CD14^+$ monocytes from the peripheral blood mononuclear cell (PBMC) fraction to flow cytometry. 50.000 cells were routinely counted after staining with CD14 FITC antibody, and the percentage of $CD14^+$ cells was determined with FlowJo 7.6.5.

3.2 Macrophage polarization assessment

3.2.1 Western Blot analysis shows activation of key macrophage effector molecules

A key requirement for the systemic analysis of macrophage polarization is a valid set of control parameters, both descriptive and functional, that can be used to test the cellular

response to the given stimulus. As the signalling cascades that are activated upon polarization are well established (see section 1.2), first assessment of the polarization efficiency was conducted by monitoring the activation of effector molecules of the MAPK cascades, the JAK/STAT pathway and the NFκB pathway (Fig. 3-2 and 3-3).

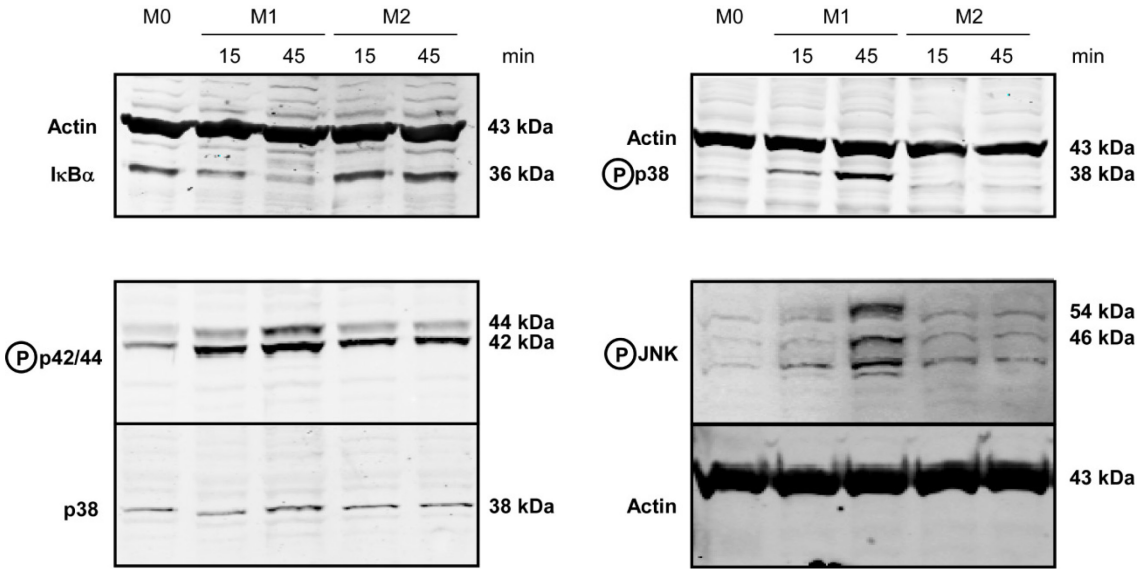

Figure 3-2: Western Blot analysis of signalling pathways in M1 macrophages. Macrophages were stimulated as indicated (M1: IFNγ (20 ng/ml) + LPS (100 ng/ml); M2: IL4 (20 ng/ml) + IL13 (20 ng/ml)) and lysed after 15 or 45 minutes in western blot lysis buffer. From each sample, 80 µg of protein were loaded and transferred to a nitrocellulose membrane by wet blot. Changes in the phosphorylation state were visualized by phospho-specific antibodies, while total protein amount was determined by pan – antibodies. Degradation of IκBα or phosphorylation of p38, p42/44 and JNK are indicative of M1 signalling pathway activation. Actin and p38 were used as loading control, respectively. One representative replicate of three is shown. Image acquisition was done on an Odyssey Infrared Imager.

Short term activation of macrophages with the M1 stimulus for 15 and 45 minutes yielded a time dependent phosphorylation and thereby activation of p42/44, p38 and JNK, and a degradation of IκBα, which is in accordance with the canonical signalling as outlined (see section 1.2.1) Phosphorylated p42/44 (ERK2 and ERK1) yielded a double band at 42 and 44 kDa, respectively, the 44 kDa band (ERK1) being a more specific marker for M1 stimulation. Phosphorylated JNK was detected at 46 kDa (p46 SAPK/JNK) and 54 kDa (p54 SAPK/JNK). A third band of unknown origin was routinely detected below 46 kDa. The observed activation of pro-inflammatory signalling was absent from cells polarized with the M2 stimulus. In order to test whether macrophages respond to the provided M2 cytokine exposure, STAT6 was assayed for phosphorylation (Fig. 3-3)

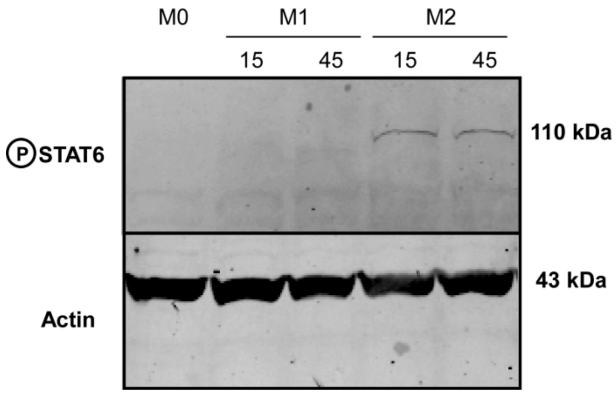

Figure 3-3: Western Blot analysis of the primary signalling pathway in M2 macrophages. Macrophages were stimulated as indicated (M1: IFNγ (20 ng/ml) + LPS (100 ng/ml); M2: IL4 (20 ng/ml) + IL13 (20 ng/ml)) and lysed after 15 or 45 minutes in western blot lysis buffer. From each sample, 80 µg of protein were loaded and transferred to a nitrocellulose membrane by wet blot. Changes in the phosphorylation state were visualized by phospho-specific antibodies, while total protein amount was determined by pan – antibodies. Phosphorylation of STAT6 is indicative of M2 signalling pathway activation. Actin was used as loading control. One representative replicate of three is shown. Image acquisition was done on an Odyssey Infrared Imager.

A weak yet specific signal revealed phosphorylation of STAT6, commonly observed in M2 macrophages. The activation profile of the stimulated macrophages as indicated by prototypical signalling pathways thus closely reflected the canonical pathway initiation patterns and served as an indicator of solid polarization quality.

3.2.2 Polarized macrophages have different bactericidal potential

In order to validate the polarization outcome on a functional level, macrophages were infected with the intracellular pathogen *Legionella pneumophila* strain Corby. Phagocytosis efficiency and intracellular killing was measured by colony forming unit (CFU) assays. The retrieved bacterial units after indicated incubation times are shown (Fig. 3-4). M1 polarized macrophages showed the highest uptake of bacteria as assessed 90 min post infection, while M2 cells showed the lowest. At 36 h post infection, clearance of bacteria was most prominent in M1 cells. In contrast, at 36 h post infection, M2 cells showed no significant difference of bacterial load in comparison to unpolarized M0 cells.

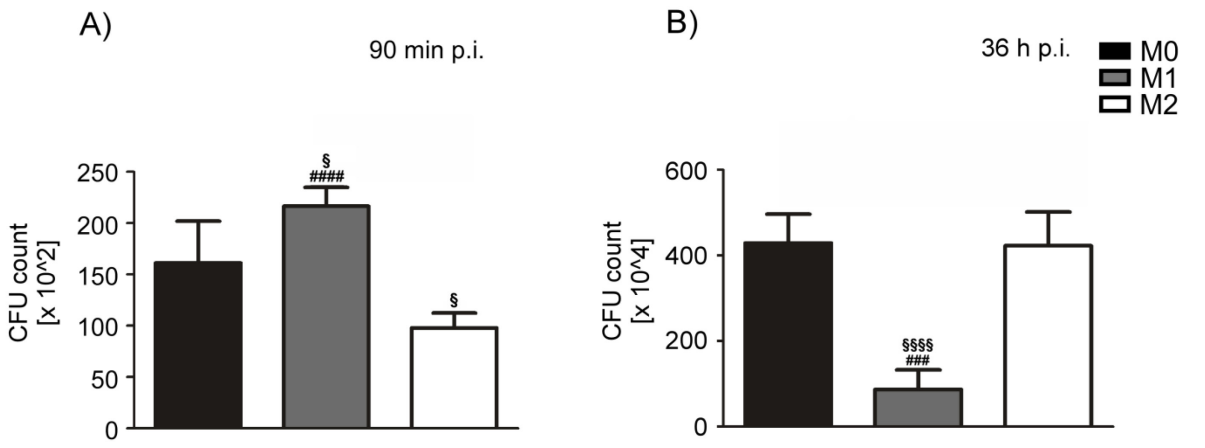

Figure 3-4: Uptake and elimination of *Legionella pneumophila* by polarized macrophages. Macrophages were polarized for 18 h (M1: IFNγ (20 ng/ml) + LPS (100 ng/ml); M2: IL4 (20 ng/ml) + IL13 (20 ng/ml)) or left un-polarized and then infected with *L. pneumophila* at a MOI of one. At 90 min and 36 h post infection, the cells were lysed by osmotic stress and rigorous pipetting, and the lysate was plated on BYCA agar plates. After three days, the bacterial colonies were counted. Phagocytotic (A) and bactericidal capacity (B) is markedly increased in M1-polarized macrophages as compared to M0 (§) and M2 (#) cells, while M2 cells show reduced uptake capacity vs. M0 (§) (A). Bars indicate mean and standard deviation. $^{§/\#}p< 0.05$; $^{§§§/\#\#\#}p<0.001$; $^{§§§§/\#\#\#\#}p<0.0001$ (n=3).

3.2.3 Cytometric analysis of polarized macrophages shows selective up-regulation of surface markers

The surface marker decoration of cells is both indicative of the cellular activation status and readily accessible to isolate specific cell types. Available transcriptome data on polarized macrophages [31] were screened for likely candidates. As the presence of a surface molecule can not necessarily be inferred by occurrence of transcript, putative markers were validated by flow cytometry. An investigation of the candidates led to dismissal of CCR7 and CD86 as putative M1 markers and of CD206 as a putative M2 marker, because their occurrence on the cell surface was irresponsive to the given stimuli (not shown). Further analysis revealed CD80 as an exclusive M1 marker and CD23 as an exclusive M2 marker (Fig. 3-5). While M1 treatment routinely led to the expression of CD80 by 80 - 90 % of the cells, only 50 % of cells treated with the M2 stimulus reacted by up-regulation of surface CD23. This required further purification to increase the percentage of $CD23^+$ cells for further analysis. To this end, cells stained with the CD23-APC antibody were magnetically labelled with anti-APC magnetic

beads and subjected to positive selection on an autoMACS Pro Separator. A prevalence of approximately 80 % of total cells expressing the respective marker after the appropriate stimulus and enrichment procedure was considered to be indicative of a homogenous polarization. In an effort to standardize, only samples that matched this criterion were considered stably polarized and eligible for subsequent RNA isolation and analysis.

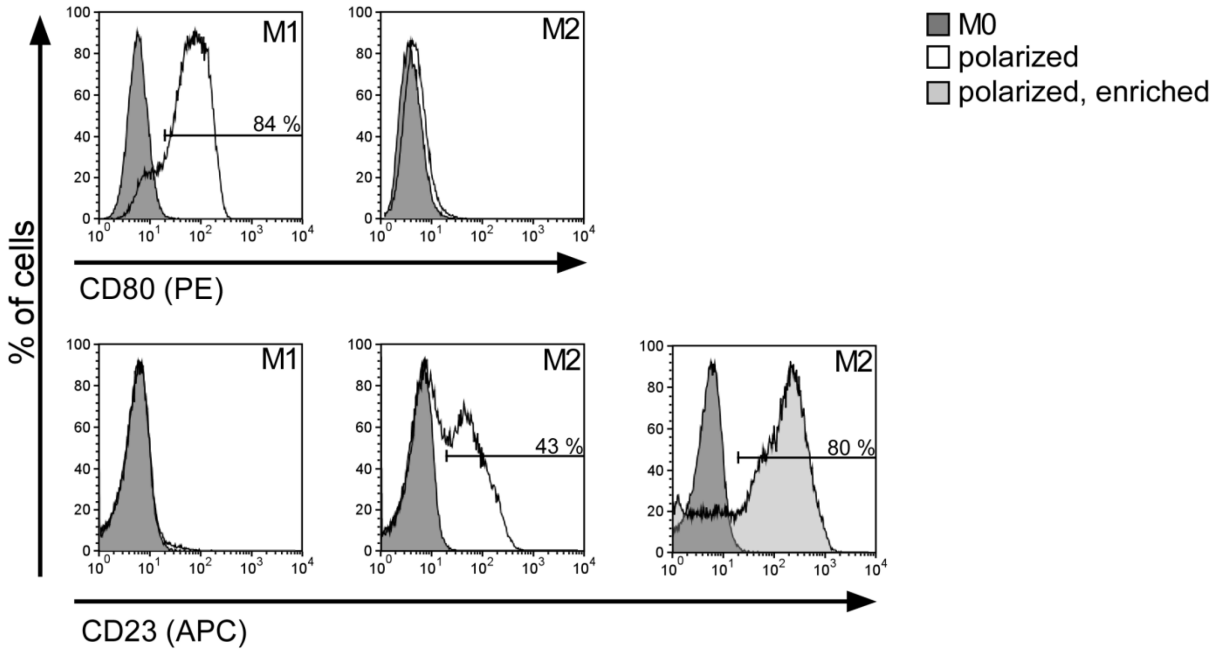

Figure 3-5: Surface marker expression of polarized macrophage subtypes. At 18 h after the polarization stimulus (M1: IFNγ (20 ng/ml) + LPS (100 ng/ml); M2: IL4 (20 ng/ml) + IL13 (20 ng/ml)) the cells were subjected to cytometric analysis. The type of polarization is indicated in the top right corner of each panel. CD80 and CD23 were determined to be specific for M1 and M2, respectively. M2-polarized CD23-stained macrophages were further enriched by anti-APC magnetic bead positive selection to meet the purity standard for subsequent RNA analysis. 50.000 cells were routinely counted after simultaneous staining with CD80 and CD23 antibody. One representative replicate of three is shown. The percentage of positive cells was determined with FlowJo 7.6.5.

3.3 Systemic profiling of macrophage subtypes reveals profound changes on the RNA level

3.3.1 Quality assessment of isolated RNA

In preparation of global RNA profiling, RNA quality from three independent biological replicates of validated and enriched polarized and unpolarized macrophages was determined by capillary gel electrophoresis on an Agilent 2100 Bioanalyzer. RNA integrity was computed from the 28s and 18s rRNA signals, and deviation from their usual ratio (2.1:1) served as an indicator of global RNA degradation. Electropherograms with RNA integrity numbers (RIN, underlined) are shown for each sample (Fig. 3-6). According to the manufacturer, a RIN of 10 reflects perfect RNA quality, while a RIN of 5 means partial degradation. Based on this guideline, RINs > 8 were considered to indicate RNA quality sufficient for further analysis [110].

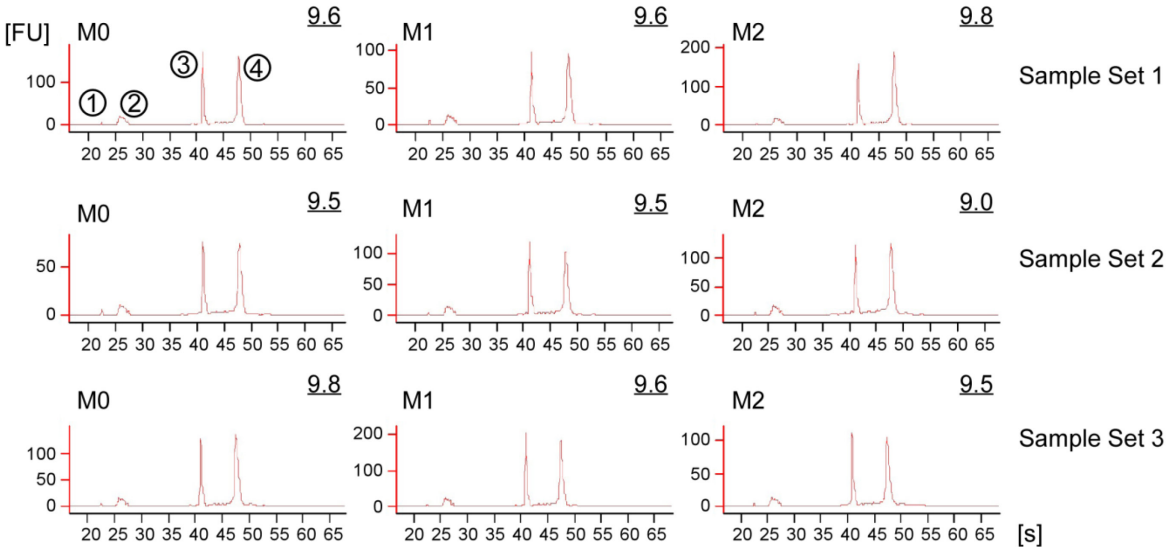

Figure 3-6: Electropherograms of total RNA isolated from three independent biological replicates of polarized macrophages. 25 – 50 ng of RNA isolated from three different donors (sample set 1 – 3) were analyzed by capillary gel electrophoresis on an Agilent 2100 Bioanalyzer. The respective polarization treatment is indicated in the top left corner of each panel (M1: IFNγ (20 ng/ml) + LPS (100 ng/ml); M2: IL4 (20 ng/ml) + IL13 (20 ng/ml)). Fluorescence units (FU) peaked when RNA was detected during the 65 second (s) run time. Underlined figures in the top right corner of each panel represent the RNA integrity number (RIN), which is deduced from the ratio of 18s and 28s rRNA. Peak ①: Marker; Peak ②: small RNA; Peak ③: 18s rRNA; Peak ④: 28s rRNA.

3.3.2 mRNA analysis identifies characteristic patterns of polarization phenotypes

mRNA analysis of polarized and unpolarized macrophages was performed on Illumina HT12 BeadChip Arrays. In a first approach, 1269 genes were found to be up-regulated in response to the polarization stimulus, and 1361 genes were determined to be down-regulated.

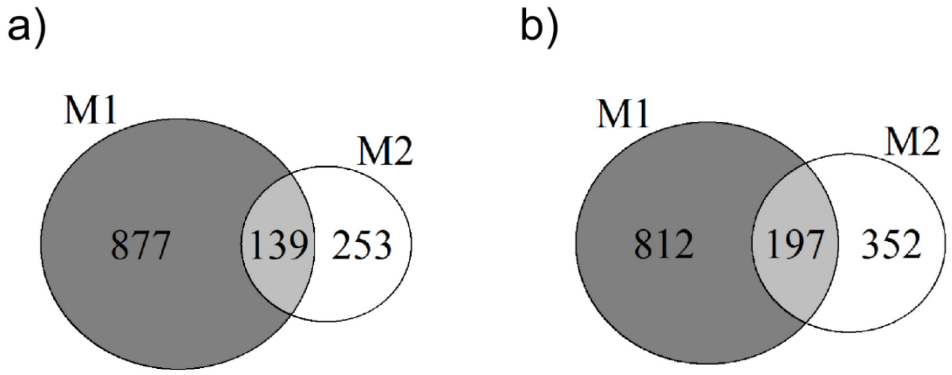

Figure 3-7: Logical relations of mRNA expression in the three distinct subsets of macrophages. The number of genes that were found to be up-regulated (a) or down-regulated (b) in polarized macrophages (M1: IFNγ (20 ng/ml) + LPS (100 ng/ml); M2: IL4 (20 ng/ml) + IL13 (20 ng/ml)) in comparison to M0 cells is shown. Genes with a linear fold change > 2 and an adjusted p value of < 0.1 were included.

The magnitude of transcriptional response that each polarization subtype exerted upon stimulus is displayed (Fig. 3-7). Of note, the stimulus' impact on the transcriptome is markedly stronger in M1-polarized cells as compared to their M2 counterpart**.** This is in accordance with the concept of M1 macrophages being considerably more active in terms of gene regulation as compared to M2 macrophages (section 1.2.3)

The samples were correlated and a heatmap was generated, indicating up- and down-regulation of transcript as a function of macrophage polarization status (Fig. 3-8). The data were considered to be in good agreement with previous transcriptome data [31], which was a further confirmation of the solidity of polarization. As shown above (Fig. 3-7), the comparatively weak response of M2 polarized macrophages to the stimulus as compared to M1 polarized macrophages is reflected in the heatmap.

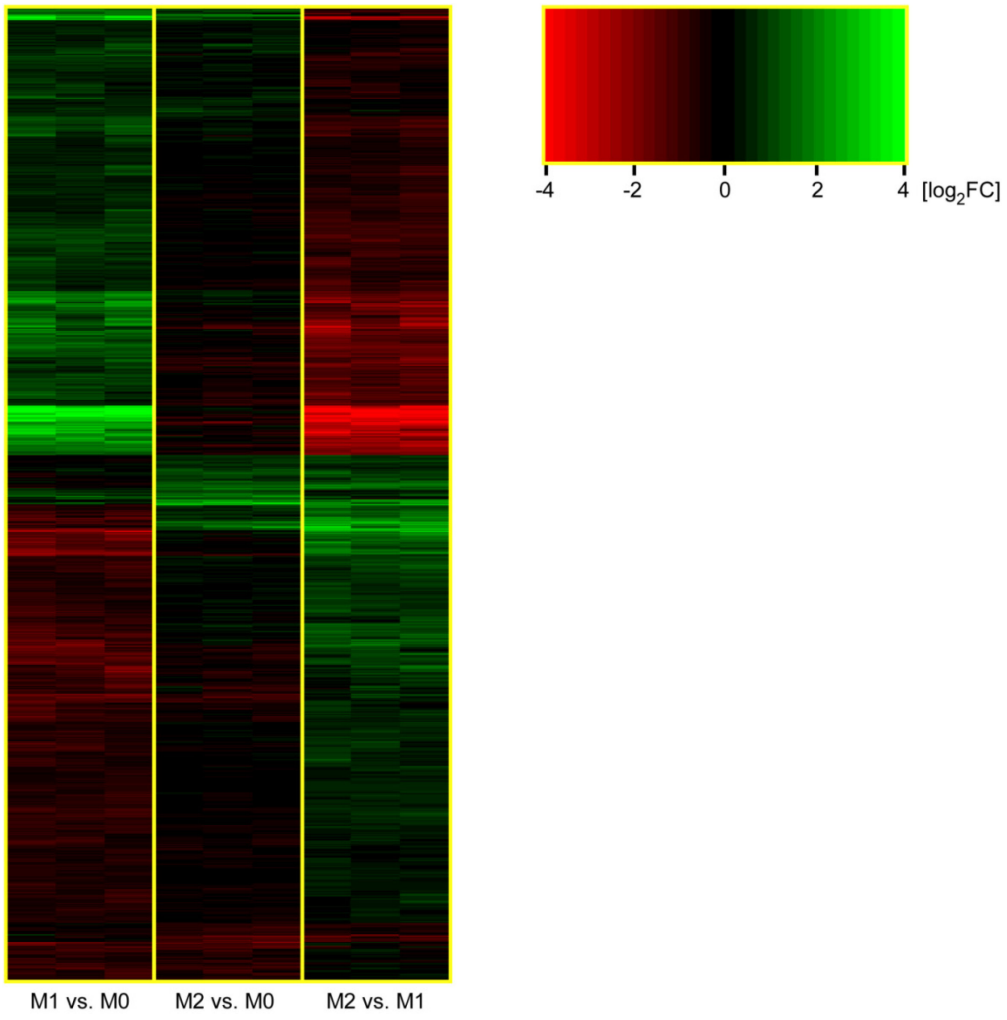

Figure 3-8: mRNA profiling of polarized macrophages on an Illumina HT12 Beadchip Array. 1 µg of total RNA from polarized (M1: IFNγ (20 ng/ml) + LPS (100 ng/ml); M2: IL4 (20 ng/ml) + IL13 (20 ng/ml)) or un-polarized macrophages was used for hybridization. 2119 differentially regulated genes were chosen for display on the basis of a $-\Delta\Delta Ct > 0.58$ and a p-value < 0.1 across 3 biological replicates. The magnitude of regulation is expressed as $\log_2$-transformed fold-change, quantile-normalized, background-corrected expression data. For graphic representation, expression values beyond -4 and +4 $\log_2$ fold change were truncated and set to -4 and +4, respectively.

In order to visualize the mRNA similarities and differences of the polarized and un-polarized macrophage subtypes, differentially regulated genes were extracted from the total expression data, yielding a high-dimensional matrix of 2119 genes x 9 individual samples. To reduce the complexity of these data to a visually accessible level, a principal component analysis (PCA, section 2.2.8.2) was performed (Fig. 3-9). The data were found to be eligible for PCA as they showed a Kaiser Meyer Olkin (KMO) criterion of 0.88 and individual measure of sampling adequacy (MSA) values of > 0.85. The overall sample variance was allocated to the first three principal components (i.e. the three eigenvectors of the co-variance matrix with the highest

eigenvalues). Principal component 1 (PC1) accounts for 83.91 %, PC2 for 11.93 % and PC3 for 2.33 % of overall data set variance. The unbiased allocation of all differentially regulated genes showed a clear clustering of the respective polarization subtypes.

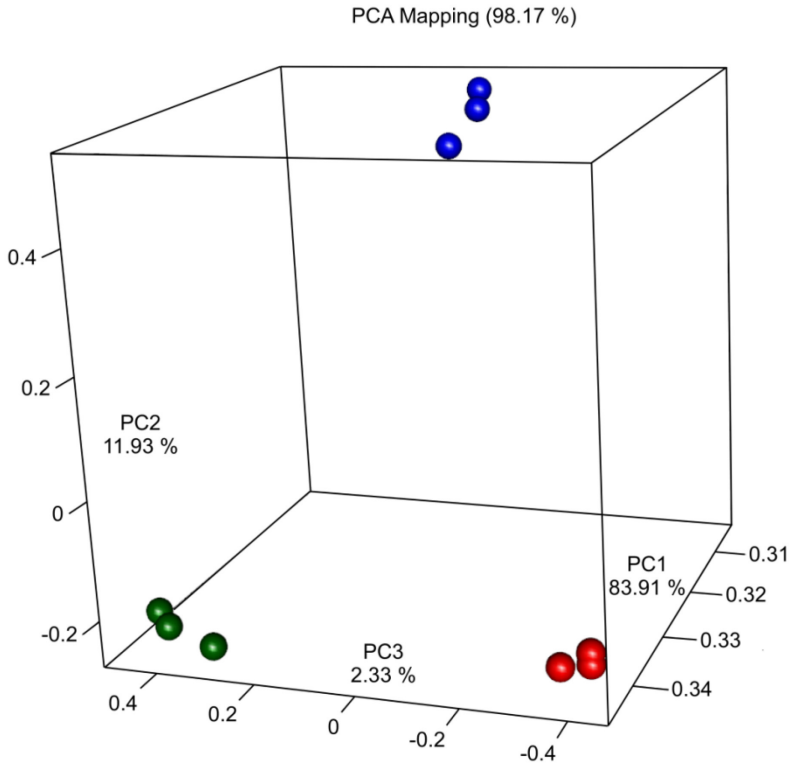

Figure 3-9: Principal component analysis of global mRNA expression data of M0, M1 and M2 macrophages. The log_2-transformed fold-change, quantile-normalized, background-corrected expression data of 2119 genes that were found to be regulated in response to polarization treatment (M1: IFNγ (20 ng/ml) + LPS (100 ng/ml); M2: IL4 (20 ng/ml) + IL13 (20 ng/ml)) was included in the calculation. By using the first three principal components, the explained variance (PCA Mapping) amounted to 98.17 %. Red: M0; blue: M1; green: M2

The identities and regulation of chosen genes out of this data set which were considered to be of particular interest for M1 macrophage activation (Fig. 3-10) and M2 macrophage activation (Fig. 3-11) are shown. In addition, the top 50 regulated genes as ranked by log_2 fold expression vs. M0 are provided for each subtype (Appendix).

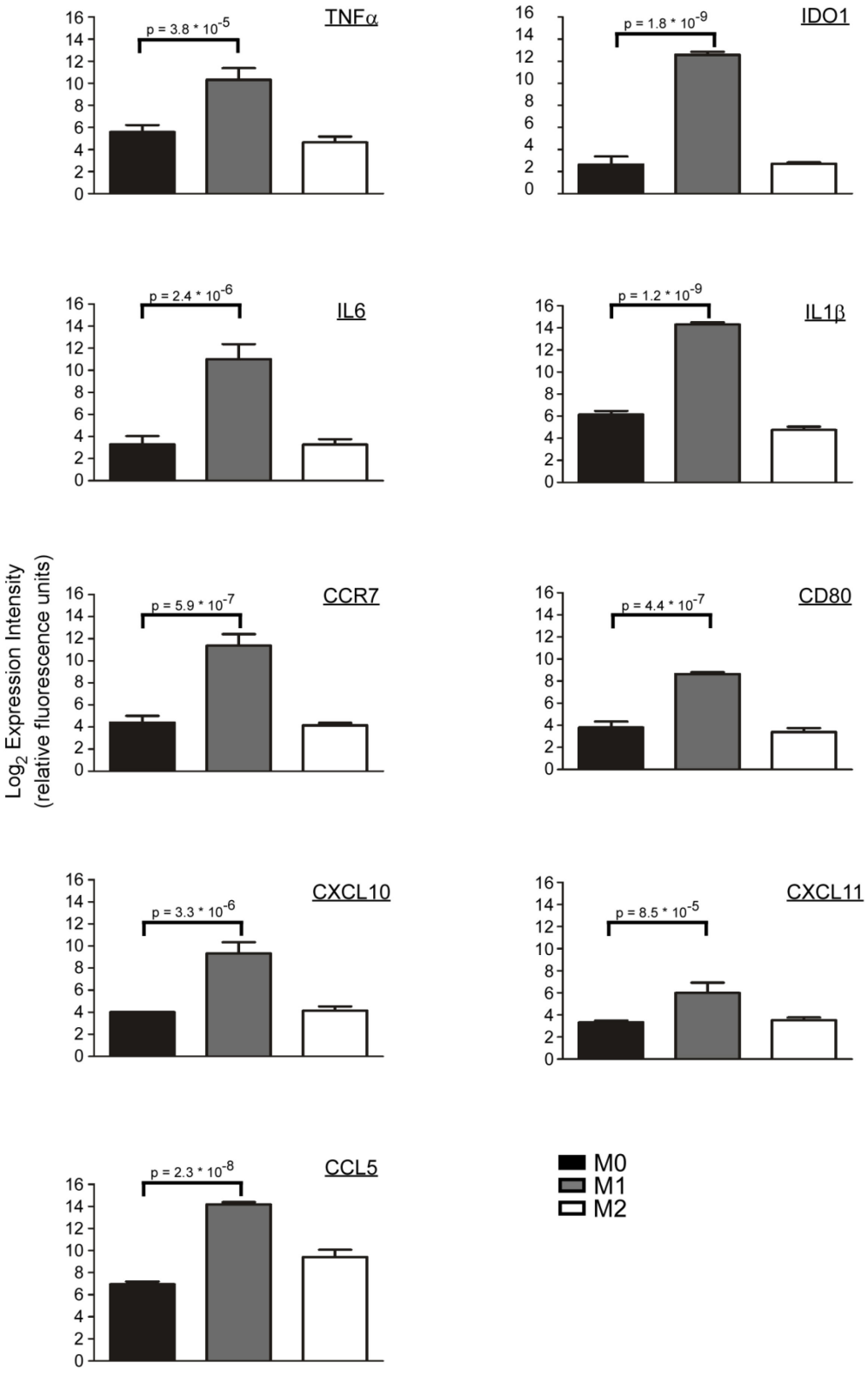

Figure 3-10: Expression levels of hallmark M1 associated genes upon polarization. Macrophages were polarized (M1: IFNγ (20 ng/ml) + LPS (100 ng/ml); M2: IL4 (20 ng/ml) + IL13 (20 ng/ml)) or left un-polarized (M0). Global gene expression levels were determined by Illumina HT12 Beadchip Array. Log_2-transformed, quantile-normalized, background-corrected expression data are shown. Hallmark M1 genes with significant regulation between the subtypes were selected. Bars represent the mean and standard deviation (n = 3).

IL-6, TNFα and IL1β are very potent cytokines which propagate pro-inflammatory activation by paracrine or autocrine signalling. CXCL10 (IP-10), CXCL11 (I-TAC) are C-X-C chemokines that belong to the ELR^- subclass, while CCL5 (RANTES) is a C-C motif chemokine. They attract T_H1-activated T cells via CCR3 (CXCL10 and CXCL11) and CCR1, CCR3 and CCR5 (CCL5). The cell surface molecule CD80 is also involved in interaction with T cells, as it binds co-stimulatory molecules such as CD28 or CTLA-4. C-C motif chemokine receptor 7 (CCR7), the receptor for CCL19 and CCL21, has been shown to be not functional on human blood derived macrophages and not inducible by pro-inflammatory treatment (Prostaglandin E2, PGE2) on the protein level [111]. Nonetheless, it is an established mRNA marker of M1-polarized macrophages [112]. Indoleamine-2,3-dioxygenase1 (IDO1) has on the one hand been described to be induced by IFNγ [113], and on the other hand it has been suggested to be involved in immunosuppression by starvation due to breakdown of the essential amino acid tryptophan [114]. In summary, this highlights both the supporting nature of M1 polarized macrophages in a T_H1-skewed inflammatory microenvironment and the concomitant activation of regulatory mechanisms.

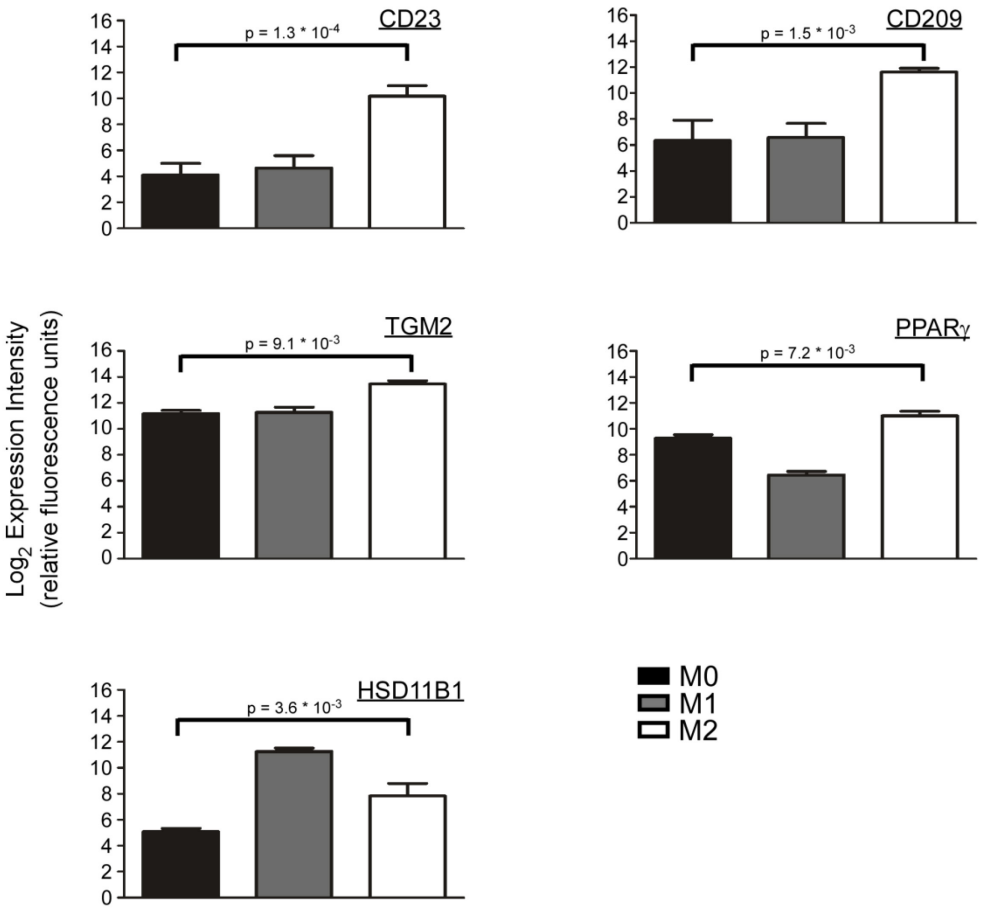

Figure 3-11: Expression levels of hallmark M2 associated genes upon polarization. Macrophages were polarized (M1: IFNγ (20 ng/ml) + LPS (100 ng/ml); M2: IL4 (20 ng/ml) + IL13 (20 ng/ml)) or left un-polarized (M0). Global gene expression levels were determined by Illumina HT12 Beadchip Array. Log_2-transformed, quantile-normalized, background-corrected expression data are shown. Hallmark M2 genes with significant regulation between the subtypes were selected. Bars represent the mean and standard deviation (n = 3).

The transcriptome analysis of the M2 polarized macrophages revealed CD23 as the most prominently up-regulated transcript (Fig. 3-11). Correspondingly, the CD23 surface protein served as the M2 specific surface marker in this study. Furthermore, CD209 (DC-SIGN) was strongly up-regulated. CD23 and DC-SIGN have been shown to form a cluster on chromosome 19p13 [115] and to be inducible by IL4 [116]. Up-regulated genes with a known role in alternatively activated macrophage biology furthermore included 11β-Hydroxysteroid Reductase Type 1 (HSD11B1) and Peroxysome Proliferator-Activated Receptor-γ (PPARγ), which have been shown to cooperate in alternative macrophage activation [117]. Briefly, PPARγ induces HSD11B1 on the transcript level. HSD11B1 has been described to be up-regulated in human macrophages that were activated by LPS and by IL-4. This bimodal way

of induction is reflected here, as HSD11B1 is up-regulated in both M1 and M2 polarized macrophages.

Recently, transglutaminase 2 (TGM2) has been found to be the only consistent and functional M2 marker upon IL-4 stimulation on mRNA and protein level in a comparative study of human and mouse [118]. It has been implicated in a plethora of processes, such as fibrosis, wound healing and apoptosis [119], all of which are closely linked to alternative macrophage activation.

3.3.3 microRNA analysis identifies characteristic patterns of polarization phenotypes

In order to correlate changes in mRNA expression to changes in miRNA expression, Taqman low density arrays (TLDA) were performed (section 2.2.2.3), using the same RNA samples. The data were analysed according to the workflow applied for the mRNA (Fig. 3-7 – 3-9). As shown for the mRNA data (Fig. 3-7), M1 macrophages show a higher degree of subtype-specific miRNA regulation as compared to M2 macrophages (Fig. 3-12).

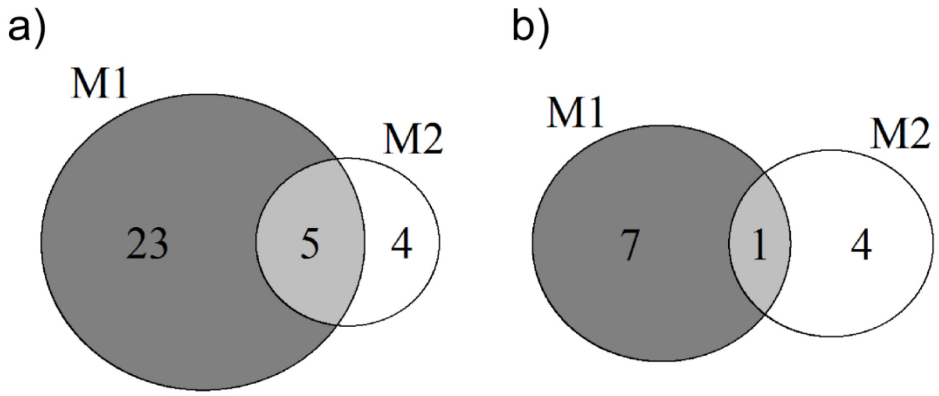

Figure 3-12: Logical relations of miRNA expression in the three distinct subsets of macrophages. The number of miRNAs that were found to be up-regulated (a) or down-regulated (b) in polarized macrophages (M1: IFNγ (20 ng/ml) + LPS (100 ng/ml); M2: IL4 (20 ng/ml) + IL13 (20 ng/ml)) in comparison to M0 cells is shown. In accordance with the mRNA profiling study, the stimulus' impact on the miRNA pattern is stronger in M1-polarized cells as compared to their M2 counterpart.

Data correlation yielded a heatmap indicating differential miRNA expression (Fig. 3-13).

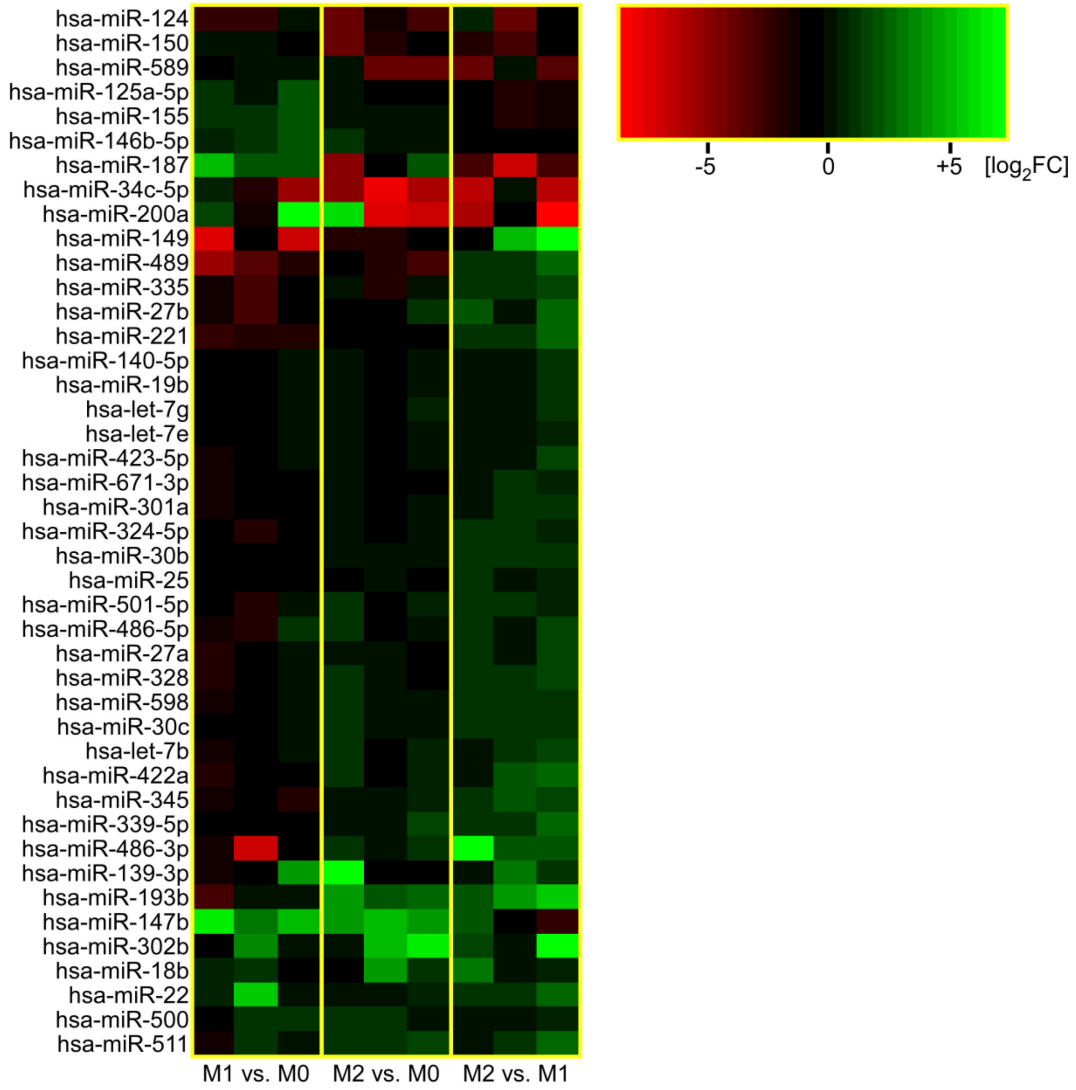

Figure 3-13: microRNA profiling of polarized macrophage subtypes. 350 – 1000 ng of total RNA from polarized (M1: IFNγ (20 ng/ml) + LPS (100 ng/ml); M2: IL4 (20 ng/ml) + IL13 (20 ng/ml)) or un-polarized macrophages was used for megaplex reverse transcription and amplification. 43 differentially regulated miRNAs were chosen for display on the basis of a $-\Delta\Delta Ct > 1$, a p-value < 0.1 across three biological replicates and an expression level of IQR (inter-quantile range) > 1.2. The magnitude of regulation is expressed as log_2-transformed fold change values as computed by the ΔΔCt method.

From these data, miRNAs were determined to be differentially expressed between the subtypes by the depicted level of confidence. Their log_2 transformed individual relative expression levels as compared to M0 are shown (Fig. 3-14).

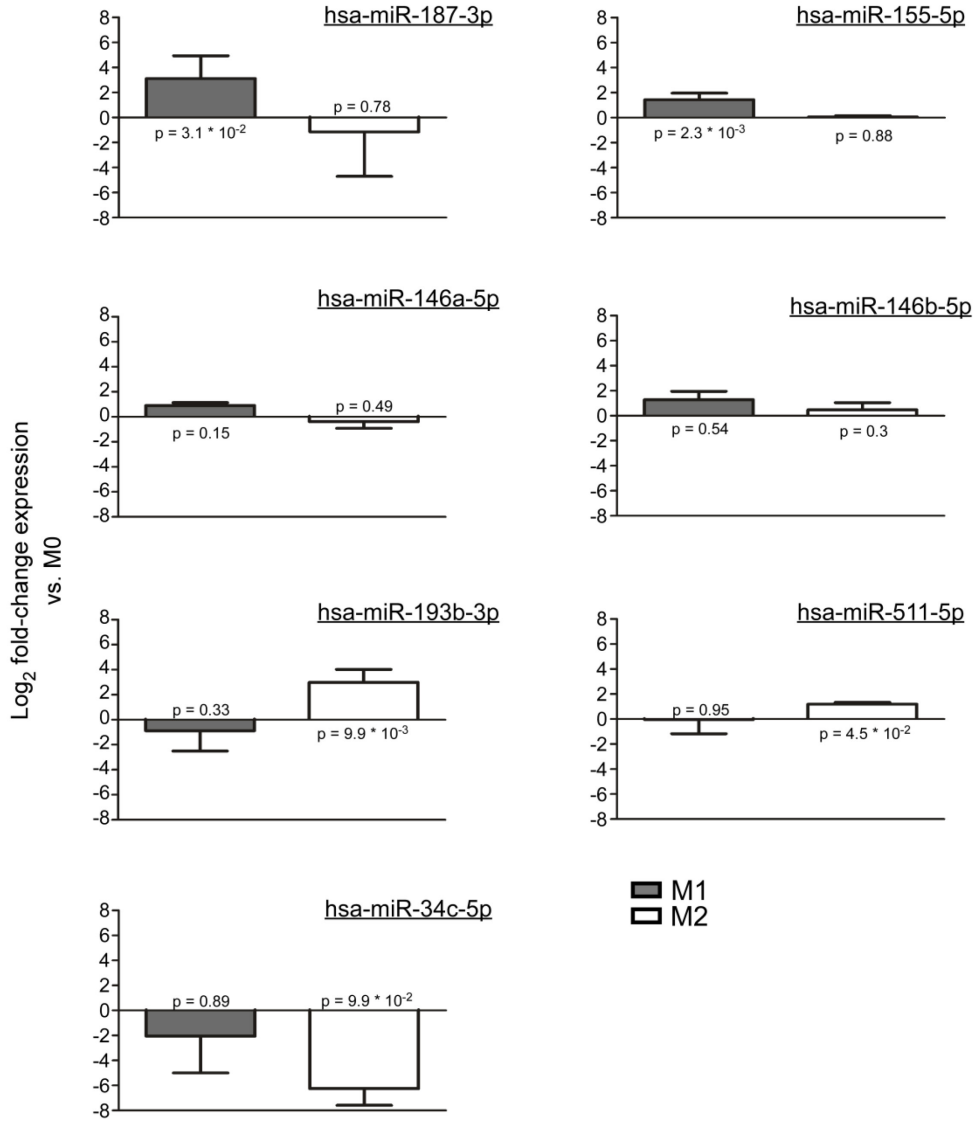

Figure 3-14: Selected miRNAs with a potentially subtype-specific expression pattern. Individual miRNAs that were found to be differentially regulated as a function of macrophage polarization (M1: IFNγ (20 ng/ml) + LPS (100 ng/ml); M2: IL4 (20 ng/ml) + IL13 (20 ng/ml)) were extracted from the miRNA screening experiments. The relative regulation as compared to the un-polarized M0 subtype is shown as log_2 transformed fold-change expression. Expression values were computed by the ΔΔCt method. p-values as adjusted for multiple testing are indicated (n=3).

As above (Fig. 3-9), a principal component analysis of these 43 miRNAs was performed in order to visually illustrate the degree of similarity or differences in miRNA expression between the individual samples (Fig. 3-15). The data were found to be eligible to PCA, showing a KMO criterion of 0.89 and individual MSA values of > 0.85.

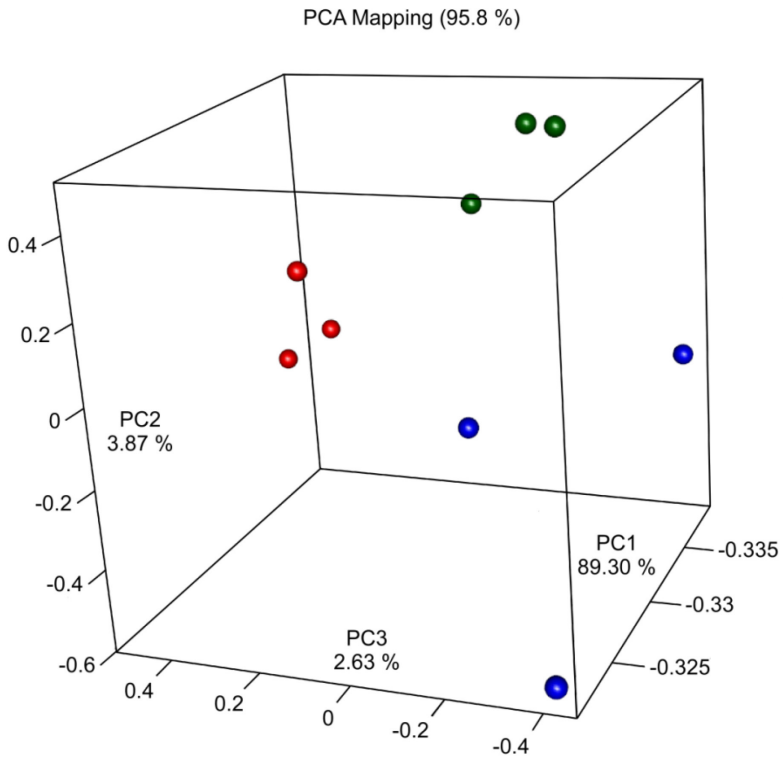

Figure 3-15: Principal component analysis of miRNA expression data. The ΔCt values of 43 miRNAs that were determined to be regulated in response to polarization treatment (M1: IFNγ (20 ng/ml) + LPS (100 ng/ml); M2: IL4 (20 ng/ml) + IL13 (20 ng/ml)) were included. By using the first three principal components, the explained variance (PCA Mapping) amounted to 95.8 %. Red: M0; blue: M1; green: M2

It is noteworthy that while sample fidelity across three biological replicates was high in the mRNA arrays and the polarization subtypes were clearly distinct (Fig. 3-9), the intra-group variance turned out to be higher in the miRNA arrays. This stressed the necessity of individual validation of miRNAs by quantitative PCR.

3.3.4 Individual validation corroborates differentially regulated microRNAs

A chosen set of miRNAs that were shown to be significantly regulated in a subtype-specific way by TLDA were individually validated by qPCR in an additional biologically independent sample. hsa-miR-146a-5p, hsa-miR146b-5p, hsa-miR-155-5p and hsa-miR-187-3p (M1, Fig.

3-16) as well as hsa-miR-193b-3p and hsa-miR-511-5p (M2, Fig. 3-17) were all confirmed to be up-regulated in the corresponding subtype as suggested by TLDA results. Due to differences in methodology and analysis, these expression data were not combined with the TLDA data. No statistics were performed, as these validation experiments were not performed in biological replicates. p-values from the TLDA experiments were as indicated (Fig. 3-14). While the TLDA results were log_2 transformed and analyzed accordingly, the linear fold change is used here (Fig 3-16 to 3-18).

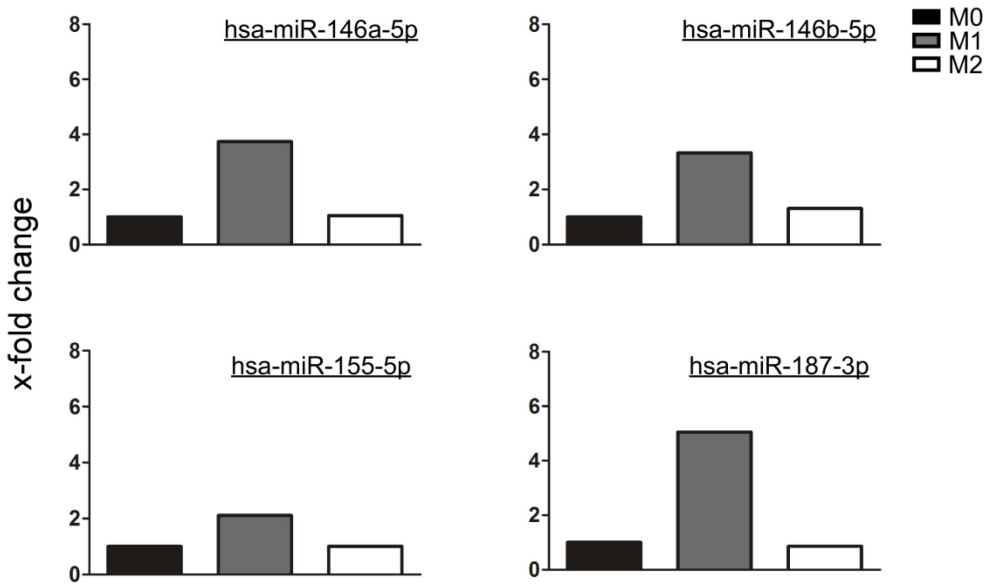

Figure 3-16: Validation of miRNA expression in M1 macrophages. Verification of miRNAs that were found to be significantly regulated in the TLDA experiments upon M1 polarization (IFNγ (20 ng/ml) + LPS (100 ng/ml)). An independent biological replicate was investigated. Differential methodology as compared to the TLDA analyses precluded an integration of these data into the TLDA results, so no statistics were performed due to the solitary nature of the data (n=1).

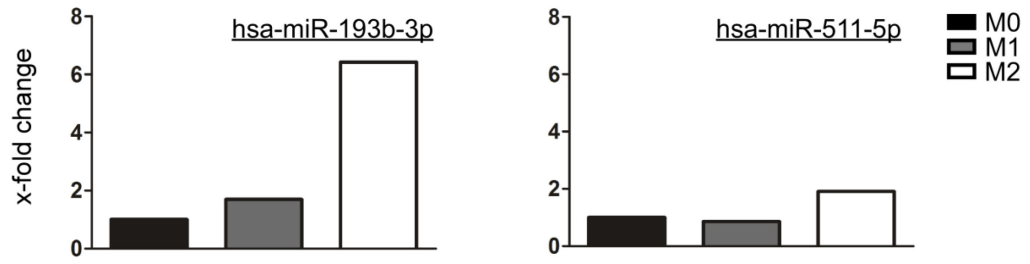

Figure 3-17: Validation of miRNA expression in M2 macrophages. Verification of miRNAs that were found to be significantly regulated in the TLDA experiments upon M2 polarization (IL4 (20 ng/ml) + IL13 (20 ng/ml)). An independent biological replicate was investigated. Differential methodology as compared to the TLDA analyses precluded an integration of these data into the TLDA results, so no statistics were performed due to the solitary nature of the data (n=1).

Of note, hsa-miR-511-5p is harboured in the MRC1/MRC1L1 gene in intron 5 [120]. MRC1L1 mRNA is significantly up-regulated in the M2 condition (Appendix and Fig. 3-19), and the magnitude of regulation matches that of hsa-miR-511-5p. The question whether MRC1 and MRC1L1 are two separate genes or not and whether they are subject to regulation by hsa-miR-511-5p will be discussed later (section 4.2).

In contrast to the aforementioned candidates, hsa-miR-34c-5p turned out to be regulated in a very volatile way. As this miRNA was almost undetectable and therefore unreliably determined to be down-regulated upon M2 stimulus in TLDA, it was pre-amplified prior to individual validation (see section 2.2.2.6.1). Due to fluctuation across donors, its regulation in the context of polarization could not be conclusively determined. Since it was expressed in individual isolates at considerable levels and responded to the M2 stimulus (Fig. 3-18), it was included in the screenings for interaction partners.

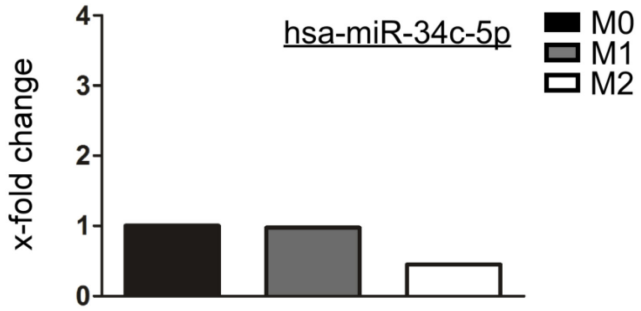

Figure 3-18: Re-investigation of hsa-miR-34c-5p expression. While this miRNA could not be conclusively profiled across all investigated samples, it was present in individual isolates and responsive to the M2 stimulus (IL4 (20 ng/ml) + IL13 (20 ng/ml)). Differential methodology as compared to the TLDA analyses precluded an integration of these data into the TLDA results, so no statistics were performed due to the solitary nature of the data (n=1).

3.4 Screening for microRNA/mRNA interaction partners

3.4.1 Bioinformatics analysis

3.4.1.1 Laws of microRNA/mRNA interaction

The likelihood of interaction of a given miRNA/mRNA pair can be expressed numerically on a metric scale of interaction scores. The score is always negative as it is a representation of a negative correlation between miRNA and mRNA expression levels. An increasing absolute score denotes an increased probability of miRNA/mRNA interaction. The score integrates various biochemical and biological aspects of miRNA and mRNA duplex formation, such as stability and sequence conservation. The putative miRNA/mRNA duplex is influenced by the free energy in the system, which, striving for a minimum, determines the thermodynamic stability of the nucleotide pairing [121]. Sequence conservation across species also impacts on the computational likelihood of interaction, since functional pairing is more likely to be conserved throughout evolution by selection pressure than non-functional pairing.

3.4.1.2 Theoretical identification of several mRNAs with an increased likelihood of microRNA-mediated regulation

After confirmation of the regulated miRNAs by qPCR, an *in silico* target prediction was performed. Potential mRNA targets that showed inverse expression as compared to the corresponding miRNA were identified (Fig. 3-19) and favourably treated by the interaction score computation algorithm (Table 3-1).

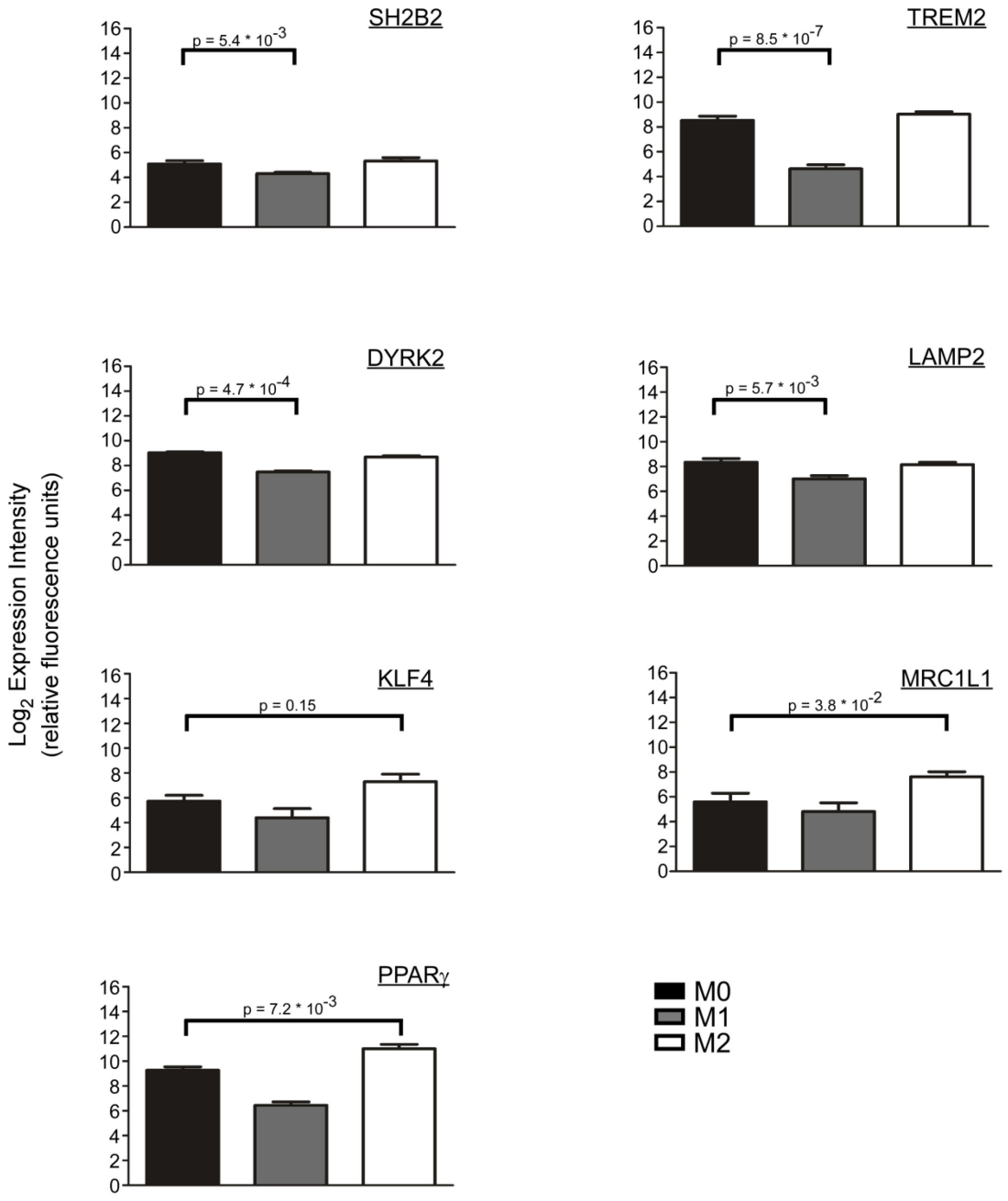

Figure 3-19: Predicted candidates for miRNA-induced regulation as extracted from the Illumina micro arrays. Selected mRNAs that were considered likely to be subject to miRNA-mediated degradation are shown by their $\log_2$ transformed expression intensity. Down-regulation of SH2B2, TREM2, DYRK2 and LAMP2 in the M1 phenotype was indicative of subtype-specific degradation of transcript. Correspondingly, up-regulation of KLF4, MRCL1L1 and PPARγ in the M2 phenotype was indicative of subtype-specific attenuated transcript destabilization. Both effects were bioinformatically linked to concomitant miRNA up- and downregulation, as the observed changes in transcript occurrence were hypothesized to be miRNA-induced. p-values as adjusted for multiple testing are shown (n=3).

In addition to universally applicable parameters (section 3.4.1.1), the adjusted score integrates several additional parameters (see section 2.2.8) in order to more accurately predict mRNA/miRNA interaction in the given macrophage setup. The publicly available miR SVR score (miRanda) as well as the adjusted score are shown for a selection of putative mRNA/miRNA interaction partners (Table 3-1).

Table 3-1: Predicted mRNA/miRNA interaction partners

Gene Symbol	Predicted microRNAs	miR SVR Score (miRanda)	Adjusted Score
DYRK2	hsa-miR-155-5p-5p	-0.82	-2.22
	hsa-miR-187-3p-3p	-0.57	-2.16
LAMP2	hsa-miR-155-5p-5p	-0.63	-1.88
	hsa-miR-187-3p-3p	-0.48	-1.35
SH2B2	hsa-miR-187-3p-3p	-1.11	-2.99
TREM2	hsa-miR-187-3p-3p	-0.57*	-1.97
PPARγ	hsa-miR-34c-5p	-1.28	-1.56
MRC1L1	hsa-miR-511-3p	-0.41*	-1.41
KLF4	hsa-miR34c-5p	-1.03	-1.72

* = prediction annulled

Asterisk-labelled scores have since been removed from the miRanda database (last update as of 2013-09: 2010-11-01), since the prediction has turned out to be invalid, which is in accordance with the luciferase-based reporter assay (section 3.4.2.1).

It has been shown that miRNAs that bind in close proximity to each other, optimally in a distance between 13 and 35 nucleotides, synergistically act on their target [122]. In the case of DYRK2, hsa-miR-155-5p and hsa-miR-187-3p were determined to bind at a distance of 152 nucleotides (position 3502 – 3654 in the 3´UTR), whereas in the LAMP2 transcript, their seed binding sites were found to lie 43 nucleotides apart (position 439 – 481 in the 3´UTR, Fig. 3-21), as determined by the miRanda target prediction algorithm. In addition to target specificity, the question of synergy was thus addressed in the following validation experiments.

3.4.2 A subset of considered microRNAs could be corroborated by experimentation

3.4.2.1 First positive evidence of microRNA/mRNA interaction could be derived from a luciferase-based reporter approach

In order to corroborate the putative miRNA targets that were found by bioinformatic prediction, a luciferase-based reporter assay was employed. 3´UTR fragments as described (section 2.1.3.1) were cloned into the psiCheck2 vector, and luminescence was determined as an indicator of miRNA-dependent mRNA regulation in HEK293 cells. A decrease of luminescence reflects a decrease of enzyme, which suggests a functional interaction with the respective miRNA, as it initiates mRNA degradation or translational inhibition. Synergy of miRNAs was assessed by equimolar co-transfection. Relative luminescence levels were as indicated (Fig 3-20 and 3-22). The signal that was detected in the samples transfected with an unspecific miRNA scramble sequence was set to 100 %, and the signal intensity from the specific transfections was calculated accordingly. For reference, a control plasmid carrying the partial 3´UTR of the PTK9 mRNA was co-transfected with hsa-miR-1. This mRNA/miRNA pair has been established to be functional, and it serves as a commercially available positive control for miRNA transfection experiments [123].

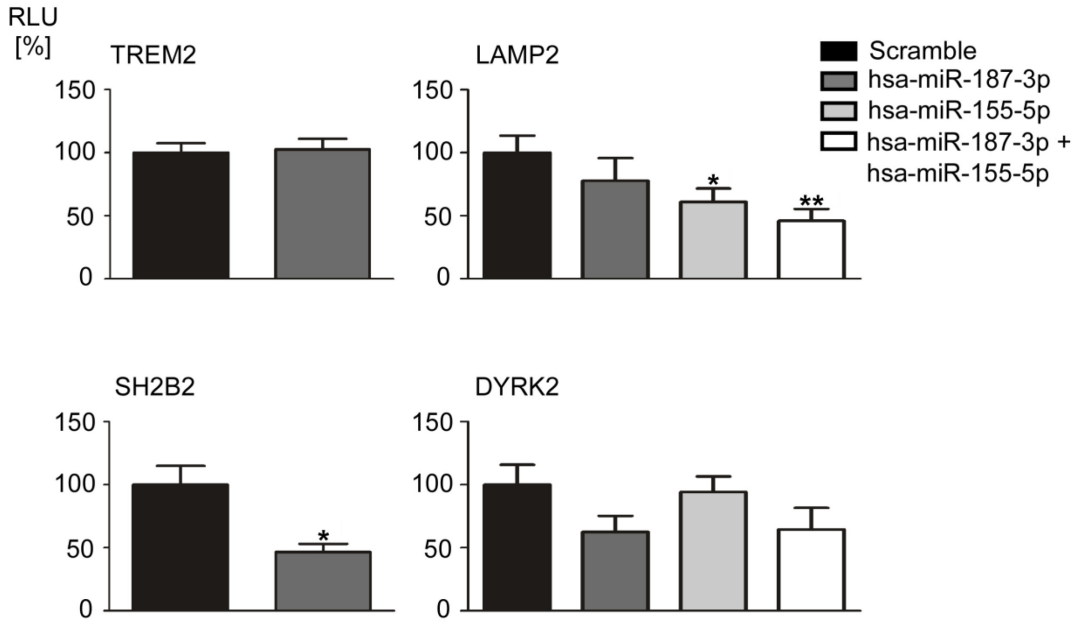

Figure 3-20: Luciferase reporter assay with M1-associated miRNAs. Co-transfection of the shown vector construct and miRNAs into HEK293 cells was performed. The specific miRNA-sensitivity of *Renilla* luciferase mRNA that carries the 3´UTR insert from the indicated mRNAs was measured as a function of luminescence. RLU: relative luminescence units. *p<0.05; **p<0.01 (n=3).

The DYRK (dual-specificity tyrosine-(Y)-phosphorylation regulated kinase) family protein kinases have been associated with several different regulatory processes. DYRK2 has been described to trigger proteasomal degradation of the transcription factors c-Jun and c-Myc, which are crucial for transition from G_1 to S phase. Accordingly, knockdown of DYRK2 leads to acceleration of cell proliferation. Macrophages do not undergo cell cycle when kept under *in vitro* conditions, and it has only recently become clear that macrophages can proliferate *in situ* under certain conditions [40]. Hence, the role of DYRK2 in macrophage biology has not been described yet. The DYRK2 construct was found to be slightly down-regulated in response to hsa-miR-187-3p, although not to a significant extent. Of note, the construct was insensitive to hsa-miR-155-5p, even though the adjusted prediction score (-2.22, Table 3-1) suggested a robust likelihood of interaction. Accordingly, no synergy could be found by co-administration of both miRNAs.

The lysosome associated membrane proteins 1 and 2 (LAMP1 and LAMP2) are situated in the membrane of lysosomes. They both possess a heavily glycosylated luminal domain, a single trans-membrane domain and a carboxyterminal domain on the cytosolic side. The glycosylation accounts for approximately 60 % of their total mass and is thought to render them resistant to the constant acidic exposure in the lysosomal lumen [124]. Their function

has been hypothesized to be protection of the lysosomal membrane as well as, in the case of LAMP2, selective uptake of cytosolic substances bound for lysosomal degradation.
The LAMP2 plasmid proofed to be slightly responsive to hsa-miR-187-3p, while transfection of hsa-miR-155-5p led to a significant decrease of the luminescence signal. Co-transfection of both miRNAs conferred the most efficient decrease of signal (approximately 50 %), which suggests a synergistic mode of action, an observation that is further corroborated by the close spatial proximity of the putative binding sites (43 nucleotides from seed region to seed region, Fig. 3-21).

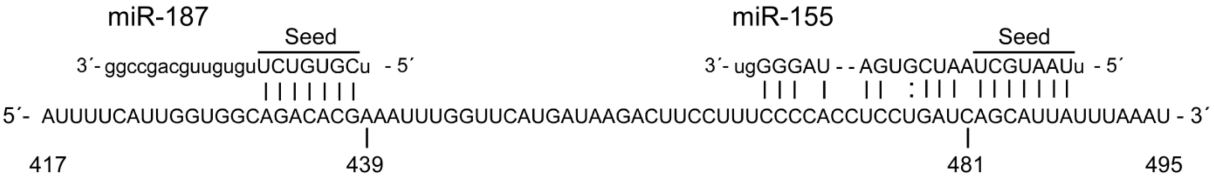

Figure 3-21: miRNA binding site distribution in the LAMP2 transcript 3´UTR. Position 417 to 495 from the LAMP2 transcript 3´UTR is shown. Vertical bars represent canonical base pairing (A-U and G-C), while the colon indicates a wobble base pair (G-U). The proximity of hsa-miR-187-3p and hsa-miR-155-5p binding sites (43 nucleotides) suggests a synergistic mode of miRNA-mediated LAMP2 transcript regulation.

The SH2B adaptor protein 2 (SH2B2 or APS, adaptor molecule containing PH and SH2 domains) is an adaptor protein with a pleckstrin homology (PH) domain that interacts with membrane-bound bi– or tri-phosphorylated phosphatidylinositol, and a src homology 2 (SH2) domain that binds to phosphorylated tyrosine residues [125, 126]. Together with SH2-B and Lnk, it is part of a family of cytokine and growth factor signalling mediators [127]. Having no catalytic activity, it was described as a scaffold molecule.
In macrophages, the function of SH2B2 has not been described yet, but its transcript is present. The SH2B2 mRNA possesses a very short 3´UTR (80 nucleotides), which was fully included in the luciferase reporter construct and which only displays one valid miRNA binding site. This site is predicted to be a target of hsa-miR-187-3p. Accordingly, transfection of hsa-miR-187-3p led to a 50 % down-regulation of signal as compared to the scramble sequence.

The triggering receptor expressed on myeloid cells 2 (TREM2) has been described as a negative regulator of TLR signalling and hence as a modulator of macrophage activation [128]. Accordingly, it has been shown to be down-regulated in M1-polarized macrophages [129] (Fig. 3-19). According to initial prediction by miRanda, TREM2 mRNA is sensitive

toward hsa-miR-187-3p. This prediction has been revoked and is no longer listed in the database (Table 3-1). In the reporter setup, TREM2 turned out to be completely irresponsive to this miRNA (Fig. 3-20).

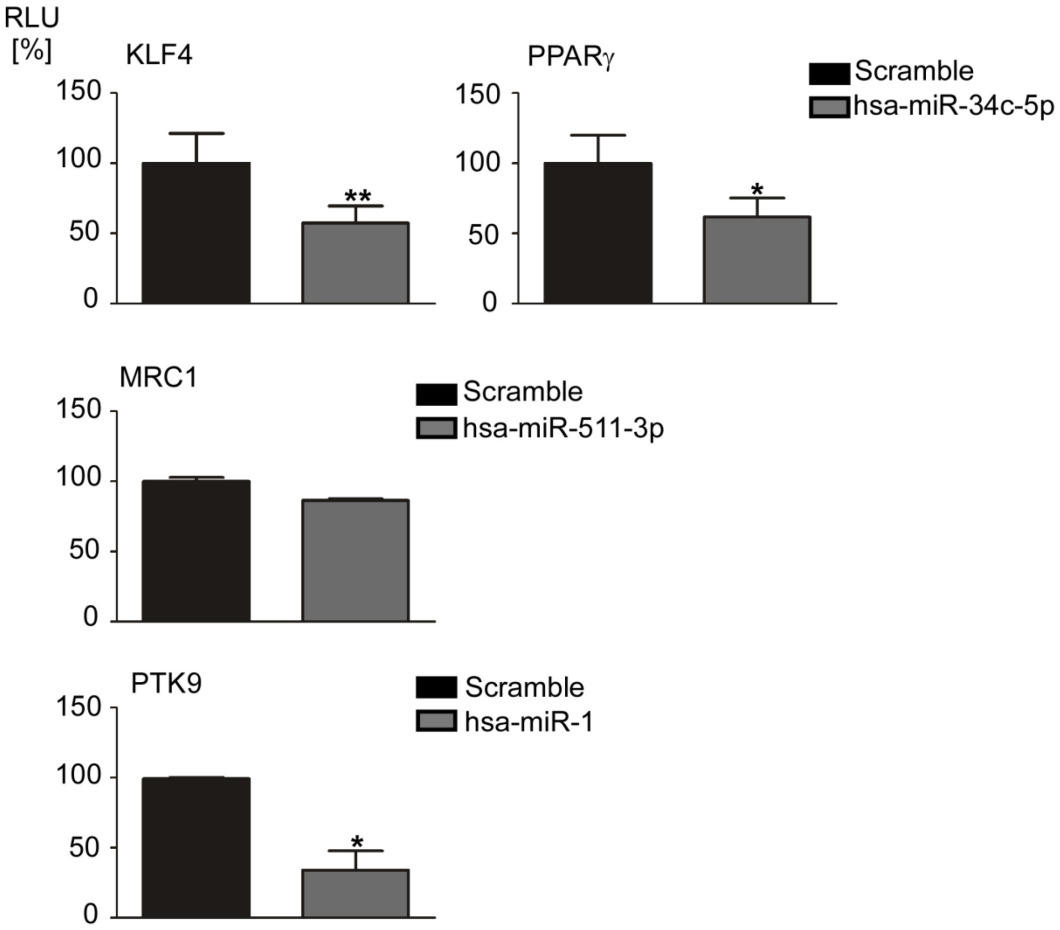

Figure 3-22: Luciferase reporter assay with M2-associated miRNAs. Co-transfection of the shown vector construct and miRNAs into HEK293 cells was performed. The specific miRNA-sensitivity of *Renilla* luciferase mRNA that carries the 3´UTR insert from the indicated mRNAs was measured as a function of luminescence. PTK9 was included as positive control. RLU: relative luminescence units. *p<0.05; **p<0.01 (n=3; PTK9: n=2).

Mannose receptor, C type 1 (MRC1/CD206) is a phagocytic carbohydrate receptor that detects both endogenous and foreign glycoproteins [130, 131]. It has been described to be inducible by IL4 and IL13, and it is acknowledged as a marker of M2-like macrophages [33]. The intronic hsa-miR-511 is encoded in the MRC1 open reading frame [132]. In addition, a putative binding site had been identified in the MRC1 3´UTR by an earlier version of the miRanda algorithm. The co-regulation of hsa-miR-511 and MRC1 and the affirmative target

prediction suggested a potential regulatory feedback mechanism that controls MRC1 expression levels. However, this prediction has been annulled and is no longer available in the miRanda database (Table 3-1). This could be confirmed here, since no effect could be shown by the reporter system.

PPARγ is a transcription factor which is activated by fatty acids or their derivatives. This receptor type is involved in cholesterol metabolism and immunoregulation, where it promotes macrophage differentiation toward the M2 type [133, 134]. The PPARγ construct showed downregulation of emitted luminescence upon hsa-miR-34c-5p transfection of approximately 50 %, which is in accordance with the target prediction score.
In close functional association with PPARγ, KLF4 has also been described to be a central factor in macrophage polarization [135]. It is a transcription factor downstream of STAT6 and is associated with numerous processes, such as anti-inflammation [136] and cancer progression [137]. Similar to PPARγ, signal decrease in the reporter assay amounted to approximately 50 % of the control scramble transfection, reflecting the affirmative prediction score.
The PTK9 construct showed a strong sensitivity to hsa-miR-1. This pair was investigated for reference only, as it represents an established positive control (n=2, Fig. 3-22).

3.4.2.2 The effect of selected microRNAs on native targets is limited

In order to more closely mimic the physiological role of miRNAs in macrophages, miRNA precursors and inhibitors were transfected by lipofection into monocyte-derived macrophages, and the effect on the native target transcript as suggested by the reporter construct was monitored. The transfection efficiency of the introduced miRNAs was routinely validated by qPCR as exemplarily shown (Fig. 3-23). The high relative amount of the mature hsa-miR-187-3p after transfection is due to its low-level occurrence in untransfected cells, as expression was normalized to the scramble-transfected sample. Accordingly, the moderate increase of mature hsa-miR-155-5p after transfection reflects the high native expression level of this miRNA in macrophages.

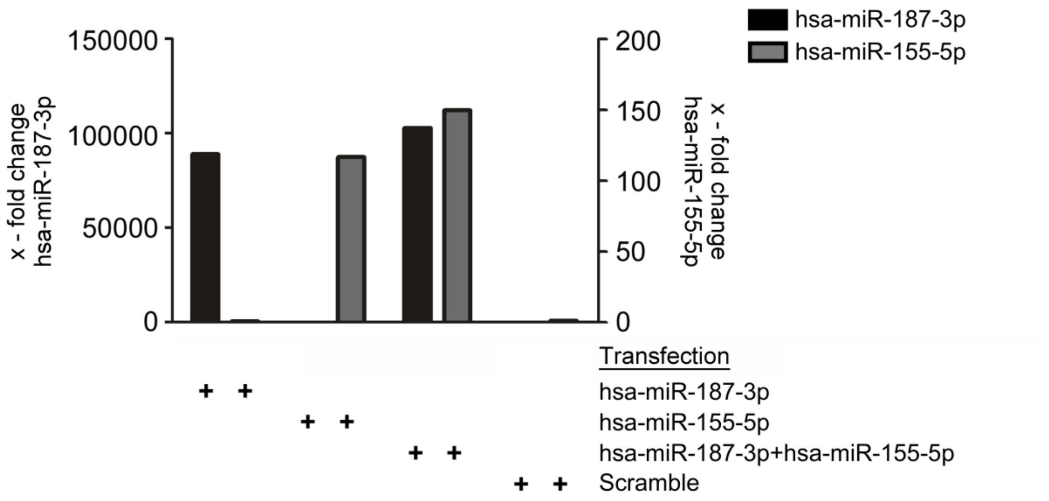

Figure 3-23: Representative example of relative miRNA expression levels after transfection. Over-expression of transfected hsa-miR-155-5p and hsa-miR-187-3p (30 nM each) was verified in blood-derived macrophages before subsequent target validation assays were performed. Each miRNA was transfected at a final concentration of 30 nM by siPort-based lipofection. Detection of the mature miRNAs was performed 24 hours post transfection by Taqman-based qPCR. All miRNA signals were normalized to RNU48.

SH2B2 mRNA regulation by hsa-miR-187-3p

The regulation of the SH2B2 transcript was the first to be investigated. The short 3´UTR and the absence of binding sites other than for hsa-miR-187-3p made it a likely candidate for miRNA-dependent regulation. Transfection of a synthetic hsa-miR-187-3p precursor at 30 nM indeed conferred a marked down-regulation of SH2B2 transcript at 24 h post transfection, as detected by qPCR (Fig. 3-24).

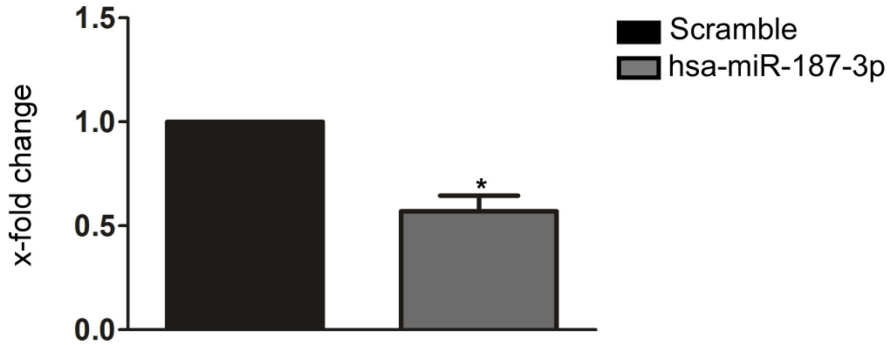

Figure 3-24: SH2B2 is down-regulated by hsa-miR-187-3p on mRNA level. Upon ectopic over-expression of hsa-miR-187-3p at 30 nM, the relative amount of SH2B2 transcript as normalized to RPS18 was shown to be reproducibly decreased. SYBR-Green based qPCR was performed at 24 h post transfection. $^{*}p<0.05$ (n = 3).

The impact of the observed regulation on the protein level of SH2B2 was not conclusively investigated, because western blot experiments with macrophage cell lysate yielded no consistent results. This was in part due to the restricted number of suitable available antibodies.

LAMP2 mRNA regulation by hsa-miR-155-5p and hsa-miR-187-3p

Since the reporter assay suggested a synergistic mode of action by hsa-miR-155-5p and hsa-miR-187-3p on the LAMP2 mRNA, it was investigated whether this regulation could be seen on the level of native transcript. To this end, monocyte-derived macrophages were transfected by lipofection. Single and combined application of hsa-miR-155-5p and hsa-miR-187-3p at 30 nM each or combined yielded no regulation of the LAMP2 transcript that was detectable by qPCR, as shown (Fig. 3-25).

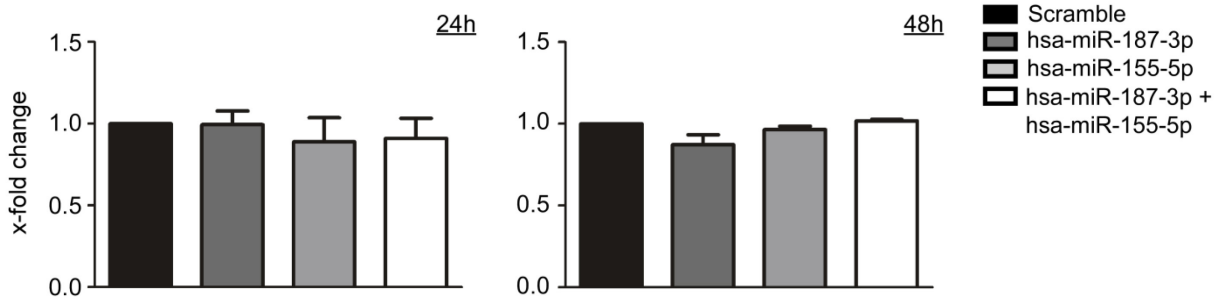

Figure 3-25: Quantification of LAMP2 transcript after indicated miRNA transfection. The relative amount of LAMP2 transcript was shown to be unresponsive to ectopic over-expression of hsa-miR-187-3p and hsa-miR-155-5p at 30 nM each or combined. Expression levels were detected by SYBR-Green based qPCR at 24 h and 48 h timepoint after transfection and normalized to RPS18 (n=2).

In order to exclude compensatory effects like enhanced transcription that might obscure degradation of transcript, a modified experimental approach was chosen [138], using the monocytic THP-1 cell line. The synthetic cytostatic actinomycin D (10 µM) was administered to the cells, thereby globally blocking transcription [139]. It could be shown that LAMP2 mRNA is highly stable under the influence of actinomycin D, as it withstands degradation for a prolonged period of up to 4 hours. TNFα mRNA, which was used as a control for actinomycin D potency, was greatly diminished (> 80 %) after 120 min (Fig 3-26).

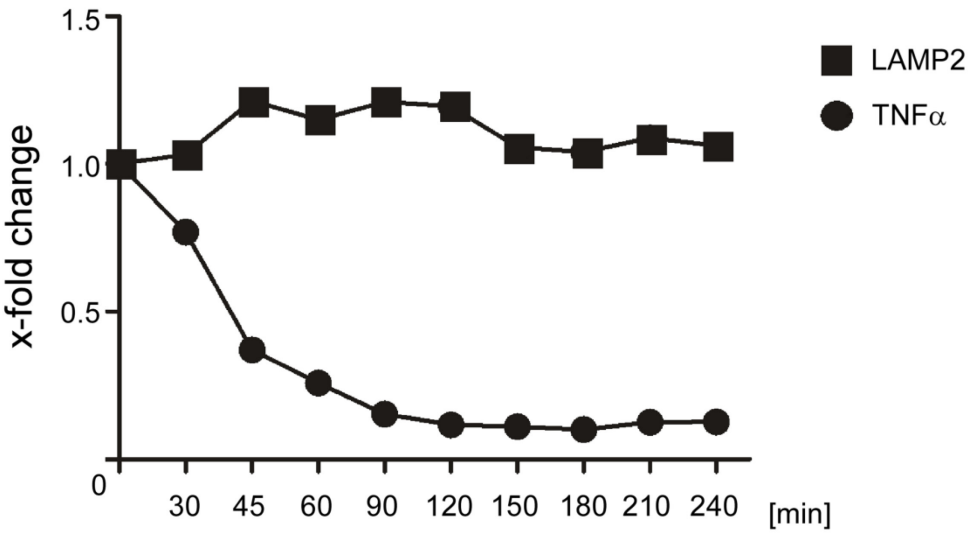

Figure 3-26: Transcript decrease of indicated genes after actinomycin D administration. THP-1 cells were treated with the cytostatic actinomycin D at a final concentration of 10 µM for the indicated time points. While TNFα mRNA is subject to rapid decrease, the LAMP2 transcript levels remain stable for up to 240 min as determined by SYBR Green based qPCR. The signal was normalized to RPS18 (n=1).

In order to show a regulatory impact of hsa-miR-187-3p and hsa-miR-155-5p on LAMP2 transcript levels, the actinomycin D treatment was supplemented by miRNA administration. In case of a functional interaction between miRNA and mRNA, which was assumed to exist given the affirmative reporter assay data, presence of either miRNA should be able to induce degradation of the LAMP2 transcript. Early time points were chosen to avoid cytotoxic side effects of actinomycin D and in accordance with literature [138].

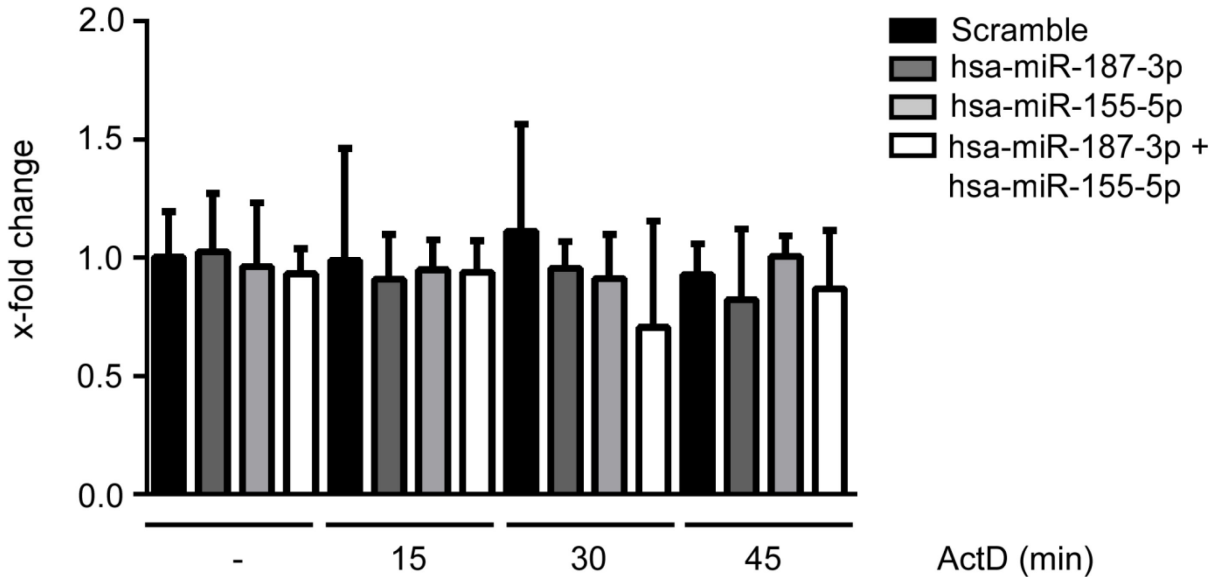

Figure 3-27: Relative quantification of LAMP2 transcript under the combined influence of actinomycin D and indicated miRNAs. Monocytic THP-1 cells were transfected with the indicated miRNAs at a final concentration of 30 nM. 18 hours after transfection, the cytostatic actinomycin D was added at a final concentration of 10 µM. RNA samples were taken at 15, 30 and 45 min and of untreated cells. Relative levels of LAMP2 transcript as normalized to RPS18 were determined by SYBR-Green based qPCR. Bars represent mean and standard deviation (n=4).

As shown, indicated miRNA overexpression under the influence of actinomycin D did not increase LAMP2 mRNA degradation on a time scale from 15 to 45 minutes (Fig. 3-27). Even though such a tendency could be observed for miRNA co-transfection at 30 min timepoint, the consecutive 45 min timepoint showed no progressive decline of transcript. Additionally, the 30 min timepoint shows a high standard deviation.

The effect of miRNA on the LAMP2 protein

Since no effect of either hsa-miR-155-5p or hsa-miR-187-3p could be detected on the transcript level, which stood in stark contrast to the data gained from the luciferase reporter assay, the possibility of miRNA-mediated translational inhibition was investigated. In order to explore the possible influence of hsa-miR-155-5p and hsa-miR-187-3p on LAMP2 protein levels, western blot analysis was performed with cell lysate from transfected monocyte-derived macrophages (Fig. 3-28). As the half-life of LAMP2 has been shown to be 48 h [140], this time point was chosen for cell lysis after miRNA transfection.

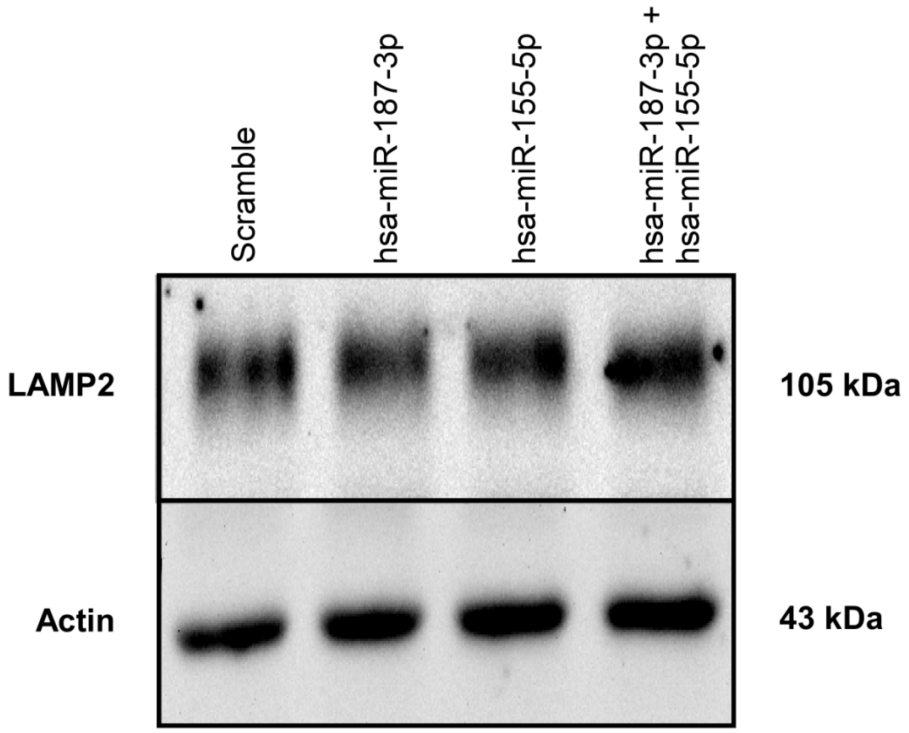

Figure 3-28: Representative example of LAMP2 detection by western blot. Blood-derived macrophages were transfected with the indicated miRNAs at a final concentration of 30 nM each, and the cells were lysed under stabilizing conditions 48 h post transfection. From each sample, 80 µg of protein were loaded and transferred to a nitrocellulose membrane by wet blot. Total LAMP2 protein amount (Isoform A and B) was determined by LAMP2 antibody staining. Actin was used as loading control. One representative replicate of four is shown.

As changes in LAMP2 expression were expected to be subtle, extracting robust data from the semi-quantitative western blot output required densitometric analysis. A set of 4 independent transfection experiments was blotted to calculate the numeric effect of the indicatd miRNAs on the LAMP2 protein level (Fig. 3-29).

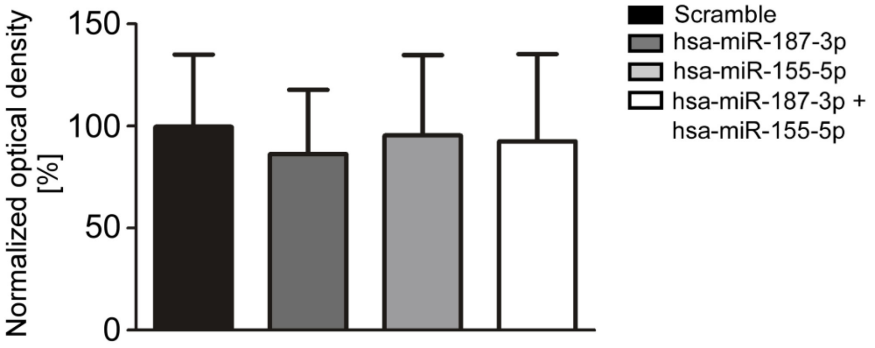

Figure 3-29: Densitometric analysis of LAMP2 protein levels as determined by western blot in response to the indicated miRNA treatment. Blood-derived macrophages were transfected with the indicated miRNAs at a final concentration of 30 nM each, and the cells were lysed under stabilizing conditions 48 h post transfection. From each sample, 80 µg of protein were loaded and transferred to a nitrocellulose membrane by wet blot. Total LAMP2 protein amount (Isoform A and B) was determined by LAMP2 antibody staining. After digital image acquisition, the western blot band volume and density were determined by the LabImage1D software. LAMP2 signal was normalized to the corresponding actin signal. Scramble transfected samples were set to 100 %. Bars represent mean and standard deviation (n= 4).

Due to considerable fluctuations in the densitometry analysis that potentially obscured regulation of LAMP2 protein by miRNAs, transfected macrophages were subjected to immunofluorescence staining in order to alternatively visualize the amount and also the distribution of LAMP2 protein (Fig. 3-30). In addition, the M1-polarized subtype was included. This was done to test whether the predicted regulation of LAMP2 by miRNAs was restricted to a specific metabolic state of the cell.

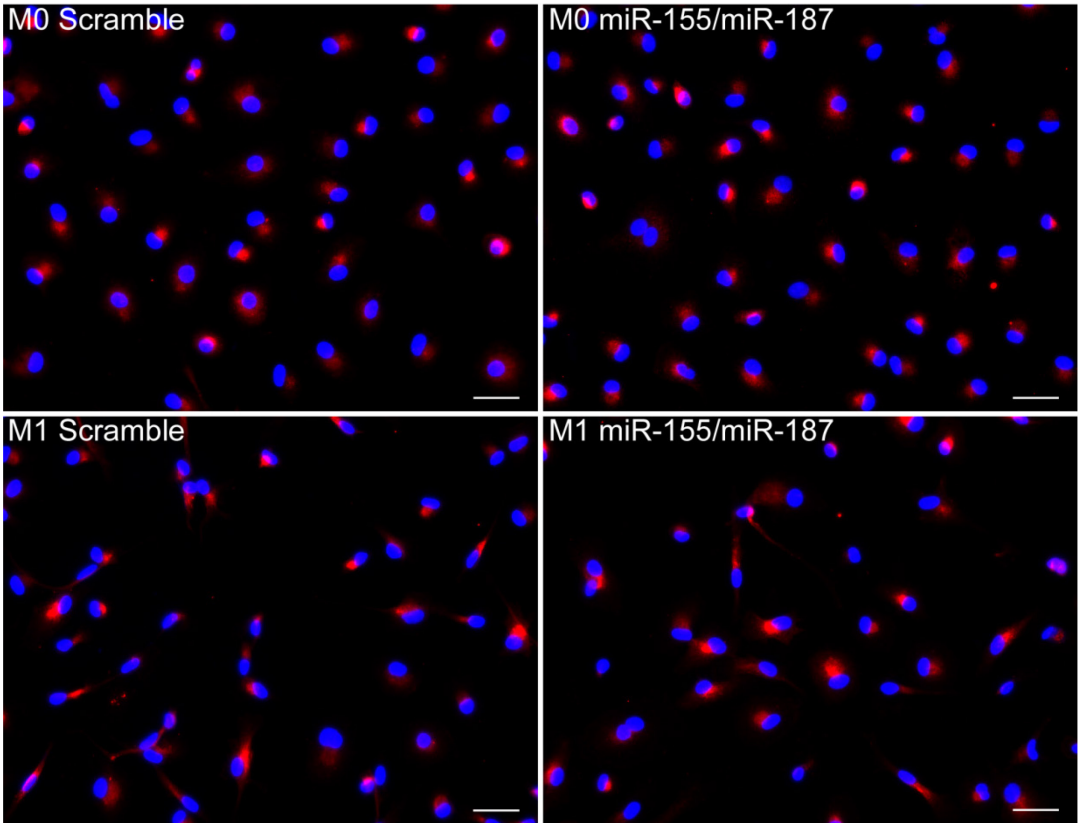

Figure 3-30: LAMP2 staining of unpolarized and M1 polarized macrophages after indicated miRNA transfection. Blood-derived macrophages were transfected with the indicated miRNAs at a final concentration of 30 nM each. After 12 h, the cells were M1-polarized or left unpolarized. Upon fixation by 4 % PFA, cells were permeabilized with 1 % Triton X100. cell Finally, cells were stained with a LAMP2-specific antibody (1:500) and a nucleus-counterstain (DAPI). Representative sections are shown. LAMP2 in red, DAPI in blue. Bar = 20 µm

Semi-quantitative screening of miRNA-transfected and scramble-transfected M0 and M1 macrophages for LAMP2 occurrence yielded no discernible change in LAMP2 quantity, irrespective of the polarization subtype. The morphological change of LAMP2 positive areas in M1 polarized cells is probably not due to an active shuttling of LAMP2, but a passive consequence of a polarization-induced change of overall cell shape. M1 polarized macrophages acquire a spindle-shaped morphology, as routinely observed by microscopy.

3.5 Macrophage-associated miRNAs are regulated in an experimental murine model of asthma

The macrophage as one of the most versatile cell types of the immune system is critically involved in a number of diseases, e.g. asthma (section 1.3.2). The gathering of a systemic, polarization-dependent macrophage miRNA and mRNA profile (section 3.3) established a referential basis that can hypothetically be used to assess the disease-driven macrophage polarization status in primary samples. Allergic asthma and the associated macrophage subtype as determined by its miRNA profile were in the focus of this effort.

Macrophages and their various subtypes have been increasingly discussed as central to the pathogenesis of allergic asthma in recent years (section 1.3.2). The acute model of eosinophilic airway inflammation, induced by sensitization and challenge of BALB/c mice, served as an experimental approximation of asthma in this study. As discussed, an M2-like macrophage phenotype was expected to dominate in eosinopilic airway inflammation.

A quickly accessible control parameter for the induction of allergic airway inflammation was the eosinophil count in the BAL fluid, which was determined by FACS analysis (Fig 3-31 and 3-32). As shown in both BAL fluid and tissue homogenate, the relative amount of eosinophils (SiglecF^{high}/CD11c^{int}) increased upon OVA challenge.

3.5.1 Cytometric macrophage isolation from healthy and asthmatic mice was performed by using specific surface markers

While macrophages constitute almost 100 % of cells present in the alveolar lumen in healthy mice, the inflammatory infiltrate that accompanies eosinophilic airway inflammation necessitates a sorting strategy that specifically isolates alveolar macrophages. Macrophages as defined by SiglecF^{high}/CD11c^{high} surface marker configuration were isolated from the BAL fluid of healthy and asthmatic mice by cytometric sorting. Interstitial macrophages from lung tissue homogenate were similarly isolated, using their SiglecF^{high}/CD11b^{low} signature or their SiglecF^{high}/CD11c^{high} signature, dependent on the health status of the donor animal (Fig. 3-31). Siglecs are lectins that mediate sialic acid binding, while CD11b and c are complement receptors.

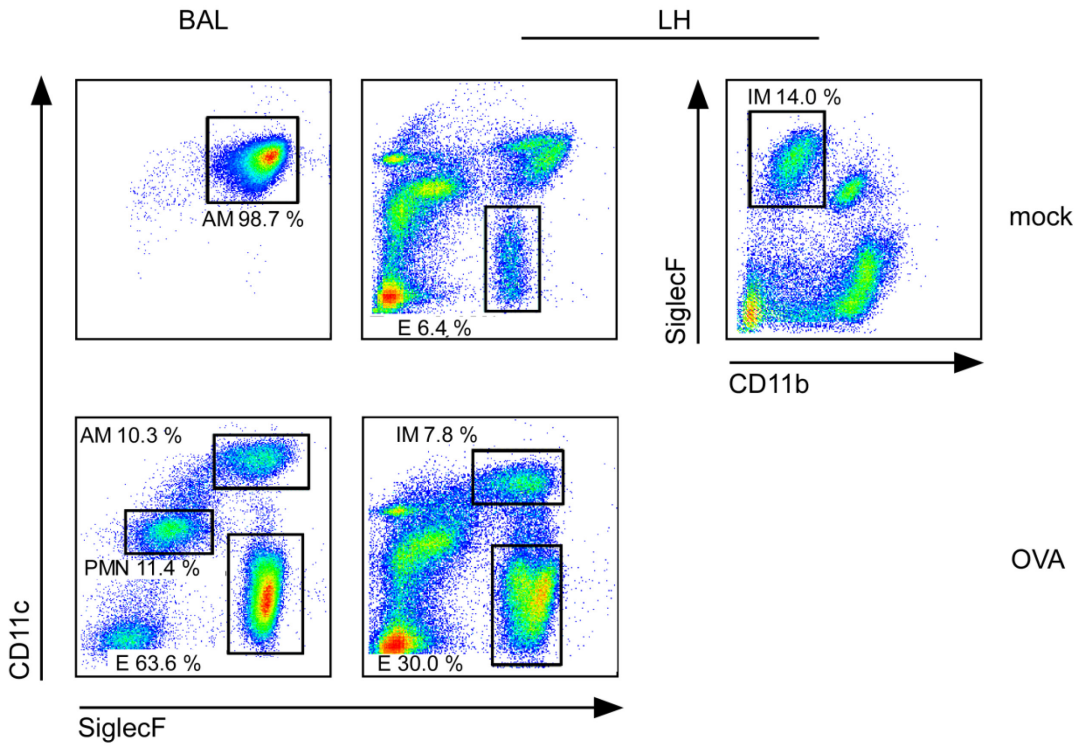

Figure 3-31: Cytometric sorting of macrophages from lavage fluid (BAL) and lung homogenate (LH) of mock and OVA treated mice. OVA - sensitized mice were sacrificed at 48 h after the final challenge with nebulized OVA or PBS, respectively. BAL fluid and lung homogenate were recovered, and cells were stained with fluorochrome-labelled antibodies. Alveolar macrophages (AM, SiglecF^{high}/CD11c^{high}**)** and interstitial macrophages (IM, SiglecF^{high}/CD11c^{high} or SiglecF^{high}/CD11b^{low}) were purified from the indicated fractions by cytometric sorting and taken up in Isol RNA Lysis Reagent for further RNA analysis. Increase of eosinophils (E, SiglecF^{high}/CD11c^{int}) was routinely observed in OVA challenged mice and is indicative of eosinophilic airway inflammation. Cells from the pan-leukocyte CD45^{+} parent gate are shown from one representative experiment out of three. For each experiment and condition, material from six mice was pooled. PMN = polymorphonuclear neutrophil

The relative cell counts from the pan-leukocyte CD45^{+} gate were averaged across three biologically independent experiments (Fig. 3-32). The high reproducibility was considered indicative of a stable induction of eosinophilic airway inflammation and warranted the subsequent isolation and analysis of the cell-type specific RNA.

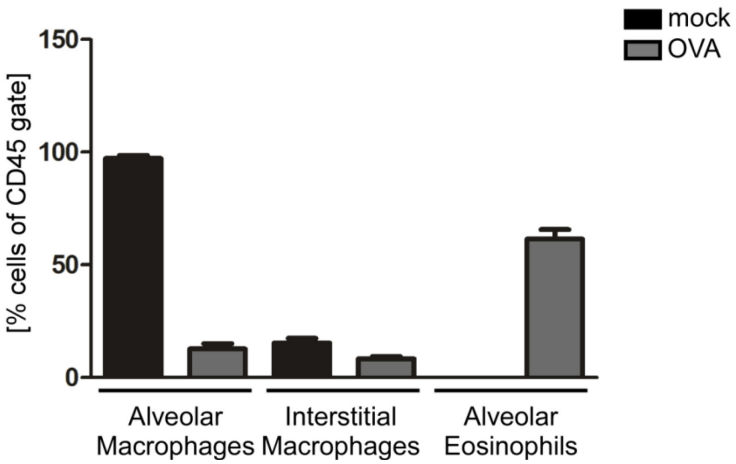

Figure 3-32: Percentages of CD45$^+$ cells in mock- and OVA-treated mice. The average relative amount of cells in the CD45$^+$ gate at 48 h after the final OVA challenge of OVA- and mock-sensitized mice was determined by flow cytometry. Influx of eosinophils (SiglecF^{high}/CD11c^{int}) was considered indicative of eosinophilic asthma and leads to a relative decrease of alveolar macrophages (SiglecF^{high}/CD11c^{high}). Bars represent mean and standard deviation. For each experiment and condition, material from six mice was pooled (n = 3).

3.5.2 Systemic profiling of isolated macrophage specimens shows regulation of microRNAs as a function of health status and compartment of residence

RNA was isolated from purified macrophage populations, and the miRNA profile was determined as described (section 2.2.2.4). The miRNA expression was found to be in parts dependent on both the macrophage´s compartment of origin and the disease status of the donor animal. The regulation pattern of the most strongly regulated miRNAs is shown as the $\log_2$ transformed expression data of asthma-related macrophages relative to the healthy control macrophages. Of all miRNAs that were probed, 32 were chosen on the basis of their statistical confidence of differential expression (Fig. 3-33).

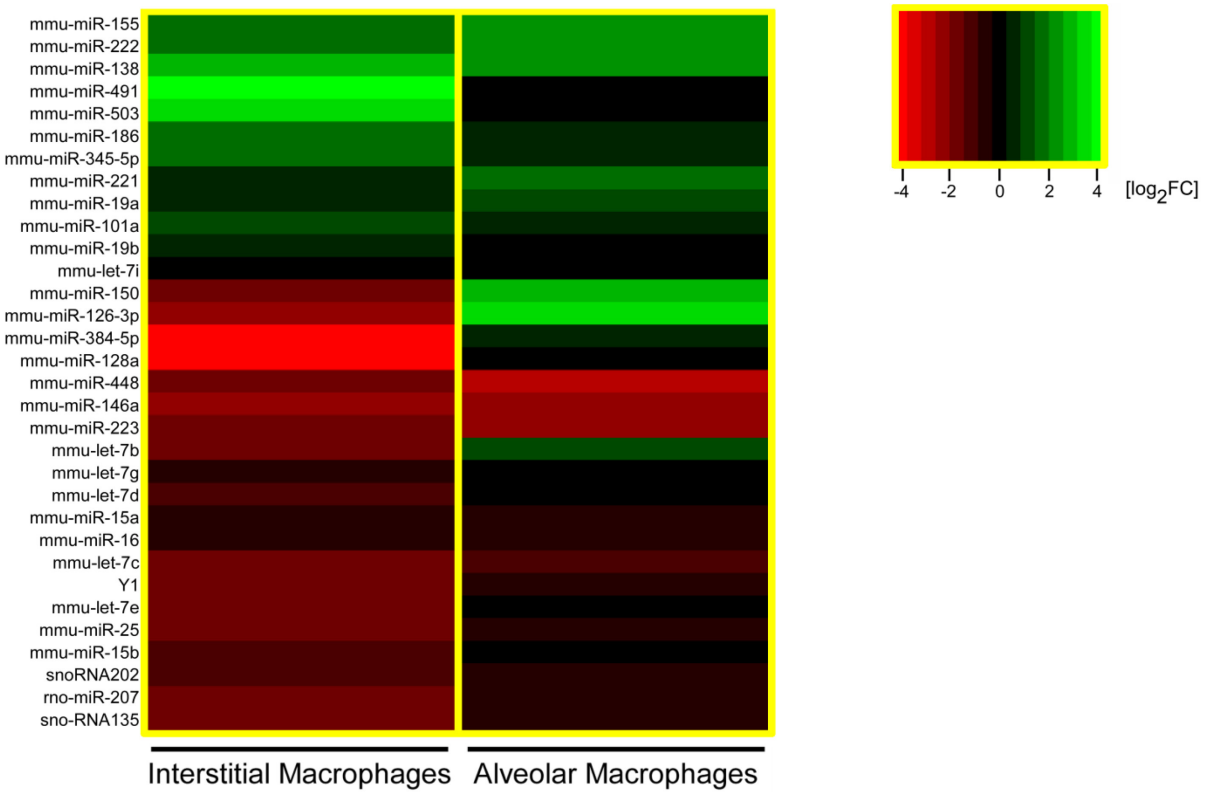

Figure 3-33: miRNA regulation in the alveolar and interstitial macrophage fractions of mice with acute eosinophilic airway inflammation as compared to corresponding macrophage fractions from mock-treated animals. At 48 h after the final OVA challenge, OVA- and mock-sensitized mice were sacrificed, the alveolar and interstitial macrophage fractions were purified, and RNA was isolated. The global asthma- and tissue-dependent miRNA regulation pattern was determined by Taqman Low Density Array (TLDA). The 32 most reliably regulated miRNAs as determined by their p-values were chosen for display, and their average regulation across three biological replicates is shown as $\log_2$ transformed fold change expression. For each experiment and condition, material from six mice was pooled (n=3).

These candidates included miRNAs with prominent modulatory roles in inflammation as described elsewhere (section 4.2), such as mmu-miR-155-5p, which is up-regulated in both the interstitial and alveolar macrophage fractions, and mmu-miR-146a-5p, which is down-regulated, correspondingly. The displayed set of miRNAs furthermore includes mmu-miR-126-3p, which shows opposing patterns of regulation upon eosinophilic airway inflammation. While up-regulated in alveolar macrophages, it is down-regulated in the interstitial macrophage fraction. The regulation of this miRNA is of particular interest, since mmu-miR-126 has been shown to promote the T_H2 response in a house dust mite model of asthma [103]. Likewise, mmu-miR-21a-5p has been shown to drive the immune response toward the T_H2

axis in OVA-induced eosinophilic airway inflammation [102]. Albeit this miRNA failed to pass the criteria for differential regulation and is therefore not listed (Fig. 3-33), it was investigated because of its known impact on eosinophilic airway inflammation. Altogether, these four miRNAs of particular interest were regulated at the depicted levels of confidence (Fig. 3-34).

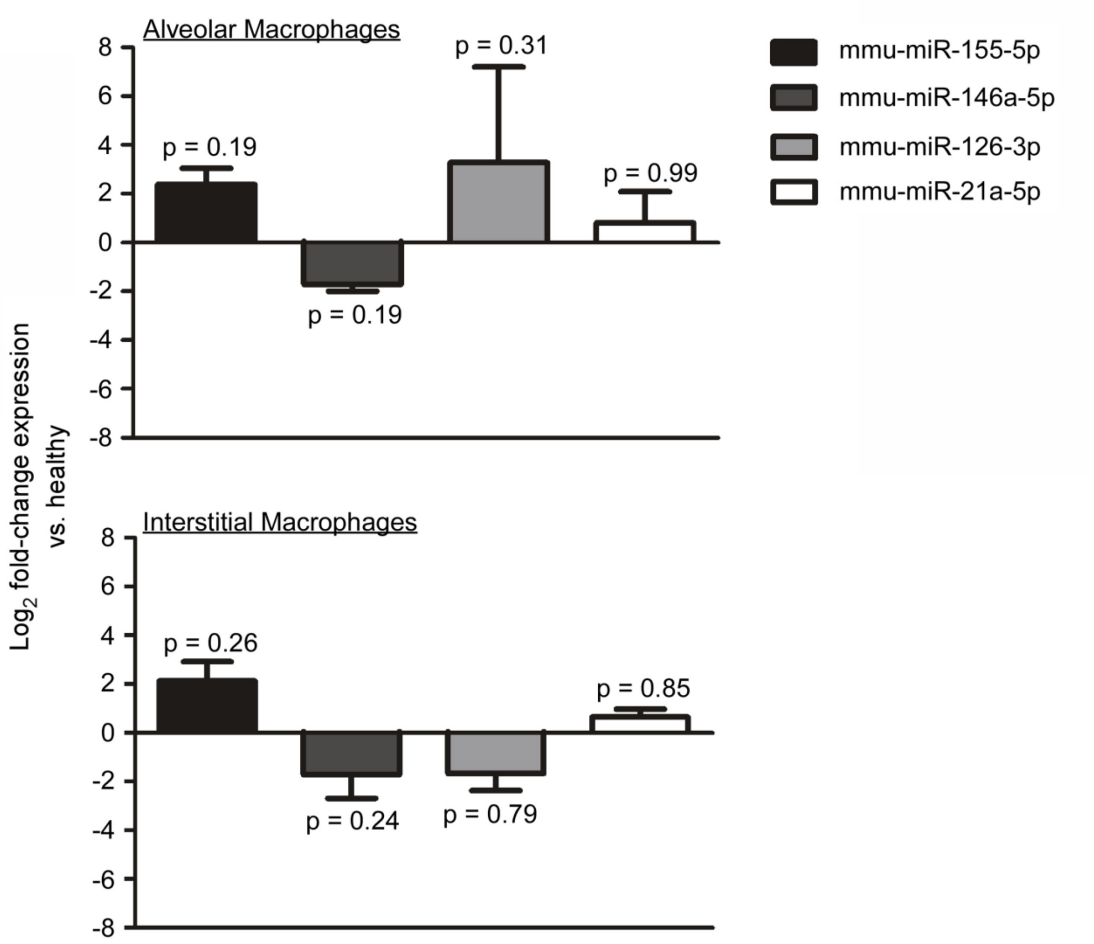

Figure 3-34: Selected miRNAs with a potentially asthma-dependent expression pattern. Individual miRNAs that were found to be differentially regulated as a function of OVA administration were extracted from the miRNA screening experiments. The relative regulation as compared to the healthy control is shown as log_2 transformed fold-change expression. Expression values were computed by the ΔΔCt method. p-values as adjusted for multiple testing are indicated. For each experiment and condition, material from six mice was pooled (n=3).

In addition to analyzing individual miRNA expression levels, the pattern of the combined set of the 32 differentiallly regulated miRNAs as identified above was considered to be a valuable indicator of the animal´s health status. Therefore, a principal component analysis was performed as described above (section 2.2.8.2) in order to visualize similarities and differences of the respective macrophage subset in health and disease. Prior to extraction of the first principal components, the Kaiser Meyer Olkin criterion (KMO) and the measure of sampling adequacy (MSA) were calculated to assess the extent of partial sample correlation. As in the human *in vitro* data (section 3.3.3), the partial sample correlation turned out to be moderate in the miRNA expression data gained from the murine alveolar (KMO = 0.82) and interstitial (KMO = 0.79) macrophages. Accordingly, some MSA values indicated weak sample correlation, ranging from 0.71 to 0.92. Altogether, these values argue for full eligibility of the data for subsequent factor analysis (Fig. 3-35).

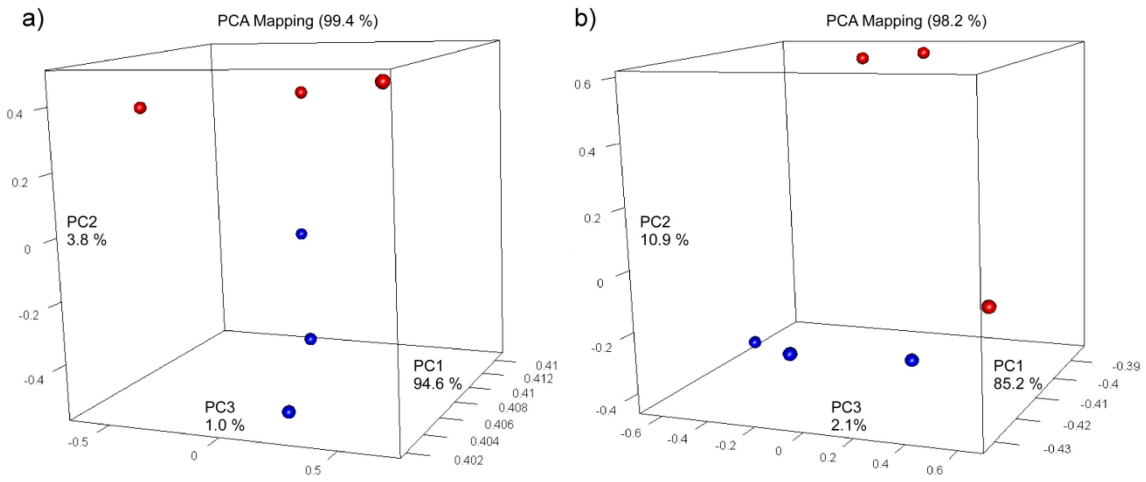

Figure 3-35: Principal Component Analysis of murine macrophage populations during eosinophilic airway inflammation. The ΔCt values of 32 miRNAs that were determined to be regulated during eosinophilic airway inflammation were used to extract the first three principal components from the alveolar (a) and the interstitial (b) macrophage expression data. Total explained variance (PCA Mapping) amounted to 99.4 % (a) and 98.2 % (b). Each data point represents pooled material from six mice. healthy = red, asthmatic = blue (n=3).

The visual correlation yielded moderate clustering of the alveolar (a) and interstitial (b) macrophages when displayed as a function of health status. Thus, the miRNA profile seems to be potentially suitable to identify the disease status of the animal.

3.5.3 Individual validation corroborates differential regulation of microRNAs in the context of asthma

Selected candidates from the list of putative differentially regulated miRNAs (Fig. 3-33) were individually validated, as has been done for the human *in vitro* experiments (section 3.3.4). Only a limited amount of RNA was available due to the scarcity of murine cell material. Thus, the validation focused on material from the interstitial macrophage fraction and on three candidates which were considered to be crucial for macrophage biology in asthma. As mmu-miR-21a-5p, mmu-miR-146a-5p and mmu-miR-126-3p have already been described to play a role in inflammatory responses [102, 103, 141], these three miRNAs were chosen for investigation. Interpretation of the TLDA analyses only revealed tendencies of their regulation at a low level of confidence (Fig. 3-34). However, the same tendencies could be shown in the interstitial macrophage fraction from a biologically independent sample that was not part of the TLDA analyses (Fig 3-36). Of note, the absolute expression of these miRNAs appeared to also be dependent the compartment of macrophage residence. As shown by the TLDA analyses, mmu-miR-126-3p was only barely detected in alveolar macrophages, while its expression was very robust in interstitial macrophages. In contrast, mmu-miR-146a-5p and mmu-miR-21a-5p were both robustly expressed in alveolar and interstitial macrophages.

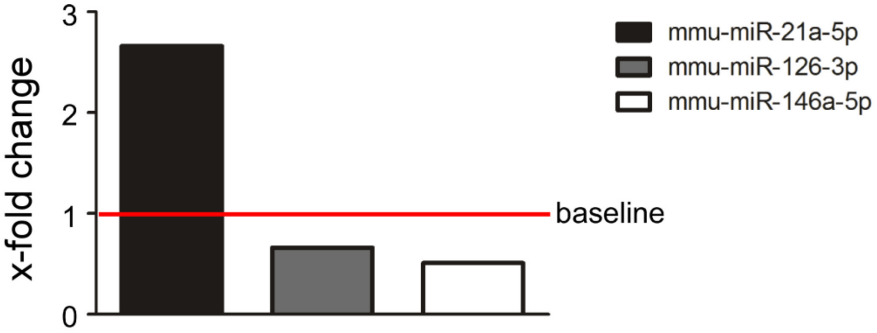

Figure 3-36: Expression of indicated miRNAs in interstitial macrophages in asthma. Upon induction of asthma, the indicated miRNAs responded by up- or down-regulation. Non-asthmatic baseline expression was set as a reference (red line). Pooled material from six mice per condition was used. The expression data were gained from an additional biologically independent sample that was not part of the TLDA analyses, so no statistics were performed due to the solitary nature of the data (n=1).

4 Discussion

The goal of this study was to understand the molecular basis of miRNA involvement in macrophage polarization, and to translate this knowledge into the context of eosinophilic airway inflammation. To this end, the mRNA and miRNA profiles of the prototypical human M1 and M2 macrophage polarization types were assessed. Apart from exploring possible mRNA/miRNA interactions, these RNA profiles were envisaged to provide generally applicable patterns that can be used to determine the polarization status of macrophages isolated from *in vivo* material. In this study, murine eosinophilic airway inflammation was used as an experimental disease model, and lung macrophages from BAL fluid and lung homogenate were isolated in an attempt to determine their polarization status on the basis of their miRNA pattern.

4.1 Human macrophage maturation and polarization can be monitored on both the mRNA and microRNA level

The *in vitro* monocyte-to-macrophage maturation stood at the beginning of this thesis. Different published maturation protocols suggested various cultivation methods and the addition of supporting cytokines, such as M-CSF [142]. However, there was reasonable concern that cultivation of monocytes in the presence of M-CSF or GM-CSF might influence the polarization capacities of mature macrophages [143-145]. It has been shown that M-CSF alone skews macrophages toward the M2 axis, and it has been hypothesized that M-CSF-induced macrophages constitute the default subtype in homeostasis *in vivo* [31, 146]. On the other hand, GM-CSF has been described to increase cellular responses to pro-inflammatory stimuli [147]. While M-CSF circulates at high concentrations in the blood, GM-CSF is predominant in the lung and regulates alveolar macrophage differentiation [148]. It has been described that cultivation in the presence of human serum gives rise to macrophages that resemble tissue macrophages that develop in the GM-CSF rich environment of the lung [149, 150]. In order to generate blood-derived macrophages *in vitro* that resemble alveolar macrophages to ensure maximal comparability with later *in vivo* lung studies, monocytes were cultured in the presence of human off-the-clot AB serum. Since naïve mature macrophages were of the utmost importance for unbiased polarization experiments, no auxiliary cytokine

was given to support the monocyte-to-macrophage transition. Macrophage maturation was closely monitored by microscopy. Furthermore, the response of the cells to the polarization stimuli was examined before RNA profiling was performed. The phosphorylation of p42/44, p38, and JNK, as well as the degradation of IκBα, indicated activation of pro-inflammatory M1-associated signalling pathways, whereas phosphorylation of STAT6 pointed to M2-related cellular activation. Functional characterization of the polarization routine was furthermore achieved by infection of polarized macrophages with *Legionella pneumophila* and subsequent assessment of phagocytic and bactericidal capacity. As described before [151], M1 polarized macrophages showed increased uptake and killing of bacteria as compared to M0 and M2 macrophages (section 3.2).

As shown in subsequent RNA analyses, the *in vitro* polarization of human monocyte-derived macrophages yielded reproducible and stable miRNA and mRNA profiles that were characteristic of the respective macrophage subtype (Fig. 3.8 and 3.13). A closer investigation of mRNAs that were regulated as a response to the M1 polarization stimulus showed hallmark inflammatory gene expression such as IL1β and IL6 as well as TNFα among the most highly induced genes (Fig. 3-10). Of note, CCR7, a potential surface marker for M1 polarized macrophages that has been dismissed in cytometric screening experiments (section 3.2.3) also showed marked up-regulation on the mRNA level. This discrepancy between very high transcript occurrence and a total lack of response on extracellular protein level might either be a temporal effect, or it might be the consequence of translational repression. The 3´UTR of CCR7 mRNA was screened *in silico* for binding sites of highly expressed miRNAs in M1 macrophages, but no matches could be found. Finally, CD80, the surface marker eventually used for M1 macrophage identification, proofed to be strongly up-regulated on mRNA level, as expected.

The transcriptome analysis of the M2 polarized macrophages revealed CD23 as the most prominently up-regulated transcript (Fig. 3-11). The CD23 protein served as the M2 specific surface marker in this study. Furthermore, CD209 (DC-SIGN) was strongly up-regulated. CD23 and DC-SIGN have been shown to form a cluster on chromosome 19p13 [115] and to be inducible by IL4 [116]. Up-regulated genes with a known role in alternatively activated macrophage biology furthermore included HSD11B1 and PPARγ, which have been shown to cooperate in alternative macrophage activation [117]. Recently, transglutaminase 2 (TGM2) has been found to be the only consistent and functional M2 marker upon IL4 stimulation in a comparative study of human and mouse [118].

As these subtype-defining factors were identified in polarized macrophages that have been raised without M-CSF, it is of particular interest to note that they are in good alignment with factors found in M-CSF-generated macrophages, on condition that the same polarization stimulus is applied [112]. In the referenced publication, CD80 was identified as a M1 surface marker, while CXCL10, CXCL11, CCL5, CCR7 and IDO1 were described as M1 mRNA markers after LPS and IFNγ administration, which is in full accordance with the data gathered from the macrophages herein that were raised without M-CSF (Fig. 3-10). This analogy was less robust in M2 polarized macrophages, where PPARγ was the only shared M2 marker on mRNA level among the investigated candidates. This might be explained by the fact that in the cited study, the M2 polarization was achieved by administration of IL4 alone, whereas in our model, a combination of IL4 and IL13 was given. Hallmark IL13 inducible genes [121] could hence be detected in the M2 polarized macrophages, such as SOCS1 and the aforementioned DC-SIGN and CD23 (FCER2), which are also described as IL4-induced. While DC-SIGN is a typical marker of alternatively activated macrophages [152], CD23, the low affinity IgE receptor, has been implicated in allergy [52], a property that will be discussed later (section 4.4).
In summary, the obtained *in vitro* polarized macrophage subtypes appeared to be in good accordance with already described phenotypes.

The affirmative data on the macrophage subtype manifestation encouraged the next step, which was the miRNA profiling of the three different polarization types (M0, M1, M2). In the light of the transcriptome data (section 3.3.2), the biological variance between the samples was considered sufficiently low. However, the data gathered from the TLDA experiments (section 3.3.3) turned out to bear considerably more variation than the mRNA data, even though the same RNA samples were used. This might be due to the technical differences of the employed detection methods. The TLDA method is based on compartmentalized qPCR reactions that run in parallel in a reaction volume of 1 µl each. Gathering of the miRNA data was accomplished by performing three individual arrays per day on three different days. The time effect variance (i.e. the variance introduced by doing experiments on different days) has been described to have the most serious impact on data collection when compared to biological, between-array and within-array variation [153]. The mRNA data were collected on an Illumina HT12 Beadchip Array by probe hybridization. The mRNA samples were measured in a single run, which minimized variation due to technical inaccuracies. Furthermore, this measurement was conducted on a standardized commercial platform (MFT

Services, Tübingen). Additionally, while 2119 differential genes were extracted from the transcriptome data, only 43 differential miRNAs were gathered from the TLDA experiments, which further increased variance of the miRNA data due to a lower number of measurements. Extraction of differentially regulated miRNAs and putative mRNA interaction partners therefore required extensive bioinformatic analyses. This work was done by Dr. Annalisa Marsico, assisted by Dr. Brian Caffrey, as part of a cooperation (Max Planck Institute for Molecular Genetics, Berlin).

Due to the technical challenge of extracting significantly regulated miRNAs from the array data, each potential candidate was individually validated by qPCR. As a result, hsa-miR-146a-5p, hsa-miR-146b-5p, hsa-miR-155-5p and hsa-miR-187-3p were shown to be up-regulated in M1 polarized macrophages, whereas hsa-miR-193b-3p and hsa-miR-511-5p were up-regulated in M2 macrophages (Fig. 3-16 and 3-17).

The evaluation of hsa-miR-34c-5p was complicated by very low or undetectable amounts in individual donor isolates. While this miRNA could be shown to be responsive to the M2 stimulus in individual samples (Fig. 3-18), the effect across all probed samples was volatile and not conclusive. In qPCR, its reliable detection required a pre-cycling step for the pre-amplification of starting material (section 3.3.4). Hypothetically, this miRNA, if present, is subjected to down-regulation upon the M2 stimulus, but this effect apparently depends on its physiologic expression value, which seems to fluctuate between donors.

4.2 The effect of microRNAs on the polarization of macrophages

The hsa-miR-146 family and hsa-miR-155-5p are very well known and broadly studied miRNAs that are centrally implicated in the immune response. In macrophages, TLR4 stimulation leads to the subsequent downstream activation of NFκB, amongst others [154]. Both miR-146a/b and hsa-miR-155-5p are NFκB-induced upon TLR4 signalling [155, 156]. These miRNAs have been shown to act in a two-tier model of dampening the pro-inflammatory immune response. While hsa-miR-146a/b contributes to subduing sub-inflammatory levels of TLR4 signalling by targeting TRAF6, IRAK1 and IRAK2, hsa-miR-155-5p is only up-regulated at supra-threshold TLR4 activity levels. It is hypothesized to take over the role of hsa-miR-146a/b, dampening TLR4 signalling by targeting TAB2 [141]. This

would make hsa-miR-155-5p, rather than hsa-miR-146a/b, the dominant negative regulator of NFκB-dependent inflammatory responses.

In addition to their role in the inflammatory context, hsa-miR-146a-5p and hsa-miR-155-5p are crucial contributors to the maturation of macrophages from hematopoietic stem cells (HSC). During lymphomyeloid development, high amounts of the Ets family transcription factor PU.1 have been shown to induce differentiation to macrophages [157]. It has recently been shown that PU.1 exerts its role in macrophage maturation at least partly via inducing hsa-miR-155-5p and hsa-miR-146a-5p [158]. Additionally, PU.1 has been shown to be a direct target of hsa-miR-155-5p, thereby implying a negative feedback mechanism [159]. In summary, hsa-miR-146a-5p and hsa-miR-155-5p seem to substantially contribute to both macrophage development and macrophage activation by inflammatory mediators.

hsa-miR-155-5p has furthermore been crucially implicated in macrophage polarization. IL13Rα1 (see section 1.2.1) has been shown to be a direct target of hsa-miR-155-5p. Via regulation of receptor expression, hsa-miR-155-5p can thus modulate pathways that are central to the M2 polarization process, most prominently the STAT6 pathway. Accordingly, STAT6 phosphorylation was shown to be significantly decreased after hsa-miR-155-5p overexpression, and this effect was shown to be caused by down-regulation of IL13Rα1 [121]. As a consequence, the transcriptional profile of M2 polarized macrophages was markedly altered, which strongly suggested a pivotal role of hsa-miR-155-5p in balancing the M1/M2 macrophage polarization spectrum.

As the hsa-miR-146 family and hsa-miR-155-5p have already been extensively studied by many different groups, the comparatively unknown remaining miRNA candidates were put into the focus of the target screening experiments in this study.

The hsa-miR-511-5p has been reported to be present in two copies in the genome, which were originally described to be harboured by MRC1 and MRC1L1 in intron 5, respectively [120]. While MRC1L1 was up-regulated in M2-polarized macrophages (Appendix), MRC1 was not. This is in accordance with the dismissal of MRC1 (CD206) as an M2 surface marker (section 3.2.3). The observed up-regulation of hsa-miR-511-5p thus seems to be dependent solely on concomitant MRC1L1 expression, which is also suggested by an equal magnitude of regulation upon M2 stimulus (Fig. 3-17 and 3-19). MRC1 and MRC1L1 were originally annotated as paralogues, i.e. two genes that arose from segment duplication. However, as of August 2013, an annotation information available for gene ID 4360 (MRC1) on NCBI states

the following: "In July 2010, the Genome Reference Consortium determined that the region contains a duplication error. Two of the clones on which MRC1L1 was based (AL928580, BX255924) will be removed from the reference assembly and only MRC1 will be present in the assembly. [28 Apr 2011]". In the luciferase reporter assay, no functional relation between MRC1 and hsa-miR-511-5p could be established (Fig. 3-22), so it was excluded from further experimentation.

The most prominently regulated miRNA in the M2 subtype was found to be hsa-miR-193b-3p, which has already been described to be up-regulated in IL4-stimulated human blood-derived macrophages [88]. Little is known about its role in macrophages, though. It was mentioned to indirectly regulate CCL2 mRNA levels in the THP-1 cell line as a side note in a study on miRNA expression in adipose tissue, which implicates its potential in inflammatory recruitment [160]. Its main function, however, seems to lie in tumour suppression [161-163]. As proliferative diseases were not central to the present thesis, the hsa-miR-193b-3p was no longer pursued.

Even though hsa-miR-34c-5p is also primarily described as tumour-suppressive [164, 165], it has, unlike hsa-miR-193b-3p, some putative targets that are vitally implicated in macrophage biology, namely Krueppel-like factor 4 (KLF4) and Peroxisome proliferator-activated receptor gamma (PPARγ) (Table 3-1). As described (section 3.2.1), STAT6 is one of the central signalling molecules of the M2 response. Downstream of STAT6, KLF4 and PPARγ have been described to be critically involved in alternative macrophage activation. In a mouse model of alternative macrophage activation, PPARγ has been shown to inhibit IL6 production, which is central to the M1 polarization programme [166]. KLF4, the other putative hsa-miR-34c-5p target, is a zinc finger class transcription factor. It is suggested to be a central regulator of the M2 polarization programme, as it negatively regulates recruitment of co-activators of NFκB, p300 and PCAF, in murine RAW264 cells, thereby inhibiting the M1 polarization programme. Accordingly, $KLF4^{-/-}$ macrophages exhibit enhanced M1 polarization. In addition to sequestration of NFκB co-factors, KLF4 has been shown to cooperatively bind with pSTAT6 at the PPARγ promoter and induce transcription [135]. This may further promote the M2 polarization status, given the important role of PPARγ in alternative macrophage activation.

Altogether, KLF4 and PPARγ are, at least in mice, central promoters of the M2 response, and both were predicted to be regulated by hsa-miR-34c-5p. In both cases, the detected decrease of luminescence was significant and of a magnitude of approximately 40 % (Fig. 3-22). The

relevance of this observation has to be carefully evaluated in the given context, since hsa-miR-34c-5p was not convincingly regulated upon M2 stimulation as shown by the TLDA analyses and the subsequent validation experiment (section 3.3.4).

The hsa-miR-187-3p turned out to be the miRNA with the most robust perspective of involvement in macrophage biology. It was reliably and stably induced upon M1 polarization and predicted to regulate targets that are in part relevant for macrophage organization and function. Its scientific coverage is scarce. One of its few known targets is Disabled homolog-2 (Dab2) [167], a mitogen-responsive phosphoprotein. It has been shown to interact with Grb2, thereby competing with son of sevenless (SOS), a GTP exchanger for RAS [125] . This displacement potentially influences the Ras/Raf pathway [168]. In turn, this pathway and Grb2 have been described to be linked to SH2B2 (APS) [125], a scaffold protein that bears a Pleckstrin Homology (PH) domain, a Shc homology 2 (SH2) domain and a tyrosine phosphorylation site. While the PH domain enables SH2B2 to bind to membrane-associated phosphatidylinositol-4,5-bisphosphate [169], it can bind the signalling molecule Grb2 upon tyrosine phosphorylation. Here, SH2B2 was identified as a possible target of hsa-miR-187-3p (section 3.4.1.2). Assuming that hsa-miR-187-3p could target the described signalling pathway from more than one angle (Fig. 4-1) supported the likelihood of a functional and conserved interaction of hsa-miR-187-3p and SH2B2, as it was bioinformatically predicted (see section 3.4.1). This hypothesis could be solidified by luciferase reporter experiments (Fig. 3-20) and the documentation of native SH2B2 transcript decrease after hsa-miR-187-3p transfection (Fig. 3-24). In a published screen of hematopoietic cell lines, SH2B2 was only found in Burkitt´s Lymphoma-derived B cells, where it was described to be tyrosine-phosphorylated upon B cell receptor stimulation. The interaction of the BCR and SH2B2 is enabled by the membrane localization of SH2B2 via its PH domain. Growth-factor-receptor bound-2 (Grb2) associates with SH2B2 after activation, while Src-homology-2 containing (Shc) binds irrespective of the activation state. Both factors are adaptor molecules that are situated upstream of the Ras signalling pathway. Thus, it was hypothesized that SH2B2 couples the B cell receptor to the Ras signalling cascade [125]. Additionally, SH2B2 was found to be tyrosine-phosphorylated in response to platelet-derived growth factor (PDGF), insulin-like growth factor (IGF) and granulocyte-macrophage colony stimulating factor (GM-CSF) in a human osteosarcoma cell line [126]. The role of SH2B2 in insulin signalling and regulation of insulin receptor protein expression has been tentatively described but remains elusive. SH2B2 can associate with the tri-phosphorylated insulin receptor, and SH2B2

kockout mice display enhanced insulin sensitivity [170]. Initially, this was attributed to SH2B2-mediated ubiquitination of insulin receptor by recruitment of c-Cbl [171]. However, this observation did not hold true in a more recent study [172]. While SH2B2 does seem to be able to negatively regulate sensitivity to insulin [170], this process does not appear to involve regulation of insulin receptor protein expression [173].

Another recent study suggests that SH2B2 can homodimerize (or heterodimerize with SH2-B) and then bind JAK2 by SH2 domain – pTyr813 interaction, yielding a heterotetrameric complex of JAK2-$(SH2B2)_2$-JAK2. Accordingly, while activation of JAK2 could be achieved by stimulating the growth hormone receptor, it could be further increased by SH2B2 overexpression. This was attributed to transactivation that was enabled by the close spatial proximity of two JAK2 molecules in the tetrameric complex [127]. Downstream signalling of JAK2 then includes STAT5 dimerization, which drives the induction of gene expression depending on the cellular context.

The importance of SH2B2 in macrophage biology remains elusive. On the protein level, regulation of SH2B2 by hsa-miR-187-3p could not be conclusively shown in this work. This was in part due to the restricted number of suitable available antibodies. Issues with specificity and signal intensity precluded a robust assessment of SH2B2 protein expression. Still, a significant impact of hsa-miR-187-3p on SH2B2 mRNA was detectable. If this phenomenon extends to cells which at least partially rely on SH2B2 for Ras/Raf signalling, e.g. B lymphocytes, hsa-miR-187-3p could be a negative regulator of this pathway by targeting both Dab2 and SH2B2, thereby modulating downstream signalling events, e.g. the phosphorylation of ERK.

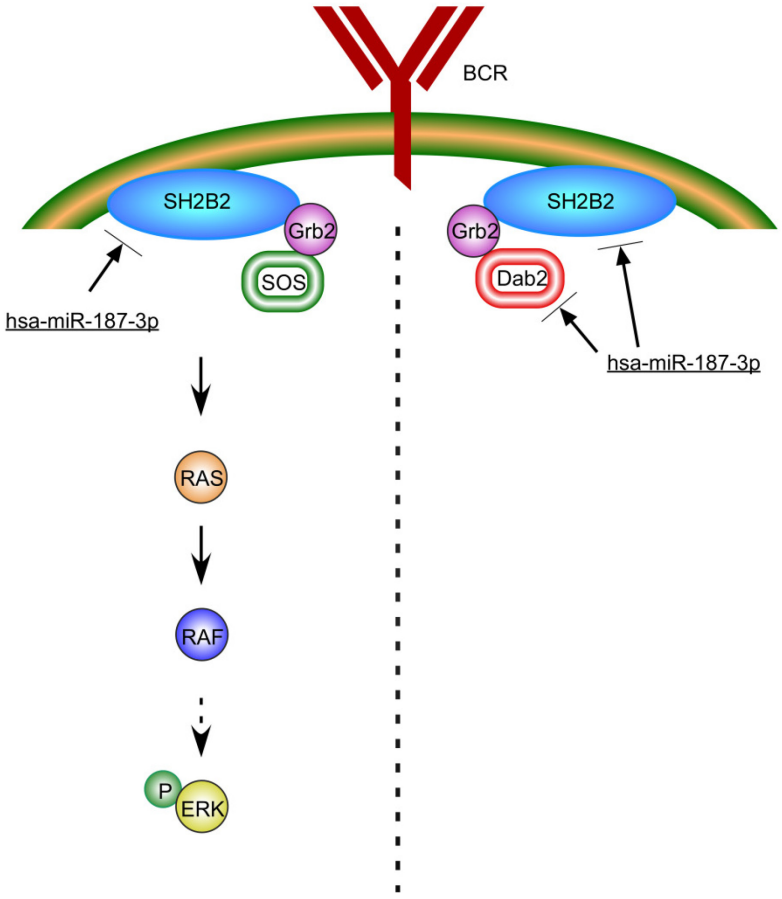

Figure 4-1: Hypothetical regulation of the BCR signalling pathway by hsa-miR-187-3p. Dab2, a validated target of hsa-miR-187-3p, has been proposed to be a negative regulator of the RAS/RAF pathway by displacing SOS from Grb2. SOS is a GTP exchanger for RAS, and its replacement by Dab2 shuts down RAS/RAF signalling. The C-terminal tyrosine phosphorylation site of SH2B2 is a docking site for Grb2, while the membrane localization of SH2B2 is mediated by its PH domain. SH2B2 is hypothetically required to link the BCR to the RAS/RAF signalling pathway. Targeting of either Dab2 or SH2B2 by hsa-miR-187-3p might thus be positively (Dab2) or negatively (SH2B2) influencing the BCR-RAS/RAF signalling axis.

In contrast to SH2B2, another predicted target of hsa-miR-187-3p, LAMP2, appeared to be of greater importance in the context of macrophage biology. Furthermore, the synergetic regulation of the LAMP2 reporter plasmid by hsa-miR-155-5p and hsa-miR-187-3p made it an interesting target also from a mechanistic point of view. As outlined above (see section 3.4.2.1), LAMP2 is a structural component of the lysosomal membrane, and it is hypothesized to work as a trans-membrane transporter [124]. It possesses three splice variants (LAMP2A, B and C). While isoform A and C both carry the hsa-miR-155-5p and hsa-miR-187-3p target

sites, LAMP2B is devoid of these sites and thus not a candidate for miRNA-directed regulation. All three isoforms have identical aminoterminal domains facing the endosomal lumen, but their cytosolic domains differ [174]. In terms of function, LAMP2A has been implicated in chaperone-mediated autophagy by mediating protein uptake into lysosomes together with heat shock protein 70 (hsc70) [175]. LAMP2C, on the other hand, has been shown to bind DNA and RNA for lysosomal uptake, a process which is part of a phenomenon that has been termed DNautophagy or RNautophagy, respectively. This mechanism has been hypothesized to make exogenous nucleic acids accessible for immune receptors such as TLR3, TLR7 and TLR9, as their nucleic acid sensing domains face toward the endosomal compartment [176].

As LAMP2B does not contain the miRNA binding sites of interest, and LAMP2C was found to be very weakly expressed in macrophages, LAMP2A was assayed for miRNA-induced regulation. On the mRNA level, no regulation could be seen upon miRNA overexpression after 24 h and 48 h (Fig. 3-25). Since the luciferase reporter assay strongly suggested an effect of hsa-miR-187-3p and hsa-miR-155-5p (Fig. 3-20), a further method was employed to show a regulatory effect on native LAMP2 transcript. A global transcriptional stop was enforced by application of actinomycin D, a synthetic cytostatic. Naturally, a decrease of transcript amount ensues because of the inherent half-life of each mRNA molecule. It has been published before that the additional administration of miRNAs can enhance specific mRNA degradation [138]. However, this approach showed no impact of either miRNA on LAMP2A transcript levels (Fig. 3-27). This might be due to the highly stable nature of the LAMP2A mRNA, as it withstands degradation under the influence of actinomycin D for at least 4 h. TNFα transcript, which was used as a positive control for actinomycin D potency, was massively down-regulated after 90 min of treatment (Fig. 3-26).

As miRNAs can also exert their function through translational silencing, LAMP2 was addressed on the protein level. The half-life of LAMP2 protein has been shown to be 48 h [140]. At this time-point after transfection, LAMP2 protein levels were investigated. No regulation of LAMP2 could be detected by western blot after transfection of hsa-miR-155-5p, hsa-miR-187-3p, or both (Fig. 3-28, 3-29). This might be due to the three LAMP2 isoforms A, B and C. The antibody used to detect LAMP2 by western blot binds both the LAMP2A and LAMP2B isoform. As LAMP2B does not possess binding sites for hsa-miR-187-3p and hsa-miR-155-5p, it might mask changes of LAMP2A protein amount that potentially occur in the wake of miRNA overexpression.

As an alternative to the western blot procedure, LAMP2 amount and cellular distribution were displayed by immunofluorescence microscopy (Fig. 3-30). In order to provide an additional molecular context for the regulation to take place, M1 polarized macrophages were included. While visual quantification of LAMP2 signal revealed no response to either hsa-miR-155-5p or hsa-miR-187-3p overexpression or polarization, the localization of LAMP2 was altered in M1 polarized cells. This effect has to be attributed to a change in cell morphology that was routinely observed upon M1 polarization. It is thus most likely a consequence of cellular behaviour and not induced by specific miRNA properties. Still, the enforced re-localization of LAMP2 in polarized macrophages might obscure changes in protein amount and distribution.
Following the actinomycin D mRNA degradation study, a similar approach could be taken to investigate degradation of LAMP2 on the protein level. The massive glycosylation of LAMP2 confers protection against the constant acidic exposure in the lysosomal lumen. Administration of endoglycosidase H cleaves asparagine-linked oligosaccharides from lysosomal membrane proteins, which leads to their rapid decomposition [124]. In such a setup, the effect of hsa-miR-187-3p and hsa-miR-155-5p on translation of the LAMP2 transcript could be closely monitored. Assuming that LAMP2 transcript is targeted by hsa-miR-155-5p and hsa-miR-187-3p, as suggested by the reporter assay, degradation of the LAMP2 protein would occur faster in the presence of these two miRNAs, as replenishment of protein would be impaired due to translational inhibition.
In conclusion, no decisive effect of the studied miRNAs on macrophage biology in the context of polarization could be shown. While hsa-miR-187-3p seems to be able to down-regulate SH2B2 transcript to a significant extent, this observation lacks perspective in the context of macrophage biology so far. On the other hand, LAMP2, which has been implicated in central aspects of macrophage organization, turned out to be completely irresponsive to miRNA treatment both on protein and mRNA level, even though the reporter system strongly suggests otherwise. This illustrates that the luciferase reporter system is only of limited value for the identification of *bona fide* miRNA targets. The introduction of putative miRNA – sensitive sequences into the *Renilla* luciferase transcript seems to only partially mimic the regulation of the native target mRNA by miRNA. One aspect limiting the value of the reporter system as it was used in this work is the, in most cases, incomplete 3´UTR that was introduced into the *Renilla* luciferase transcript. The sequences were truncated to various degrees (Table 2-1) and thus lacked binding sites for collateral miRNAs that are present in the native transcript and might be targeted under physiologic circumstances. An additional obstacle that precludes direct transfer of an observation from the reporter assay into the native

cell is the secondary RNA structure. The accessibility of the 3´UTR might be decreased in the native target transcript due to e.g. hairpin structures, while an exposed *Renilla* luciferase 3´UTR might accommodate miRNA binding. Site accessibility has been shown to be as important as seed sequence match for the determination of miRNA efficiency [177]. As a consequence, it should be avoided to use truncated 3´UTR sequences for the design of further reporter vectors.

An additional limiting aspect of the chosen approach is the multitude of regulatory mechanisms that any mRNA is subjected to. The miRNA target prediction on the basis of the miRNA and mRNA array data relied in part on down-regulation of transcript. In case of parallel up-regulation of putatively specific miRNAs, this combined observation was interpreted as a potential regulatory mechanism. However, there are other factors besides miRNAs that determine mRNA stability. Tristetraprolin, or zinc finger protein 36 (ZFP36), has been described to bind AU rich elements in the 3´UTR of mRNA, thereby causing de-adenylation and enhanced transcript degradation. TNFα is a well-known target of ZFP36 [178], which is why TNFα was used as an indicator of actinomycin D potency (Fig. 3-26). In accordance with literature [179], M1-polarized macrophages showed a slight up-regulation of ZFP36 (Appendix), thereby potentially accounting for subtle down-regulation of transcript. These unmonitored regulatory events that invariably occur in the chosen system might both obscure or exaggerate miRNA effects on any given mRNA.

4.3 Macrophage polarization phenotypes are known to differentially influence asthma pathogenesis

Building on the human *in vitro* - generated macrophage polarization profiles, I aimed to categorize macrophage subtypes that were isolated from murine lungs in a model of eosinophilic airway inflammation. As outlined above (section 4.1), GM-CSF plays a crucial role in macrophage activation, and is particularly important for alveolar macrophage homeostasis. It has been hypothesized that a shift toward an M-CSF dominated environment in the wake of allergic bronchial inflammation could change the activation status of alveolar macrophages in the lung [180]. Macrophages both require and promote a distinct microenvironment, and their activation status is the product of this delicate interplay. In the T_H2 dominated environment of an eosinophilic lung inflammation, alveolar macrophages

have been described to further skew the immune response toward the T_H2 axis and thereby promote lung eosinophilia [50, 59, 181]. A series of studies in two different rat strains could identify the cytokine secretion of alveolar macrophages as a possible reason for the different susceptibility to allergic asthma as observed in these strains [182, 183]. While the Brown Norway strain (BN) shares many features of human allergic asthma upon allergen challenge, Sprague Dawley rats (SD) do not develop allergic asthma. It was hypothesized that different patterns of cytokines that are secreted by alveolar macrophages are the cause of this differential susceptibility. Alveolar macrophages from SD rats were shown to produce more TNFα in comparison to BN rats, while the latter produce more IL10 and IL13. In the case of TNFα, the T_H1 impact on the local immune response is suggested to protect SD rats against asthma, while the T_H2 skew provoked by IL10 and IL13 is thought to predispose BN rats to allergic airway inflammation. Along this line of reasoning, it was shown that adoptively transferred alveolar macrophages from SD rats could attenuate airway hyper-responsiveness upon OVA challenge in BN rats [183]. As this effect was attributed to the macrophage activation status, a consecutive study was performed that addressed the crosstalk of lung microenvironment and alveolar macrophages. It was shown that *ex vivo* culture of alveolar macrophages from allergic lungs of BN rats could reduce airway hyper-responsiveness (AHR) upon re-introduction into the lung. This effect was attributed to the withdrawal of the T_H2 skewed lung microenvironment. *Ex vivo* culture was shown to induce the T_H1 cytokines IFNγ and IL12p40 in alveolar macrophages. Instillation of these re-programmed macrophages protected BN rats against development of AHR [61]. In summary, these studies strongly suggest an influence of the macrophage subtype on the manifestation of allergic airway inflammation that depends on the polarization status.

A study in mice further stressed the importance of the T_H1 and T_H2 dichotomy in the development of AHR. It was reported that an OVA pulse combined with an inflammatory mediator (IFNγ) increased the antigen presenting capacities of lung macrophages. This skewed the T cell response toward the T_H1 axis, thus weakening the T_H2 inflammation that drives AHR [184]. This observation is of particular interest since it was described before that OVA-sensitization alone seems to eliminate the protective role of alveolar macrophages in AHR [59]. The additional IFNγ stimulus seems to vitally contribute to the regulatory properties of lung macrophages, most likely increasing their M1-like properties and thus enabling them to more efficiently establish a protective T_H1 environment.

The clear model of a protective (T_H1) and permissive (T_H2) microenvironment in allergic airway inflammation is not universally applicable, though. There are severe forms of asthma that are insensitive to glucocorticoid treatment and that seem to originate from a different immunological context. As outlined above, a T_H1 skew of the microenvironment can confer protection against AHR in the context of a T_H2 driven eosinophilic airway inflammation. Severe corticosteroid resistant asthma, on the contrary, has been described to be caused by classical activation of alveolar macrophages by LPS in the BALF [49, 185]. M1 polarized alveolar macrophages are thus hypothesized to play a crucial role in the exacerbation of asthma. Hence, the full extent of the macrophage polarization spectrum needs to be considered when evaluating the detrimental or beneficial effect of these cells on the different manifestations of allergic asthma.

4.4 Macrophage polarization phenotypes as defined by their microRNA profile seem to be heterogeneous in experimental asthma

The versatility of macrophages as discussed above (sections 1.2 and 1.3.2) requires a thorough investigation of marker molecules when assessing their polarization status in any given setup. The identification of prototypical human *in vitro* - derived M1 and M2 macrophages was performed on the basis of a single surface molecule (M1: CD80, M2: CD23). While those markers were suitable for macrophage isolation, they are by no means sufficient for a comprehensive subtype characterization. In spite of presenting confirmed polarization markers, cells can functionally divert from their stereotypic M1 or M2 properties. CD80, a T cell co-stimulatory molecule, has been reported to be increased on the alveolar macrophages of asthmatic subjects, enhancing their antigen presentation to T_H2 lymphocytes [186]. Thereby, they support T_H2-driven inflammation, showing that their polarization state is not *bona fide* M1. Furthermore, it was shown that the low affinity IgE receptor (CD23) is present on alveolar macrophages from healthy and asthmatic patients. While stimulation with IgE leads to the release of both pro- and anti-inflammatory cytokines, it was demonstrated that alveolar macrophages from asthmatic donors initially secrete more TNFα and less IL10 compared to their healthy counterparts, thus favouring a pro-inflammatory microenvironment in the airways and the lung [187]. This bias in the TNFα/IL10 axis is commonly associated with M1 polarized macrophages. The inflammatory nature of asthma implies a range of pro-

inflammatory mechanisms at work that dynamically shape the disease manifestation. Hence, both M1 and M2 macrophages and their dynamically shaped hybrid forms seem to contribute at different stages of the disease [49]. The pro-inflammatory nature of airway macrophages that has been described in patients with corticosteroid-resistant asthma as discussed above (section 4.3) has been documented by higher expression levels of typical M1 associated genes, such as TNFα, IL1β, IL8, CXCL1, CCL3 and CXCL2, all of which can be confirmed by the mRNA profiling experiments of the present study (Fig. 3-10 and Appendix). The proinflammatory properties of airway macrophages in severe asthma have been attributed to activation of the TNFα axis [188, 189], which is also crucially involved in classical macrophage polarization [190].

The complexity of macrophage activation in the pathogenesis of allergic airway inflammation requires in-depth analyses of subtype-defining regulatory events. As miRNAs have been shown to vitally contribute to many aspects of immunology in general and macrophage biology in particular, the global miRNA setup of alveolar and interstitial macrophages from the lungs of mice with acute OVA-induced eosinophilic airway inflammation was investigated with a special focus on their potential in macrophage polarization. In a first step, a principal component analysis was performed on the basis of the 32 most stably differentially regulated miRNAs in the investigated setup. The miRNA profile from both the alveolar and interstitial macrophages showed a certain dependency on the health situation of the animals (Fig. 3-35). This finding encouraged further investigation. To this end, three miRNAs were selected for individual validation in the interstitial macrophage samples, being mmu-miR-21a-5p, mmu-miR-126-3p and mmu-miR146a-5p. Due to material scarcity, no RNA from the alveolar macrophage fraction was left after the TLDA analyses, so validation was restricted to the interstitial macrophage pool. This revealed an opposing pattern of mmu-miR-21a-5p, which was up-regulated, and mmu-miR-126-3p, which was down-regulated (Fig. 3-36). The mmu-miR-21 has been described to target IL12p35 in T cells, thereby contributing to an attenuated T_H1 response by limiting the activation of the IL12/IFNγ axis [102]. As IL12 is an important molecule in the macrophage M1 subtype manifestation, this regulatory property of mmu-miR-21 is of particular interest when assessing the macrophage polarization status in the T_H2 dominated microenvironment of eosinophilic airway inflammation. The observed up-regulation of mmu-miR-21a-5p in the interstitial macrophage fraction (Fig. 3-34, 3-36) suggests an active suppression of M1-associated signalling pathways in these cells. This assumption is complicated, however, by the observed concomitant down-regulation of mmu-

miR-126-3p. This miRNA has been described to reduce allergic airway inflammation when antagonized by limiting the T_H2 effector function. This has been attributed to an up-regulation of the transcription factor PU.1 and a subsequent down-regulation of GATA3 upon anti-miR-126 treatment [103]. It was furthermore described that mmu-miR-126 was up-regulated in the airways of chronically OVA-challenged mice, and that antagonizing this miRNA led to reduced eosinophil recruitment [191]. In summary, antagonizing mmu-miR-126 seems to attenuate the T_H2-dominated pathogenesis of eosinophilic asthma, which is at odds with the observed down-regulation of this miRNA in the interstitial macrophage fraction from OVA-challenged mice (Fig. 3-34, 3-36). However, the observed miRNA pattern has not been described in macrophages before. PU.1 is an important transcription factor in macrophages with a broad role in both maturation and pro-inflammatory activation [192], which might exceed its function in T cells.

In order to assess the extent of M1 type pro-inflammatory activation patterns of interstitial macrophages in the acute OVA model, the regulation of the hallmark pro-inflammatory mmu-miR-146a-5p was investigated. As suggested by the TLDA analyses, it was confirmed to be down-regulated in these cells, which argues against a prototypical, fully M1-type activation, as this miRNA is described as up-regulated in M1 macrophages, as is shown in the present study in the context of *in vitro* polarized human macrophages (Fig. 3-16). For a further investigation of the miRNAs that were differentially regulated in asthma, no validation experiments of individual candidates could be performed, because the scarce RNA material was exhausted after the analyses described above. It is noteworthy, however, that more candidates are included in the list of differentially expressed miRNAs (Fig. 3-33), e.g. the mmu-miR-155-5p, which appears to be solidly up-regulated in both alveolar and interstitial macrophages, and could also be shown to be induced in M1-type macrophages (Fig. 3-16). The apparent reciprocal regulation of mmu-miR-146a-5p (down) and mmu-miR-155-5p (up) (Fig. 3-34) is of particular interest, since both miRNAs have been shown to often be co-induced [141]. If this observation can be corroborated, it might be a defining feature of eosinophilic airway inflammation.

Additionally, the let-7 family seems to be regulated in repsonse to OVA. This miRNA family has been shown to down-regulate IL13 in T cells and thereby alleviate allergic airway inflammation [193]. As they all share the same binding site in the IL13 3´UTR, there is a sterical competition. In the alveolar macrophage fraction, there seems to be OVA-induced regulation of let-7b (up) and let7c (down), while in the interstitial macrophage population, a down-regulation of let-7e can be observed (Fig. 3-33). It remains to be investigated whether

these patterns are functionally permissive of IL13 up-regulation and thereby contribute to the T_H2 - dominated condition of eosinophilic airway inflammation. As shown in the human miRNA screening experiments, hsa-let-7b is slightly induced in M2-polarized macrophages. Whether this observation can help to define the activation status of macrophages in eosinophilic asthma remains to be investigated.

In summary, the envisioned global comparison of murine miRNA profiles with their *in vitro*-derived human counterparts is currently hindered by the limited intersection of the human and murine data material. This can potentially be improved by including more mice in the study and by employing an additional model, e.g. house dust mite-induced airway inflammation. However, individual miRNAs show reliable patterns of induction or repression upon OVA challenge, as described above. These miRNAs and their role in experimental and clinical asthma as well as their contribution to macrophage polarization will be in the focus of future research.

4.5 Outlook

In order to further employ the knowledge that has been gained in this study, the question of macrophage polarization and their involvement in asthma will be addressed from additional angles. Shortcomings of the chosen approach that have been identified will thus be minimized.

The *in vitro* subtype generation of human blood-derived macrophages has some inherent limitations that hinder the application of the identified mRNA and miRNA patterns to the specimens obtained from the mouse model. Apart from the species barrier, the extreme phenotypes that were obtained by *in vitro* polarization are not likely to be present in primary lung macrophages, as the latter are shaped by the complex and volatile dynamics of an ongoing immune response. In order to more accurately mimic the situation as found in the animal model, we are planning to mix *in vitro* generated macrophage subtypes at defined percentages by cytometric sorting. This will yield hybrid populations with mixed characteristics, which will be more suitable as a reference for macrophage subtypes obtained from *in vivo* sources, because it takes sample heterogeneity into account and allows quantification thereof.

In order to complement the miRNA data from the murine model of eosinophilic airway inflammation, global mRNA profiling has been performed in order to find putative

mRNA/miRNA interaction partners as has been done in the human *in vitro* model. The data are currently being interpreted. Once available, it will constitute an additional data basis to assess the macrophage polarization status in eosinophilic asthma. Furthermore, alveolar macrophages from human healthy and asthmatic donors are currently being acquired. Their miRNA profile might be more suitable for comparison with the *in vitro* polarized human reference samples.

The investigation of direct miRNA/mRNA interaction partners by luciferase reporter assay and qPCR turned out to only scarcely shed light on the mechanisms of macrophage polarization in the chosen models. Nevertheless, miRNA expression patterns do change upon *in vitro* polarization and in *in vivo* inflammation models. In an attempt to explore the sum of miRNA-mediated regulatory events, including indirect effects, ectopic disturbance of the miRNA profile in the context of polarization was performed. To this end, unpolarized and M1 polarized macrophages were transfected with hsa-anti-miR-155-5p and hsa-pre-miR-187-3p, respectively. In the present study, both miRNAs have been found to be regulated in response to the M1 stimulus. As hsa-miR-155-5p is strongly expressed in macrophages even at basal levels, it was chosen to silence it by anti-miR application. In contrast, hsa-miR-187-3p, only weakly expressed even upon induction, was over-expressed by pre-miR administration. The resulting global impact on the mRNA profile was investigated by microarray screening. As of submittal of this thesis, the data were not fully interpreted. The analysis will focus on both direct miRNA-mediated translational control and on indirect effects. These indirect effects include, e.g., miRNA-mediated regulation of a transcription factor, which potentially has downstream effects on gene expression, or down-regulation of an inhibitor, with subsequent de-repression of an agonist. If enrichment of putative candidates in functionally linked processes can be shown, this will yield important insights into their role in cellular organization. These data will be used, if suitable, to further define the properties of polarized macrophages and to understand the underlying RNA-based mechanisms.

The effect of a given miRNA on cellular biology has to ultimately be shown on the protein level. Identification of individual targets by Western Blot, as attempted in this study, could be too narrow-focused in some cases, as it might miss important secondary effects. This problem might be addressed by a proteomics approach, e.g. 2D gel electrophoresis, which visualizes the composition of heterogeneous protein samples by a combined approach of isoelectric focussing and gel electrophoresis. Changes in the characteristic protein pattern after miRNA over-expression or silencing (as employed above) can then be interpreted by use of annotation databases (like UniProt-GOA).

In summary, the envisioned approaches might help to identify the polarization status of macrophages collected from the lungs of mice within the model of OVA-induced airway inflammation, and from the BAL fluid of healthy and asthmatic human donors. Knowledge about the physiologic and disease-driven polarization state of primary lung macrophages might provide clues on their involvement in asthma and on how to ameliorate disease progression by manipulating macrophage subtype manifestation.

Appendix

Table 1: Gene expression profiles of M1 vs. M0 macrophages, ranked by expression value

Gene	Description	log2 fold change vs. M0	P-value	Rank
IDO1	indoleamine 2,3-dioxygenase 1	9.95	1.80E-09	1
CXCL9	chemokine (C-X-C motif) ligand 9	9.54	8.41E-10	2
EBI3	Epstein-Barr virus induced 3	8.37	2.29E-09	3
CD38	CD38 molecule	8.20	9.44E-09	4
IL1B	interleukin 1, beta	8.16	1.25E-09	5
IL6	interleukin 6 (interferon, beta 2)	7.72	2.38E-06	6
CCL1	chemokine (C-C motif) ligand 1	7.43	5.07E-05	7
CCL5	chemokine (C-C motif) ligand 5	7.24	2.34E-08	8
LOC730249	PREDICTED: Homo sapiens similar to Immune-responsive protein 1 (LOC730249), mRNA.	7.24	2.02E-07	9
CCL8	chemokine (C-C motif) ligand 8	7.09	3.33E-06	10
CCR7	chemokine (C-C motif) receptor 7	6.96	5.95E-07	11
IL7R	PREDICTED: Homo sapiens interleukin 7 receptor (IL7R), mRNA.	6.94	1.35E-06	12
CFB	complement factor B	6.82	1.63E-07	13
PTGS2	prostaglandin-endoperoxide synthase 2 (prostaglandin G/H synthase and cyclooxygenase)	6.79	4.64E-08	14
ISG20	interferon stimulated exonuclease gene 20kDa	6.77	5.44E-08	15
IFI27	interferon, alpha-inducible protein 27	6.62	6.34E-05	16
CCL20	chemokine (C-C motif) ligand 20	6.52	2.63E-07	17
MCOLN2	mucolipin 2	6.51	3.56E-08	18
SLAMF1	signaling lymphocytic activation molecule family member 1	6.34	9.52E-07	19
ANKRD22	ankyrin repeat domain 22	6.31	5.44E-08	20
UBD	ubiquitin D	6.29	4.79E-07	21
NFS1	NFS1 nitrogen fixation 1 homolog (S. cerevisiae)25	6.28	2.34E-08	22
GBP5	guanylate binding protein 5	6.25	2.19E-06	23
HSD11B1	hydroxysteroid (11-beta) dehydrogenase 1	6.24	5.96E-07	24
IFI44L	interferon-induced protein 44-like	6.12	1.93E-07	25
GBP4	guanylate binding protein 4	5.95	2.33E-07	26
ADORA2A	adenosine A2a receptor	5.63	5.06E-08	27
PTGES	prostaglandin E synthase	5.62	1.51E-05	28
CCL19	chemokine (C-C motif) ligand 19	5.62	2.40E-07	29
TNIP3	TNFAIP3 interacting protein 3	5.61	5.44E-08	30
IL2RA	interleukin 2 receptor, alpha	5.45	9.52E-07	31
TNFAIP6	tumor necrosis factor, alpha-induced protein 6	5.42	1.29E-06	32

CRISPLD2	cysteine-rich secretory protein LCCL domain containing 2	5.38	2.13E-07	33
LAMP3	lysosomal-associated membrane protein 3	5.35	5.74E-05	34
CXCL10	chemokine (C-X-C motif) ligand 10	5.32	3.25E-06	35
CA12	carbonic anhydrase XII	5.30	1.67E-07	36
G0S2	G0/G1switch 2	5.21	5.48E-07	37
STAT4	signal transducer and activator of transcription 4	5.17	1.70E-05	38
IFITM3	interferon induced transmembrane protein 3 (1-8U)	4.99	0.0003	39
OSM	oncostatin M	4.95	6.90E-06	40
MUCL1	mucin-like 1	4.89	0.0028	41
PDE4B	phosphodiesterase 4B, cAMP-specific (phosphodiesterase E4 dunce homolog, Drosophila)	4.88	7.40E-06	42
CXCL2	chemokine (C-X-C motif) ligand 2	4.85	6.85E-06	43
CD80	CD80 molecule	4.84	4.39E-07	44
CYP26A1	cytochrome P450, family 26, subfamily A, polypeptide 1	4.77	2.33E-07	45
TNF	tumor necrosis factor (TNF superfamily, member 2)	4.73	3.85E-05	46
IL27	interleukin 27	4.72	5.37E-07	47
IL12B	interleukin 12B (natural killer cell stimulatory factor 2, cytotoxic lymphocyte maturation factor 2, p40)	4.71	0.0005	48
SOD2	superoxide dismutase 2, mitochondrial	4.66	8.83E-07	49
GCH1	GTP cyclohydrolase 1	4.66	2.75E-06	50
IL8	interleukin 8	3.84	0.0001	76
CXCL1	chemokine (C-X-C motif) ligand 1 (melanoma growth stimulating activity, alpha)	3.69	1.71E-05	88
CCL3	chemokine (C-C motif) ligand 3	3.07	1.70E-05	128
CXCL11	chemokine (C-X-C motif) ligand 11	2.65	0.0007	177
ZFP36	zinc finger protein 36, C3H type, homolog (mouse)	1.48	0.0046	465

Table 2: Gene expression profiles of M2 vs. M0 macrophages, ranked by expression value

Gene	Description	log2 fold change vs. M0	P-value	Rank
FCER2	Fc fragment of IgE, low affinity II, receptor for (CD23)	6.08	1.34E-04	1
CH25H	cholesterol 25-hydroxylase	5.29	3.94E-05	2
CD209	CD209 molecule	5.28	1.55E-03	3

MMP12	matrix metallopeptidase 12 (macrophage elastase)	4.70	3.94E-05	4
HOPX	HOP homeobox	4.68	2.26E-03	5
RAMP1	receptor (G protein-coupled) activity modifying protein 1	4.47	2.36E-04	6
FCGR2B	Fc fragment of IgG, low affinity IIb, receptor (CD32)	3.89	1.74E-04	7
CCL4L2	Homo sapiens chemokine (C-C motif) ligand 4-like 2 (CCL4L2), mRNA.	3.84	2.63E-04	8
GUCA1A	guanylate cyclase activator 1A (retina)	3.81	3.94E-05	9
CCL26	chemokine (C-C motif) ligand 26	3.81	3.94E-05	10
CISH	cytokine inducible SH2-containing protein	3.80	9.02E-04	11
SOCS1	suppressor of cytokine signaling 1	3.71	1.78E-04	12
MAOA	monoamine oxidase A	3.69	3.03E-05	13
FARP1	FERM, RhoGEF (ARHGEF) and pleckstrin domain protein 1 (chondrocyte-derived)	3.62	1.63E-04	14
CTNNAL1	catenin (cadherin-associated protein), alpha-like 1	3.55	4.43E-03	15
SPINT2	serine peptidase inhibitor, Kunitz type, 2	3.54	9.09E-05	16
ESPNL	espin-like	3.51	2.02E-03	17
SLAMF1	signaling lymphocytic activation molecule family member 1	3.51	1.30E-03	18
C17orf87	Homo sapiens chromosome 17 open reading frame 87 (C17orf87), mRNA.	3.39	6.19E-04	19
ALDH1A2	aldehyde dehydrogenase 1 family, member A2	3.27	3.94E-05	20
F13A1	coagulation factor XIII, A1 polypeptide	3.25	6.80E-02	21
FAM110B	family with sequence similarity 110, member B	3.23	2.25E-04	22
FOXC1	forkhead box C1	3.23	1.34E-04	23
EFNA1	ephrin-A1	3.15	8.38E-03	24
BATF3	basic leucine zipper transcription factor, ATF-like 3	3.14	2.89E-04	25
SIGLEC10	sialic acid binding Ig-like lectin 10	3.13	2.89E-04	26
CLEC10A	C-type lectin domain family 10, member A	3.09	1.45E-02	27
FAR2	fatty acyl CoA reductase 2	2.97	2.22E-04	28
DNASE1L3	deoxyribonuclease I-like 3	2.96	1.61E-03	29
C10orf128	chromosome 10 open reading frame 128	2.93	4.34E-04	30
TGFA	transforming growth factor, alpha	2.93	3.84E-02	31
STAMBPL1	STAM binding protein-like 1	2.90	2.44E-03	32
SYT17	synaptotagmin XVII	2.89	4.53E-03	33
HSD11B1	hydroxysteroid (11-beta) dehydrogenase 1	2.84	3.59E-03	34
ACOT7	acyl-CoA thioesterase 7	2.78	2.32E-03	35
MS4A6E	membrane-spanning 4-domains, subfamily A, member 6E	2.76	1.33E-02	36

ENPP2	ectonucleotide pyrophosphatase/phosphodiesterase 2	2.73	2.01E-02	37
IRF7	interferon regulatory factor 7	2.69	1.09E-03	38
HOMER2	homer homolog 2 (Drosophila)	2.65	0.0002	39
CDH1	cadherin 1, type 1, E-cadherin (epithelial)	2.63	9.02E-04	40
FCRLB	Fc receptor-like B	2.62	0.0001	41
DACT1	dapper, antagonist of beta-catenin, homolog 1 (Xenopus laevis)	2.60	7.13E-04	42
ANPEP	alanyl (membrane) aminopeptidase	2.60	1.92E-03	43
SLC47A1	solute carrier family 47, member 1	2.59	9.78E-03	44
LIMA1	LIM domain and actin binding 1	2.57	2.25E-04	45
TRAF5	TNF receptor-associated factor 5	2.50	1.40E-03	46
PARM1	prostate androgen-regulated mucin-like protein 1	2.50	1.43E-03	47
CCL3	chemokine (C-C motif) ligand 3	2.49	0.0006	48
CCL5	chemokine (C-C motif) ligand 5	2.46	1.86E-03	49
ABCG2	ATP-binding cassette, sub-family G (WHITE), member 2	2.41	2.58E-03	50
TGM2	transglutaminase 2 (C polypeptide, protein-glutamine-gamma-glutamyltransferase)	2.12	0.0091	66
MRC1L1	mannose receptor, C type 1-like 1	2.03	0.0383	73
PPARG	peroxisome proliferator-activated receptor gamma	1.73	0.0073	100

TaqMan® Human MicroRNA Array A

	1	2	3	4	5	6	7	8	9	10	11	12	13	14	15	16	17	18	19	20	21	22	23	24
A	hsa-let-7a	hsa-let-7c	hsa-let-7d	hsa-let-7e	hsa-let-7f	hsa-let-7g	hsa-miR-1	hsa-miR-9	hsa-miR-10a	hsa-miR-10b	Mamm U6	Mamm U6	hsa-miR-15a	hsa-miR-15b	hsa-miR-16	hsa-miR-17	hsa-miR-18a	hsa-miR-18b	hsa-miR-19a	hsa-miR-19b	hsa-miR-20a	hsa-miR-20b	hsa-miR-21	hsa-miR-22
B	hsa-miR-23a	hsa-miR-23b	hsa-miR-24	hsa-miR-25	hsa-miR-26a	hsa-miR-26b	hsa-miR-27a	hsa-miR-27b	hsa-miR-28-3p	hsa-miR-28-5p	Mamm U6	Mamm U6	hsa-miR-29a	hsa-miR-29b	hsa-miR-29c	hsa-miR-30b	hsa-miR-30c	hsa-miR-31	hsa-miR-32	hsa-miR-33b	hsa-miR-34a	hsa-miR-34c-5p	hsa-miR-92a	hsa-miR-93
C	hsa-miR-95	hsa-miR-96	hsa-miR-98	hsa-miR-99a	hsa-miR-99b	hsa-miR-100	hsa-miR-101	hsa-miR-103	hsa-miR-105	hsa-miR-106a	RNU44	hsa-miR-106b	hsa-miR-107	hsa-miR-122	hsa-miR-124	hsa-miR-125a-3p	hsa-miR-125a-5p	hsa-miR-125b	hsa-miR-126	hsa-miR-127-3p	hsa-miR-127-5p	hsa-miR-128	hsa-miR-129-3p	hsa-miR-129-5p
D	hsa-miR-130a	hsa-miR-130b	hsa-miR-132	hsa-miR-133a	hsa-miR-133b	hsa-miR-134	hsa-miR-135a	hsa-miR-135b	hsa-miR-136	hsa-miR-137	hsa-miR-138	hsa-miR-139-3p	hsa-miR-139-5p	hsa-miR-140-3p	hsa-miR-140-5p	hsa-miR-141	hsa-miR-142-3p	hsa-miR-142-5p	hsa-miR-143	hsa-miR-145	hsa-miR-146a	hsa-miR-146b-3p	hsa-miR-146b-5p	hsa-miR-147b
E	hsa-miR-148a	hsa-miR-148b	hsa-miR-149	hsa-miR-150	hsa-miR-152	hsa-miR-153	hsa-miR-154	hsa-miR-181a	hsa-miR-181c	hsa-miR-182	RNU48	hsa-miR-183	hsa-miR-184	hsa-miR-185	hsa-miR-186	hsa-miR-187	hsa-miR-188-3p	hsa-miR-190	hsa-miR-191	hsa-miR-192	hsa-miR-193a-3p	hsa-miR-193a-5p	hsa-miR-193b	hsa-miR-194
F	hsa-miR-195	hsa-miR-196b	hsa-miR-197	hsa-miR-198	hsa-miR-199a-5p	hsa-miR-199a-3p	hsa-miR-199b-5p	hsa-miR-200a	hsa-miR-200b	hsa-miR-200c	hsa-miR-202	hsa-miR-203	hsa-miR-204	hsa-miR-205	hsa-miR-208b	hsa-miR-210	hsa-miR-214	hsa-miR-215	hsa-miR-216a	hsa-miR-216b	hsa-miR-217	hsa-miR-218	hsa-miR-219-5p	hsa-miR-221
G	hsa-miR-222	hsa-miR-223	hsa-miR-224	hsa-miR-296-3p	hsa-miR-296-5p	hsa-miR-299-3p	hsa-miR-299-5p	hsa-miR-301a	hsa-miR-301b	hsa-miR-302a	ath-miR-159a	hsa-miR-302b	hsa-miR-302c	hsa-miR-320	hsa-miR-323-3p	hsa-miR-324-3p	hsa-miR-324-5p	hsa-miR-326	hsa-miR-328	hsa-miR-329	hsa-miR-330-3p	hsa-miR-330-5p	hsa-miR-331-3p	hsa-miR-331-5p
H	hsa-miR-335	hsa-miR-337-5p	hsa-miR-338-3p	hsa-miR-339-3p	hsa-miR-339-5p	hsa-miR-340	hsa-miR-155	hsa-let-7b	hsa-miR-342-3p	hsa-miR-342-5p	hsa-miR-345	hsa-miR-361-5p	hsa-miR-362-3p	hsa-miR-362-5p	hsa-miR-363	hsa-miR-365	hsa-miR-367	hsa-miR-369-3p	hsa-miR-369-5p	hsa-miR-370	hsa-miR-371-3p	hsa-miR-372	hsa-miR-373	hsa-miR-374a
I	hsa-miR-374b	hsa-miR-375	hsa-miR-376a	hsa-miR-376b	hsa-miR-377	hsa-miR-379	hsa-miR-380	hsa-miR-381	hsa-miR-382	hsa-miR-383	hsa-miR-409-5p	hsa-miR-410	hsa-miR-411	hsa-miR-422a	hsa-miR-423-5p	hsa-miR-424	hsa-miR-425	hsa-miR-429	hsa-miR-431	hsa-miR-433	hsa-miR-449a	hsa-miR-449b	hsa-miR-450a	hsa-miR-450b-3p
J	hsa-miR-450b-5p	hsa-miR-451	hsa-miR-452	hsa-miR-453	hsa-miR-454	hsa-miR-455-3p	hsa-miR-455-5p	hsa-miR-483-5p	hsa-miR-484	hsa-miR-485-3p	hsa-miR-485-5p	hsa-miR-486-3p	hsa-miR-486-5p	hsa-miR-487a	hsa-miR-487b	hsa-miR-488	hsa-miR-489	hsa-miR-490-3p	hsa-miR-491-3p	hsa-miR-491-5p	hsa-miR-493	hsa-miR-494	hsa-miR-495	hsa-miR-496
K	hsa-miR-499-3p	hsa-miR-499-5p	hsa-miR-500	hsa-miR-501-3p	hsa-miR-501-5p	hsa-miR-502-3p	hsa-miR-502-5p	hsa-miR-503	hsa-miR-504	hsa-miR-505	hsa-miR-507	hsa-miR-508-3p	hsa-miR-508-5p	hsa-miR-509-5p	hsa-miR-510	hsa-miR-512-3p	hsa-miR-512-5p	hsa-miR-513-5p	hsa-miR-515-3p	hsa-miR-515-5p	hsa-miR-516a-5p	hsa-miR-516b	hsa-miR-517a	hsa-miR-517c
L	hsa-miR-518a-3p	hsa-miR-518a-5p	hsa-miR-518b	hsa-miR-518c	hsa-miR-518d-3p	hsa-miR-518d-5p	hsa-miR-518e	hsa-miR-518f	hsa-miR-519a	hsa-miR-519d	hsa-miR-519e	hsa-miR-520a-3p	hsa-miR-520a-5p	hsa-miR-520d-5p	hsa-miR-520g	hsa-miR-521	hsa-miR-522	hsa-miR-523	hsa-miR-524-5p	hsa-miR-525-3p	hsa-miR-525-5p	hsa-miR-526b	hsa-miR-532-3p	hsa-miR-532-5p
M	hsa-miR-539	hsa-miR-541	hsa-miR-542-3p	hsa-miR-542-5p	hsa-miR-544	hsa-miR-545	hsa-miR-548a-3p	hsa-miR-548a-5p	hsa-miR-548b-3p	hsa-miR-548b-5p	hsa-miR-548c-3p	hsa-miR-548c-5p	hsa-miR-548d-3p	hsa-miR-548d-5p	hsa-miR-551b	hsa-miR-556-3p	hsa-miR-556-5p	hsa-miR-561	hsa-miR-570	hsa-miR-574-3p	hsa-miR-576-3p	hsa-miR-576-5p	hsa-miR-579	hsa-miR-582-3p
N	hsa-miR-582-5p	hsa-miR-589	hsa-miR-590-5p	hsa-miR-597	hsa-miR-598	hsa-miR-615-3p	hsa-miR-615-5p	hsa-miR-616	hsa-miR-618	hsa-miR-624	hsa-miR-625	hsa-miR-627	hsa-miR-628-5p	hsa-miR-629	hsa-miR-636	hsa-miR-642	hsa-miR-651	hsa-miR-652	hsa-miR-653	hsa-miR-654-3p	hsa-miR-654-5p	hsa-miR-655	hsa-miR-660	hsa-miR-671-3p
O	hsa-miR-672	hsa-miR-674	hsa-miR-708	hsa-miR-744	hsa-miR-758	hsa-miR-871	hsa-miR-872	hsa-miR-873	hsa-miR-874	hsa-miR-875-3p	hsa-miR-876-3p	hsa-miR-876-5p	hsa-miR-885-3p	hsa-miR-885-5p	hsa-miR-886-3p	hsa-miR-886-5p	hsa-miR-887	hsa-miR-888	hsa-miR-889	hsa-miR-890	hsa-miR-891a	hsa-miR-891b	hsa-miR-892a	hsa-miR-147
P	hsa-miR-208	hsa-miR-211	hsa-miR-212	hsa-miR-219-1-3p	hsa-miR-219-2-3p	hsa-miR-220	hsa-miR-220b	hsa-miR-220c	hsa-miR-298	hsa-miR-325	hsa-miR-346	hsa-miR-376c	hsa-miR-384	hsa-miR-412	hsa-miR-448	hsa-miR-492	hsa-miR-506	hsa-miR-509-3-5p	hsa-miR-511	hsa-miR-517b	hsa-miR-519c-3p	hsa-miR-520b	hsa-miR-520e	hsa-miR-520f

TaqMan® Rodent MicroRNA Array A

	1	2	3	4	5	6	7	8	9	10	11	12	13	14	15	16	17	18	19	20	21	22	23	24
A	mmu-let-7b	mmu-let-7c	mmu-let-7d	mmu-let-7e	mmu-let-7g	mmu-let-7i	mmu-miR-1	rno-miR-1	mmu-miR-7a	mmu-miR-7b	Mamm U6	Mamm U6	mmu-miR-9	mmu-miR-10a	mmu-miR-10b	mmu-miR-15a	mmu-miR-15b	mmu-miR-16	rno-miR-17-3p	mmu-miR-18a	mmu-miR-18b	mmu-miR-19a	mmu-miR-19b	mmu-miR-20a
B	mmu-miR-20b	rno-miR-20b-3p	mmu-miR-21	mmu-miR-23b	mmu-miR-24	mmu-miR-25	mmu-miR-26a	mmu-miR-26b	mmu-miR-27a	mmu-miR-27b	Mamm U6	Mamm U6	mmu-miR-28	mmu-miR-29b	mmu-miR-29c	mmu-miR-30b	mmu-miR-30c	mmu-miR-30d	mmu-miR-32	mmu-miR-34a	mmu-miR-34c	mmu-miR-93	mmu-miR-96	mmu-miR-98
C	mmu-miR-99a	mmu-miR-99b	mmu-miR-100	mmu-miR-101a	mmu-miR-103	mmu-miR-105	mmu-miR-107	mmu-miR-122	mmu-miR-124	mmu-miR-125a-3p	mmu-miR-125a-5p	mmu-miR-125b-5p	mmu-miR-126-3p	mmu-miR-126-5p	mmu-miR-127	mmu-miR-128a	mmu-miR-129-3p	mmu-miR-130a	mmu-miR-130b	mmu-miR-132	mmu-miR-133a	mmu-miR-133b	mmu-miR-134	mmu-miR-135a
D	mmu-miR-135b	mmu-miR-136	mmu-miR-137	mmu-miR-138	mmu-miR-139-3p	mmu-miR-139-5p	mmu-miR-140	mmu-miR-141	mmu-miR-142-3p	mmu-miR-142-5p	snoRNA 135	mmu-miR-145	mmu-miR-146a	mmu-miR-146b	mmu-miR-147	mmu-miR-148a	mmu-miR-148b	mmu-miR-150	mmu-miR-151-3p	mmu-miR-152	mmu-miR-153	mmu-miR-154	mmu-miR-181a	mmu-miR-181c
E	mmu-miR-182	mmu-miR-183	mmu-miR-184	mmu-miR-185	mmu-miR-186	mmu-miR-190	mmu-miR-191	mmu-miR-192	mmu-miR-193	mmu-miR-193b	mmu-miR-194	mmu-miR-195	mmu-miR-196b	rno-miR-196c	mmu-miR-197	mmu-miR-199a-3p	mmu-miR-199a-5p	mmu-miR-200a	mmu-miR-200b	mmu-miR-200c	mmu-miR-201	mmu-miR-202-3p	mmu-miR-205-5p	mmu-miR-203
F	mmu-miR-204	mmu-miR-205	mmu-miR-207	rno-miR-207	mmu-miR-208	mmu-miR-208b	mmu-miR-210	mmu-miR-211	mmu-miR-214	mmu-miR-215	snoRNA 202	mmu-miR-216a	mmu-miR-216b	mmu-miR-217	mmu-miR-218	mmu-miR-219	mmu-miR-220	mmu-miR-221	mmu-miR-222	mmu-miR-223	mmu-miR-224	mmu-miR-290-3p	mmu-miR-291a-3p	mmu-miR-291b-5p
G	mmu-miR-292-3p	mmu-miR-293	mmu-miR-294	mmu-miR-295	mmu-miR-296-3p	mmu-miR-296-5p	mmu-miR-297c	mmu-miR-297b-5p	mmu-miR-298	mmu-miR-301a	mmu-miR-301b	mmu-miR-302a	mmu-miR-302c	mmu-miR-302d	mmu-miR-320	mmu-miR-323-3p	mmu-miR-324-5p	mmu-miR-325	rno-miR-327	mmu-miR-328	mmu-miR-329	mmu-miR-330	mmu-miR-331-3p	mmu-miR-331-5p
H	rno-miR-333	mmu-miR-335-3p	mmu-miR-335-5p	rno-miR-336	mmu-miR-337-3p	mmu-miR-337-5p	mmu-miR-338-3p	mmu-miR-339-3p	rno-miR-339-3p	mmu-miR-339-5p	U87	mmu-miR-340-3p	mmu-miR-340-5p	mmu-miR-342-3p	mmu-miR-342-5p	rno-miR-343	mmu-miR-344	rno-miR-344-3p	rno-miR-344-5p	mmu-miR-345-3p	rno-miR-345-3p	mmu-miR-345-5p	mmu-miR-346	rno-miR-346
I	rno-miR-347	rno-miR-349	mmu-miR-350	rno-miR-351	mmu-miR-361	mmu-miR-362-3p	mmu-miR-363	mmu-miR-365	mmu-miR-367	mmu-miR-369-3p	mmu-miR-369-5p	mmu-miR-370	mmu-miR-375	mmu-miR-376a	mmu-miR-376b	mmu-miR-376c	mmu-miR-377	rno-miR-377	mmu-miR-379	mmu-miR-380-3p	mmu-miR-380-5p	mmu-miR-381	mmu-miR-382	mmu-miR-383
J	mmu-miR-384-3p	mmu-miR-384-5p	mmu-miR-409-3p	mmu-miR-409-5p	mmu-miR-410	mmu-miR-411	rno-miR-421	mmu-miR-423-5p	mmu-miR-425	mmu-miR-429	Y1	mmu-miR-431	mmu-miR-433	mmu-miR-434-3p	mmu-miR-434-5p	mmu-miR-448	mmu-miR-449a	mmu-miR-449b	mmu-miR-450a-5p	mmu-miR-450b-5p	mmu-miR-451	mmu-miR-453	mmu-miR-455	mmu-miR-465a-3p
K	mmu-miR-465a-5p	mmu-miR-465b-5p	rno-miR-466b	rno-miR-466c	mmu-miR-466h	mmu-miR-467a	mmu-miR-467c	mmu-miR-467d	mmu-miR-467e	mmu-miR-470	mmu-miR-484	mmu-miR-486	mmu-miR-487b	mmu-miR-489	mmu-miR-491	mmu-miR-493	mmu-miR-494	mmu-miR-495	mmu-miR-497	mmu-miR-499	mmu-miR-500	mmu-miR-501-3p	mmu-miR-503	mmu-miR-504
L	mmu-miR-505	mmu-miR-509-3p	mmu-miR-509-5p	mmu-miR-511	mmu-miR-532-3p	mmu-miR-532-5p	rno-miR-532-5p	mmu-miR-539	mmu-miR-540-3p	mmu-miR-540-5p	ath-miR-159a	mmu-miR-542-3p	mmu-miR-542-5p	mmu-miR-543	rno-miR-543	mmu-miR-544	mmu-miR-551b	mmu-miR-574-3p	mmu-miR-582-3p	mmu-miR-582-5p	mmu-miR-590-5p	mmu-miR-598	rno-miR-598-5p	mmu-miR-615-3p
M	mmu-miR-615-5p	mmu-miR-654-3p	mmu-miR-654-5p	mmu-miR-665	mmu-miR-666-5p	mmu-miR-669a	mmu-miR-671-3p	mmu-miR-672	rno-miR-673	mmu-miR-674	mmu-miR-708	mmu-miR-741	mmu-miR-742	rno-miR-742	mmu-miR-743b-3p	mmu-miR-743b-5p	mmu-miR-743a	rno-miR-743b	mmu-miR-744	rno-miR-758	rno-miR-760-5p	mmu-miR-770-3p	mmu-miR-802	mmu-miR-871
N	rno-miR-871	mmu-miR-872	mmu-miR-873	mmu-miR-874	mmu-miR-875-3p	mmu-miR-876-3p	mmu-miR-876-5p	rno-miR-878	mmu-miR-878-5p	mmu-miR-879	mmu-miR-881	rno-miR-881	mmu-miR-883a-3p	mmu-miR-883b-3p	mmu-miR-883a-5p	mmu-miR-125b-3p	mmu-miR-143	rno-miR-219-1-3p	rno-miR-219-2-3p	rno-miR-224	mmu-miR-324-3p	mmu-miR-351	rno-miR-381	rno-miR-409-5p
O	rno-miR-450a	mmu-miR-452	mmu-miR-464	mmu-miR-467b	mmu-miR-468	mmu-miR-469	mmu-miR-488	mmu-miR-490	mmu-miR-496	rno-miR-505	mmu-miR-546	mmu-miR-547	mmu-miR-652	mmu-miR-667	mmu-miR-668	mmu-miR-670	mmu-miR-675-3p	mmu-miR-675-5p	mmu-miR-676	mmu-miR-677	mmu-miR-679	mmu-miR-680	mmu-miR-682	mmu-miR-683
P	mmu-miR-684	mmu-miR-685	mmu-miR-686	mmu-miR-687	mmu-let-7a	mmu-let-7f	mmu-miR-106b	mmu-miR-155	mmu-miR-17	mmu-miR-23a	mmu-miR-29a	mmu-miR-30a	mmu-miR-30e	mmu-miR-31	mmu-miR-34b-3p	mmu-miR-92a	rno-miR-190b	mmu-miR-129-5p	mmu-miR-187	mmu-miR-188-3p	mmu-miR-106a	mmu-miR-188-5p	mmu-miR-302b	mmu-miR-322

Danksagung

Ich danke Herrn Professor Bernd Schmeck für die problemlose Finanzierung und Betreuung meiner Doktorarbeit an der Charité Berlin und an der Philipps Universität Marburg. Die mir gebotenen Entfaltungsmöglichkeiten sowie das in mich gesetzte Vertrauen trugen wesentlich zu meinem wissenschaftlichen und persönlichen Weiterkommen bei.

Weiterhin danke ich Herrn Professor Suttorp und Herrn Professor Hippenstiel, die mir an der Charité Berlin den Einstieg in meine Doktorarbeit ermöglicht haben.

Bei Herrn Professor Richard Lucius und Herrn Professor Nils Blüthgen möchte ich mich für die Übernahme der Begutachtung meiner Doktorarbeit an der Humboldt Universität zu Berlin bedanken.

Mein besonderer Dank gilt Dr. Annalisa Marsico, die mit der bioinformatischen Auswertung der erhobenen Hochdurchsatzdaten wesentlich zur Entstehung dieser Arbeit beigetragen hat.

Nicht zuletzt möchte ich meinen Arbeitskollegen für die herausragende und freundschaftliche Arbeitsatmosphäre und die wissenschaftliche Unterstützung danken. Ganz besonderes danken möchte ich hierbei Dr. Alexandra Sittka, deren Expertise und Unterstützung mir an vielen Stellen entscheidend weiter geholfen hat. Dr. Kerstin Seidel danke ich für ihre Hilfe beim Etablieren und Durchführen der Isolation von murinen Lungenmakrophagen. Christine Schulz möchte ich danken für ihre Unterstützung bei meinem Einstieg in die RNA Biologie. Elisa Jentho gebührt mein Dank für Ihre Mithilfe bei der Durchführung der LAMP2 mRNA Studie.

Abschließend danken möchte ich Ulli sowie meiner Familie, insbesondere meinen Eltern, die mir Rückhalt in allen Lebenssituationen gegeben haben und die mir diese Doktorarbeit erst ermöglicht haben.

Declaration

I hereby declare that this dissertation is the result of my own work. No other person´s work has been used without due acknowledgement. Dr. Annalisa Marsico is credited with the advanced bioinformatic expertise herein. The Principal Component Analyses I did by myself. This dissertation has not been submitted for the award of any other degree or diploma in any other institution.

Erklärung

Ich versichere hiermit, dass die von mir vorgelegte Dissertation selbstständig angefertigt wurde. Die nötige bioinformatische Expertise wurde im Rahmen einer Kooperation von Dr. Annalisa Marsico zur Verfügung gestellt. Die Hauptkomponentenanalysen habe ich selbst durchgeführt. Ich habe die Stellen der Arbeit, die anderen Werken in Wortlaut oder Sinn nach entnommen sind, in jedem Einzelfall als Entlehnung kenntlich gemacht.
Diese Dissertation wurde noch keiner anderen Fakultät zur Prüfung vorgelegt.

Marburg, 15.05.2014

Bibliography

1. Abbas, A.K., A.H. Lichtman, and S. Pillai, *Cellular and molecular immunology*. 6th ed2007, Philadelphia: Saunders Elsevier. viii, 566 p.

2. Mazo, I.B., S. Massberg, and U.H. von Andrian, *Hematopoietic stem and progenitor cell trafficking.* Trends Immunol, 2011. **32**(10): p. 493-503.

3. Ziegler-Heitbrock, L., et al., *Nomenclature of monocytes and dendritic cells in blood.* Blood, 2010. **116**(16): p. e74-80.

4. Mantovani, A., et al., *Macrophage plasticity and polarization in tissue repair and remodelling.* J Pathol, 2013. **229**(2): p. 176-85.

5. Geissmann, F., et al., *Unravelling mononuclear phagocyte heterogeneity.* Nat Rev Immunol, 2010. **10**(6): p. 453-460.

6. Tacke, F., et al., *Monocyte subsets differentially employ CCR2, CCR5, and CX3CR1 to accumulate within atherosclerotic plaques.* J Clin Invest, 2007. **117**(1): p. 185-94.

7. Cros, J., et al., *Human CD14dim monocytes patrol and sense nucleic acids and viruses via TLR7 and TLR8 receptors.* Immunity, 2010. **33**(3): p. 375-86.

8. Etzrodt, M., et al., *Regulation of monocyte functional heterogeneity by miR-146a and Relb.* Cell Rep, 2012. **1**(4): p. 317-24.

9. Fogg, D.K., et al., *A clonogenic bone marrow progenitor specific for macrophages and dendritic cells.* Science, 2006. **311**(5757): p. 83-7.

10. Liu, K., et al., *In vivo analysis of dendritic cell development and homeostasis.* Science, 2009. **324**(5925): p. 392-7.

11. Schulz, C., et al., *A lineage of myeloid cells independent of Myb and hematopoietic stem cells.* Science, 2012. **336**(6077): p. 86-90.

12. Chorro, L. and F. Geissmann, *Development and homeostasis of 'resident' myeloid cells: the case of the Langerhans cell.* Trends Immunol, 2010. **31**(12): p. 438-45.

13. Pixley, F.J., *Macrophage Migration and Its Regulation by CSF-1.* Int J Cell Biol, 2012. **2012**: p. 501962.

14. Pixley, F.J. and E.R. Stanley, *CSF-1 regulation of the wandering macrophage: complexity in action.* Trends Cell Biol, 2004. **14**(11): p. 628-38.

15. Hansson, G.K. and K. Edfeldt, *Toll to be paid at the gateway to the vessel wall.* Arterioscler Thromb Vasc Biol, 2005. **25**(6): p. 1085-7.

16. Kawai, T. and S. Akira, *The role of pattern-recognition receptors in innate immunity: update on Toll-like receptors.* Nat Immunol, 2010. **11**(5): p. 373-84.

17. Raetz, C.R. and C. Whitfield, *Lipopolysaccharide endotoxins.* Annu Rev Biochem, 2002. **71**: p. 635-700.

18. Wright, S.D., et al., *CD14, a receptor for complexes of lipopolysaccharide (LPS) and LPS binding protein.* Science, 1990. **249**(4975): p. 1431-3.

19. Doyle, S.L. and L.A. O'Neill, *Toll-like receptors: from the discovery of NFkappaB to new insights into transcriptional regulations in innate immunity.* Biochem Pharmacol, 2006. **72**(9): p. 1102-13.

20. Adhikari, A., M. Xu, and Z.J. Chen, *Ubiquitin-mediated activation of TAK1 and IKK.* Oncogene, 2007. **26**(22): p. 3214-26.

21. Morlon, A., A. Munnich, and A. Smahi, *TAB2, TRAF6 and TAK1 are involved in NF-kappaB activation induced by the TNF-receptor, Edar and its adaptator Edaradd.* Hum Mol Genet, 2005. **14**(23): p. 3751-7.

22. Wang, C., et al., *TAK1 is a ubiquitin-dependent kinase of MKK and IKK.* Nature, 2001. **412**(6844): p. 346-51.

23. Mercurio, F., et al., *IKK-1 and IKK-2: cytokine-activated IkappaB kinases essential for NF-kappaB activation.* Science, 1997. **278**(5339): p. 860-6.

24. Israel, A., *The IKK complex, a central regulator of NF-kappaB activation.* Cold Spring Harb Perspect Biol, 2010. **2**(3): p. a000158.

25. Jiang, H., M.B. Harris, and P. Rothman, *IL-4/IL-13 signaling beyond JAK/STAT.* J Allergy Clin Immunol, 2000. **105**(6 Pt 1): p. 1063-1070.

26. Junttila, I.S., et al., *Tuning sensitivity to IL-4 and IL-13: differential expression of IL-4Ralpha, IL-13Ralpha1, and gammac regulates relative cytokine sensitivity.* J Exp Med, 2008. **205**(11): p. 2595-608.

27. Hu, X., et al., *Sensitization of IFN-gamma Jak-STAT signaling during macrophage activation.* Nat Immunol, 2002. **3**(9): p. 859-66.

28. Biswas, S.K., et al., *Macrophage polarization and plasticity in health and disease.* Immunol Res, 2012. **53**(1-3): p. 11-24.

29. Steinberg, B.E., et al., *A cation counterflux supports lysosomal acidification.* J Cell Biol, 2010. **189**(7): p. 1171-86.

30. Lah, T.T., et al., *Gamma-interferon causes a selective induction of the lysosomal proteases, cathepsins B and L, in macrophages.* FEBS Lett, 1995. **363**(1-2): p. 85-9.

31. Martinez, F.O., et al., *Transcriptional profiling of the human monocyte-to-macrophage differentiation and polarization: new molecules and patterns of gene expression.* J Immunol, 2006. **177**(10): p. 7303-7311.

32. Mantovani, A., et al., *The chemokine system in diverse forms of macrophage activation and polarization.* Trends Immunol, 2004. **25**(12): p. 677-686.

33. Mosser, D.M. and J.P. Edwards, *Exploring the full spectrum of macrophage activation.* Nat Rev Immunol, 2008. **8**(12): p. 958-969.

34. Duffield, J.S., *Macrophages and immunologic inflammation of the kidney.* Semin Nephrol, 2010. **30**(3): p. 234-54.

35. Lucas, M., et al., *Apoptotic cells and innate immune stimuli combine to regulate macrophage cytokine secretion.* J Immunol, 2003. **171**(5): p. 2610-5.

36. Barron, L. and T.A. Wynn, *Fibrosis is regulated by Th2 and Th17 responses and by dynamic interactions between fibroblasts and macrophages.* Am J Physiol Gastrointest Liver Physiol, 2011. **300**(5): p. G723-8.

37. Fleming, B.D. and D.M. Mosser, *Regulatory macrophages: setting the threshold for therapy.* Eur J Immunol, 2011. **41**(9): p. 2498-502.

38. Mosser, D.M. and X. Zhang, *Activation of murine macrophages.* Curr Protoc Immunol, 2008. **Chapter 14**: p. Unit 14 2.

39. Xue, J., et al., *Transcriptome-based network analysis reveals a spectrum model of human macrophage activation.* Immunity, 2014. **40**(2): p. 274-88.

40. Jenkins, S.J., et al., *Local macrophage proliferation, rather than recruitment from the blood, is a signature of TH2 inflammation.* Science, 2011. **332**(6035): p. 1284-8.

41. Murray, P.J. and T.A. Wynn, *Protective and pathogenic functions of macrophage subsets.* Nat Rev Immunol, 2011. **11**(11): p. 723-37.

42. Hagemann, T., et al., *Ovarian cancer cells polarize macrophages toward a tumor-associated phenotype.* J Immunol, 2006. **176**(8): p. 5023-32.

43. Hagemann, T., et al., *"Re-educating" tumor-associated macrophages by targeting NF-kappaB.* J Exp Med, 2008. **205**(6): p. 1261-1268.

44. Duluc, D., et al., *Interferon-gamma reverses the immunosuppressive and protumoral properties and prevents the generation of human tumor-associated macrophages.* Int J Cancer, 2009. **125**(2): p. 367-73.

45. Gordon, E.D., et al., *A protective role for periostin and TGF-beta in IgE-mediated allergy and airway hyperresponsiveness.* Clin Exp Allergy, 2012. **42**(1): p. 144-55.

46. Just, J., et al., *Novel severe wheezy young children phenotypes: boys atopic multiple-trigger and girls nonatopic uncontrolled wheeze.* J Allergy Clin Immunol, 2012. **130**(1): p. 103-10 e8.

47. Hammad, H. and B.N. Lambrecht, *Dendritic cells and airway epithelial cells at the interface between innate and adaptive immune responses.* Allergy, 2011. **66**(5): p. 579-87.

48. Wenzel, S.E., *Asthma: defining of the persistent adult phenotypes.* Lancet, 2006. **368**(9537): p. 804-13.

49. Moreira, A.P. and C.M. Hogaboam, *Macrophages in allergic asthma: fine-tuning their pro- and anti-inflammatory actions for disease resolution.* J Interferon Cytokine Res, 2011. **31**(6): p. 485-91.

50. Peters-Golden, M., *The alveolar macrophage: the forgotten cell in asthma.* Am J Respir Cell Mol Biol, 2004. **31**(1): p. 3-7.

51. Akiho, H., et al., *Role of IL-4, IL-13, and STAT6 in inflammation-induced hypercontractility of murine smooth muscle cells.* Am J Physiol Gastrointest Liver Physiol, 2002. **282**(2): p. G226-32.

52. Balhara, J. and A.S. Gounni, *The alveolar macrophages in asthma: a double-edged sword.* Mucosal Immunol, 2012. **5**(6): p. 605-9.

53. Lambrecht, B.N., et al., *Myeloid dendritic cells induce Th2 responses to inhaled antigen, leading to eosinophilic airway inflammation.* J Clin Invest, 2000. **106**(4): p. 551-9.

54. Mattes, J., et al., *Antagonism of microRNA-126 suppresses the effector function of TH2 cells and the development of allergic airways disease.* Proc Natl Acad Sci U S A, 2009. **106**(44): p. 18704-9.

55. Conrad, M.L., et al., *Comparison of adjuvant and adjuvant-free murine experimental asthma models.* Clin Exp Allergy, 2009. **39**(8): p. 1246-54.

56. Landsman, L. and S. Jung, *Lung macrophages serve as obligatory intermediate between blood monocytes and alveolar macrophages.* J Immunol, 2007. **179**(6): p. 3488-94.

57. Zaslona, Z., et al., *Transcriptome profiling of primary murine monocytes, lung macrophages and lung dendritic cells reveals a distinct expression of genes involved in cell trafficking.* Respir Res, 2009. **10**: p. 2.

58. Bedoret, D., et al., *Lung interstitial macrophages alter dendritic cell functions to prevent airway allergy in mice.* J Clin Invest, 2009. **119**(12): p. 3723-38.

59. Careau, E., et al., *Antigen sensitization modulates alveolar macrophage functions in an asthma model.* Am J Physiol Lung Cell Mol Physiol, 2006. **290**(5): p. L871-9.

60. Song, C., et al., *IL-17-producing alveolar macrophages mediate allergic lung inflammation related to asthma.* J Immunol, 2008. **181**(9): p. 6117-24.

61. Pouliot, P., et al., *Alveolar macrophages from allergic lungs are not committed to a pro-allergic response and can reduce airway hyperresponsiveness following ex vivo culture.* Clin Exp Allergy, 2008. **38**(3): p. 529-38.

62. Li, J.J., et al., *IL-27/IFN-gamma induce MyD88-dependent steroid-resistant airway hyperresponsiveness by inhibiting glucocorticoid signaling in macrophages.* J Immunol, 2010. **185**(7): p. 4401-9.

63. Izant, J.G. and H. Weintraub, *Inhibition of thymidine kinase gene expression by anti-sense RNA: a molecular approach to genetic analysis.* Cell, 1984. **36**(4): p. 1007-15.

64. Nellen, W. and G. Sczakiel, *In vitro and in vivo action of antisense RNA.* Mol Biotechnol, 1996. **6**(1): p. 7-15.

65. Hammond, S.M., A.A. Caudy, and G.J. Hannon, *Post-transcriptional gene silencing by double-stranded RNA.* Nat Rev Genet, 2001. **2**(2): p. 110-9.

66. Brenner, S., *The genetics of Caenorhabditis elegans.* Genetics, 1974. **77**(1): p. 71-94.

67. Lee, R.C., R.L. Feinbaum, and V. Ambros, *The C. elegans heterochronic gene lin-4 encodes small RNAs with antisense complementarity to lin-14.* Cell, 1993. **75**(5): p. 843-54.

68. Takayama, K.M. and M. Inouye, *Antisense RNA.* Crit Rev Biochem Mol Biol, 1990. **25**(3): p. 155-84.

69. Simons, R.W., *Naturally occurring antisense RNA control--a brief review.* Gene, 1988. **72**(1-2): p. 35-44.

70. Dougherty, W.G. and T.D. Parks, *Transgenes and gene suppression: telling us something new?* Curr Opin Cell Biol, 1995. **7**(3): p. 399-405.

71. Fire, A., et al., *Potent and specific genetic interference by double-stranded RNA in Caenorhabditis elegans.* Nature, 1998. **391**(6669): p. 806-11.

72. Tabara, H., A. Grishok, and C.C. Mello, *RNAi in C. elegans: soaking in the genome sequence.* Science, 1998. **282**(5388): p. 430-1.

73. Tabara, H., et al., *The rde-1 gene, RNA interference, and transposon silencing in C. elegans.* Cell, 1999. **99**(2): p. 123-32.

74. Montgomery, M.K., S. Xu, and A. Fire, *RNA as a target of double-stranded RNA-mediated genetic interference in Caenorhabditis elegans.* Proc Natl Acad Sci U S A, 1998. **95**(26): p. 15502-7.

75. Tuschl, T., et al., *Targeted mRNA degradation by double-stranded RNA in vitro.* Genes Dev, 1999. **13**(24): p. 3191-7.

76. Zamore, P.D., et al., *RNAi: double-stranded RNA directs the ATP-dependent cleavage of mRNA at 21 to 23 nucleotide intervals.* Cell, 2000. **101**(1): p. 25-33.

77. Sijen, T., et al., *On the role of RNA amplification in dsRNA-triggered gene silencing.* Cell, 2001. **107**(4): p. 465-76.

78. Hammond, S.M., et al., *An RNA-directed nuclease mediates post-transcriptional gene silencing in Drosophila cells.* Nature, 2000. **404**(6775): p. 293-6.

79. Stein, P., et al., *RNAi: mammalian oocytes do it without RNA-dependent RNA polymerase.* RNA, 2003. **9**(2): p. 187-92.

80. Ambros, V., et al., *MicroRNAs and other tiny endogenous RNAs in C. elegans.* Curr Biol, 2003. **13**(10): p. 807-18.

81. Hutvagner, G., et al., *A cellular function for the RNA-interference enzyme Dicer in the maturation of the let-7 small temporal RNA.* Science, 2001. **293**(5531): p. 834-8.

82. Lagos-Quintana, M., et al., *Identification of novel genes coding for small expressed RNAs.* Science, 2001. **294**(5543): p. 853-8.

83. Lau, N.C., et al., *An abundant class of tiny RNAs with probable regulatory roles in Caenorhabditis elegans.* Science, 2001. **294**(5543): p. 858-62.

84. Lee, R.C. and V. Ambros, *An extensive class of small RNAs in Caenorhabditis elegans.* Science, 2001. **294**(5543): p. 862-4.

85. Ambros, V., *microRNAs: tiny regulators with great potential.* Cell, 2001. **107**(7): p. 823-6.

86. Wang, Y., et al., *DGCR8 is essential for microRNA biogenesis and silencing of embryonic stem cell self-renewal.* Nat Genet, 2007. **39**(3): p. 380-5.

87. Kim, V.N., J. Han, and M.C. Siomi, *Biogenesis of small RNAs in animals.* Nat Rev Mol Cell Biol, 2009. **10**(2): p. 126-39.

88. Graff, J.W., et al., *Identifying Functional MicroRNAs in Macrophages with Polarized Phenotypes.* J Biol Chem, 2012. **287**(26): p. 21816-25.

89. Braun, J.E., et al., *GW182 proteins directly recruit cytoplasmic deadenylase complexes to miRNA targets.* Mol Cell, 2011. **44**(1): p. 120-33.

90. Guo, H., et al., *Mammalian microRNAs predominantly act to decrease target mRNA levels.* Nature, 2010. **466**(7308): p. 835-40.

91. Krol, J., I. Loedige, and W. Filipowicz, *The widespread regulation of microRNA biogenesis, function and decay.* Nat Rev Genet, 2010. **11**(9): p. 597-610.

92. Eulalio, A., et al., *A candidate approach implicates the secreted Salmonella effector protein SpvB in P-body disassembly.* PLoS One, 2011. **6**(3): p. e17296.

93. Orom, U.A., F.C. Nielsen, and A.H. Lund, *MicroRNA-10a binds the 5'UTR of ribosomal protein mRNAs and enhances their translation.* Mol Cell, 2008. **30**(4): p. 460-71.

94. Ma, F., et al., *MicroRNA-466l Upregulates IL-10 Expression in TLR-Triggered Macrophages by Antagonizing RNA-Binding Protein Tristetraprolin-Mediated IL-10 mRNA Degradation.* J Immunol, 2010.

95. Almeida, M.I., R.M. Reis, and G.A. Calin, *MicroRNA history: discovery, recent applications, and next frontiers.* Mutat Res, 2011. **717**(1-2): p. 1-8.

96. Chen, X., et al., *Characterization of microRNAs in serum: a novel class of biomarkers for diagnosis of cancer and other diseases.* Cell Res, 2008. **18**(10): p. 997-1006.

97. Rossbach, M., *Small non-coding RNAs as novel therapeutics.* Curr Mol Med, 2010. **10**(4): p. 361-8.

98. van Rooij, E., W.S. Marshall, and E.N. Olson, *Toward microRNA-based therapeutics for heart disease: the sense in antisense.* Circ Res, 2008. **103**(9): p. 919-28.

99. Khan, A.A., et al., *Transfection of small RNAs globally perturbs gene regulation by endogenous microRNAs.* Nat Biotechnol., 2009. **27**(6): p. 549-555.

100. Yang, J.S., et al., *Widespread regulatory activity of vertebrate microRNA* species.* RNA, 2011. **17**(2): p. 312-26.

101. Griffiths-Jones, S., et al., *miRBase: tools for microRNA genomics.* Nucleic Acids Res, 2008. **36**(Database issue): p. D154-8.

102. Lu, T.X., et al., *MicroRNA-21 limits in vivo immune response-mediated activation of the IL-12/IFN-gamma pathway, Th1 polarization, and the severity of delayed-type hypersensitivity.* J Immunol, 2011. **187**(6): p. 3362-73.

103. Mattes, J., et al., *Antagonism of microRNA-126 suppresses the effector function of TH2 cells and the development of allergic airways disease.* Proc Natl Acad Sci U S A, 2009. **106**(44): p. 18704-18709.

104. Garbacki, N., et al., *MicroRNAs profiling in murine models of acute and chronic asthma: a relationship with mRNAs targets.* PLoS One, 2011. **6**(1): p. e16509.

105. Rozen, S. and H. Skaletsky, *Primer3 on the WWW for general users and for biologist programmers.* Methods Mol Biol, 2000. **132**: p. 365-86.

106. R Development Core Team, *R: A language and environment for statistical computing*, 2012: Vienna, Austria.

107. John, B., et al., *Human MicroRNA targets.* PLoS Biol, 2004. **2**(11): p. e363.

108. Lewis, B.P., C.B. Burge, and D.P. Bartel, *Conserved seed pairing, often flanked by adenosines, indicates that thousands of human genes are microRNA targets.* Cell, 2005. **120**(1): p. 15-20.

109. Cureton, E.E. and R.B. D'Agostino, *Factor analysis, an applied approach*1983, Hillsdale, N.J.: L. Erlbaum Associates. xxi, 457 p.

110. Harrington, C.A., M. Winther, and M.M. Garred, *Use of bioanalyzer electropherograms for quality control and target evaluation in microarray expression profiling studies of ocular tissues.* J Ocul Biol Dis Infor, 2009. **2**(4): p. 243-249.

111. Allaire, M.A., et al., *Prostaglandin E 2 Does Not Modulate CCR7 Expression and Functionality after Differentiation of Blood Monocytes into Macrophages.* Int J Inflam, 2013. **2013**: p. 918016.

112. Jaguin, M., et al., *Polarization profiles of human M-CSF-generated macrophages and comparison of M1-markers in classically activated macrophages from GM-CSF and M-CSF origin.* Cell Immunol, 2013. **281**(1): p. 51-61.

113. Taylor, M.W. and G.S. Feng, *Relationship between interferon-gamma, indoleamine 2,3-dioxygenase, and tryptophan catabolism.* FASEB J, 1991. **5**(11): p. 2516-22.

114. Mellor, A.L. and D.H. Munn, *Tryptophan catabolism and regulation of adaptive immunity.* J Immunol, 2003. **170**(12): p. 5809-13.

115. Soilleux, E.J., R. Barten, and J. Trowsdale, *DC-SIGN; a related gene, DC-SIGNR; and CD23 form a cluster on 19p13.* J Immunol, 2000. **165**(6): p. 2937-42.

116. Kijimoto-Ochiai, S., *CD23 (the low-affinity IgE receptor) as a C-type lectin: a multidomain and multifunctional molecule.* Cell Mol Life Sci, 2002. **59**(4): p. 648-64.

117. Chinetti-Gbaguidi, G., et al., *Peroxisome proliferator-activated receptor-gamma activation induces 11beta-hydroxysteroid dehydrogenase type 1 activity in human alternative macrophages.* Arterioscler Thromb Vasc Biol, 2012. **32**(3): p. 677-85.

118. Martinez, F.O., et al., *Genetic programs expressed in resting and IL-4 alternatively activated mouse and human macrophages: similarities and differences.* Blood, 2013.

119. Mehta, K., A. Kumar, and H.I. Kim, *Transglutaminase 2: a multi-tasking protein in the complex circuitry of inflammation and cancer.* Biochem Pharmacol, 2010. **80**(12): p. 1921-9.

120. Tserel, L., et al., *MicroRNA expression profiles of human blood monocyte-derived dendritic cells and macrophages reveal miR-511 as putative positive regulator of Toll-like receptor 4.* J Biol Chem, 2011. **286**(30): p. 26487-95.

121. Martinez-Nunez, R.T., F. Louafi, and T. Sanchez-Elsner, *The interleukin 13 (IL-13) pathway in human macrophages is modulated by microrna-155 via direct targeting of interleukin 13 receptor alpha1 (IL13R{alpha}1).* J Biol Chem, 2010.

122. Saetrom, P., et al., *Distance constraints between microRNA target sites dictate efficacy and cooperativity.* Nucleic Acids Res, 2007. **35**(7): p. 2333-42.

123. Lim, L.P., et al., *Microarray analysis shows that some microRNAs downregulate large numbers of target mRNAs.* Nature, 2005. **433**(7027): p. 769-73.

124. Eskelinen, E.L., Y. Tanaka, and P. Saftig, *At the acidic edge: emerging functions for lysosomal membrane proteins.* Trends Cell Biol, 2003. **13**(3): p. 137-45.

125. Yokouchi, M., et al., *Cloning and characterization of APS, an adaptor molecule containing PH and SH2 domains that is tyrosine phosphorylated upon B-cell receptor stimulation.* Oncogene, 1997. **15**(1): p. 7-15.

126. Yokouchi, M., et al., *APS, an adaptor protein containing PH and SH2 domains, is associated with the PDGF receptor and c-Cbl and inhibits PDGF-induced mitogenesis.* Oncogene, 1999. **18**(3): p. 759-67.

127. Nishi, M., et al., *Kinase activation through dimerization by human SH2-B.* Mol Cell Biol, 2005. **25**(7): p. 2607-21.

128. Sharif, O. and S. Knapp, *From expression to signaling: roles of TREM-1 and TREM-2 in innate immunity and bacterial infection.* Immunobiology, 2008. **213**(9-10): p. 701-13.

129. Turnbull, I.R., et al., *Cutting edge: TREM-2 attenuates macrophage activation.* J Immunol, 2006. **177**(6): p. 3520-4.

130. Martinez, F.O., L. Helming, and S. Gordon, *Alternative Activation of Macrophages: An Immunologic Functional Perspective.* Annu Rev Immunol, 2008.

131. Taylor, P.R., et al., *Macrophage receptors and immune recognition.* Annu Rev Immunol, 2005. **23**: p. 901-944.

132. Squadrito, M.L., et al., *miR-511-3p modulates genetic programs of tumor-associated macrophages.* Cell Rep, 2012. **1**(2): p. 141-54.

133. Chinetti, G., J.C. Fruchart, and B. Staels, *Peroxisome proliferator-activated receptors: new targets for the pharmacological modulation of macrophage gene expression and function.* Curr Opin Lipidol, 2003. **14**(5): p. 459-68.

134. Bouhlel, M.A., et al., *Unlike PPARgamma, PPARalpha or PPARbeta/delta activation does not promote human monocyte differentiation toward alternative macrophages.* Biochem Biophys Res Commun, 2009.

135. Liao, X., et al., *Kruppel-like factor 4 regulates macrophage polarization.* J Clin Invest, 2011. **121**(7): p. 2736-49.

136. Zahlten, J., et al., *TLR9- and Src-dependent expression of KLF4 controls IL-10 expression in pneumonia.* Eur Respir J, 2012.

137. Song, E., et al., *Attenuation of kruppel-like factor 4 facilitates carcinogenesis by inducing g1/s phase arrest in clear cell renal cell carcinoma.* PLoS One, 2013. **8**(7): p. e67758.

138. Rossato, M., et al., *IL-10-induced microRNA-187 negatively regulates TNF-alpha, IL-6, and IL-12p40 production in TLR4-stimulated monocytes.* Proc Natl Acad Sci U S A, 2012. **109**(45): p. E3101-10.

139. Sobell, H.M., *Actinomycin and DNA transcription.* Proc Natl Acad Sci U S A, 1985. **82**(16): p. 5328-31.

140. Andrejewski, N., et al., *Normal lysosomal morphology and function in LAMP-1-deficient mice.* J Biol Chem, 1999. **274**(18): p. 12692-701.

141. Schulte, L.N., A.J. Westermann, and J. Vogel, *Differential activation and functional specialization of miR-146 and miR-155 in innate immune sensing.* Nucleic Acids Res, 2013. **41**(1): p. 542-53.

142. Becker, S., M.K. Warren, and S. Haskill, *Colony-stimulating factor-induced monocyte survival and differentiation into macrophages in serum-free cultures.* J Immunol, 1987. **139**(11): p. 3703-9.

143. Fleetwood, A.J., et al., *Granulocyte-macrophage colony-stimulating factor (CSF) and macrophage CSF-dependent macrophage phenotypes display differences in cytokine profiles and transcription factor activities: implications for CSF blockade in inflammation.* J Immunol, 2007. **178**(8): p. 5245-52.

144. Fleetwood, A.J., et al., *GM-CSF- and M-CSF-dependent macrophage phenotypes display differential dependence on type I interferon signaling.* J Leukoc Biol, 2009. **86**(2): p. 411-21.

145. Verreck, F.A., et al., *Human IL-23-producing type 1 macrophages promote but IL-10-producing type 2 macrophages subvert immunity to (myco)bacteria.* Proc Natl Acad Sci U S A, 2004. **101**(13): p. 4560-4565.

146. Hashimoto, S., et al., *Serial analysis of gene expression in human monocytes and macrophages.* Blood, 1999. **94**(3): p. 837-44.

147. Hamilton, J.A., *GM-CSF in inflammation and autoimmunity.* Trends Immunol, 2002. **23**(8): p. 403-8.

148. Shibata, Y., et al., *GM-CSF regulates alveolar macrophage differentiation and innate immunity in the lung through PU.1.* Immunity, 2001. **15**(4): p. 557-67.

149. Waldo, S.W., et al., *Heterogeneity of human macrophages in culture and in atherosclerotic plaques.* Am J Pathol, 2008. **172**(4): p. 1112-26.

150. Akagawa, K.S., K. Kamoshita, and T. Tokunaga, *Effects of granulocyte-macrophage colony-stimulating factor and colony-stimulating factor-1 on the proliferation and*

differentiation of murine alveolar macrophages. J Immunol, 1988. **141**(10): p. 3383-90.

151. Benoit, M., B. Desnues, and J.L. Mege, *Macrophage polarization in bacterial infections.* J Immunol, 2008. **181**(6): p. 3733-3739.

152. Martinez, F.O., L. Helming, and S. Gordon, *Alternative activation of macrophages: an immunologic functional perspective.* Annu Rev Immunol, 2009. **27**: p. 451-83.

153. Chen, J.J., et al., *Analysis of variance components in gene expression data.* Bioinformatics, 2004. **20**(9): p. 1436-46.

154. Sha, W.C., et al., *Targeted disruption of the p50 subunit of NF-kappa B leads to multifocal defects in immune responses.* Cell, 1995. **80**(2): p. 321-30.

155. Taganov, K.D., et al., *NF-kappaB-dependent induction of microRNA miR-146, an inhibitor targeted to signaling proteins of innate immune responses.* Proc Natl Acad Sci U S A, 2006. **103**(33): p. 12481-12486.

156. Ma, X., et al., *MicroRNAs in NF-kappaB signaling.* J Mol Cell Biol, 2011. **3**(3): p. 159-66.

157. DeKoter, R.P. and H. Singh, *Regulation of B lymphocyte and macrophage development by graded expression of PU.1.* Science, 2000. **288**(5470): p. 1439-41.

158. Ghani, S., et al., *Macrophage development from HSCs requires PU.1-coordinated microRNA expression.* Blood, 2011. **118**(8): p. 2275-84.

159. Martinez-Nunez, R.T., et al., *MicroRNA-155 modulates the pathogen binding ability of dendritic cells (DCs) by down-regulation of DC-specific intercellular adhesion molecule-3 grabbing non-integrin (DC-SIGN).* J Biol Chem, 2009. **284**(24): p. 16334-42.

160. Arner, E., et al., *Adipose tissue microRNAs as regulators of CCL2 production in human obesity.* Diabetes, 2012. **61**(8): p. 1986-93.

161. Rauhala, H.E., et al., *miR-193b is an epigenetically regulated putative tumor suppressor in prostate cancer.* Int J Cancer, 2010. **127**(6): p. 1363-72.

162. Xu, C., et al., *MicroRNA-193b regulates proliferation, migration and invasion in human hepatocellular carcinoma cells.* Eur J Cancer, 2010. **46**(15): p. 2828-36.

163. Chen, J., et al., *miR-193b Regulates Mcl-1 in Melanoma.* Am J Pathol, 2011. **179**(5): p. 2162-8.

164. Hagman, Z., et al., *miR-34c is downregulated in prostate cancer and exerts tumor suppressive functions.* Int J Cancer, 2010. **127**(12): p. 2768-76.

165. Migliore, C., et al., *MicroRNAs impair MET-mediated invasive growth.* Cancer Res, 2008. **68**(24): p. 10128-36.

166. Odegaard, J.I., et al., *Macrophage-specific PPARgamma controls alternative activation and improves insulin resistance.* Nature, 2007. **447**(7148): p. 1116-20.

167. Chao, A., et al., *Regulation of ovarian cancer progression by microRNA-187 through targeting Disabled homolog-2.* Oncogene, 2012. **31**(6): p. 764-75.

168. Xu, X.X., et al., *Disabled-2 (Dab2) is an SH3 domain-binding partner of Grb2.* Oncogene, 1998. **16**(12): p. 1561-9.

169. Harlan, J.E., et al., *Pleckstrin homology domains bind to phosphatidylinositol-4,5-bisphosphate.* Nature, 1994. **371**(6493): p. 168-70.

170. Minami, A., et al., *Increased insulin sensitivity and hypoinsulinemia in APS knockout mice.* Diabetes, 2003. **52**(11): p. 2657-65.

171. Ahmed, Z., B.J. Smith, and T.S. Pillay, *The APS adapter protein couples the insulin receptor to the phosphorylation of c-Cbl and facilitates ligand-stimulated ubiquitination of the insulin receptor.* FEBS Lett, 2000. **475**(1): p. 31-4.

172. Kishi, K., et al., *APS-mediated ubiquitination of the insulin receptor enhances its internalization, but does not induce its degradation.* Endocr J, 2007. **54**(1): p. 77-88.

173. Desbuquois, B., N. Carre, and A.F. Burnol, *Regulation of insulin and type 1 insulin-like growth factor signaling and action by the Grb10/14 and SH2B1/B2 adaptor proteins.* FEBS J, 2013. **280**(3): p. 794-816.

174. Eskelinen, E.L., et al., *Unifying nomenclature for the isoforms of the lysosomal membrane protein LAMP-2.* Traffic, 2005. **6**(11): p. 1058-61.

175. Dice, J.F., *Chaperone-mediated autophagy.* Autophagy, 2007. **3**(4): p. 295-9.

176. Fujiwara, Y., et al., *Direct uptake and degradation of DNA by lysosomes.* Autophagy, 2013. **9**(8).

177. Kertesz, M., et al., *The role of site accessibility in microRNA target recognition.* Nat Genet, 2007. **39**(10): p. 1278-84.

178. Deleault, K.M., S.J. Skinner, and S.A. Brooks, *Tristetraprolin regulates TNF TNF-alpha mRNA stability via a proteasome dependent mechanism involving the combined action of the ERK and p38 pathways.* Mol Immunol, 2008. **45**(1): p. 13-24.

179. Chen, Y.L., et al., *Transcriptional regulation of tristetraprolin by NF-kappaB signaling in LPS-stimulated macrophages.* Mol Biol Rep, 2013. **40**(4): p. 2867-77.

180. Naessens, T., et al., *Innate imprinting of murine resident alveolar macrophages by allergic bronchial inflammation causes a switch from hypoinflammatory to hyperinflammatory reactivity.* Am J Pathol, 2012. **181**(1): p. 174-84.

181. Moon, K.A., et al., *Allergen-induced CD11b+ CD11c(int) CCR3+ macrophages in the lung promote eosinophilic airway inflammation in a mouse asthma model.* Int Immunol, 2007. **19**(12): p. 1371-81.

182. Sirois, J. and E.Y. Bissonnette, *Alveolar macrophages of allergic resistant and susceptible strains of rats show distinct cytokine profiles.* Clin Exp Immunol, 2001. **126**(1): p. 9-15.

183. Careau, E. and E.Y. Bissonnette, *Adoptive transfer of alveolar macrophages abrogates bronchial hyperresponsiveness.* Am J Respir Cell Mol Biol, 2004. **31**(1): p. 22-7.

184. Tang, C., et al., *Th type 1-stimulating activity of lung macrophages inhibits Th2-mediated allergic airway inflammation by an IFN-gamma-dependent mechanism.* J Immunol, 2001. **166**(3): p. 1471-81.

185. Goleva, E., et al., *Corticosteroid-resistant asthma is associated with classical antimicrobial activation of airway macrophages.* J Allergy Clin Immunol, 2008. **122**(3): p. 550-9 e3.

186. Burastero, S.E., et al., *Increased expression of the CD80 accessory molecule by alveolar macrophages in asthmatic subjects and its functional involvement in allergen presentation to autologous TH2 lymphocytes.* J Allergy Clin Immunol, 1999. **103**(6): p. 1136-42.

187. Gosset, P., et al., *Production of chemokines and proinflammatory and antiinflammatory cytokines by human alveolar macrophages activated by IgE receptors.* J Allergy Clin Immunol, 1999. **103**(2 Pt 1): p. 289-97.

188. Berry, M.A., et al., *Evidence of a role of tumor necrosis factor alpha in refractory asthma.* N Engl J Med, 2006. **354**(7): p. 697-708.

189. Howarth, P.H., et al., *Tumour necrosis factor (TNFalpha) as a novel therapeutic target in symptomatic corticosteroid dependent asthma.* Thorax, 2005. **60**(12): p. 1012-8.

190. Mosser, D.M. and J.P. Edwards, *Exploring the full spectrum of macrophage activation.* Nat Rev Immunol, 2008. **8**(12): p. 958-69.

191. Collison, A., et al., *Altered expression of microRNA in the airway wall in chronic asthma: miR-126 as a potential therapeutic target.* BMC Pulm Med, 2011. **11**: p. 29.

192. Karpurapu, M., et al., *Functional PU.1 in macrophages has a pivotal role in NF-kappaB activation and neutrophilic lung inflammation during endotoxemia.* Blood, 2011. **118**(19): p. 5255-66.

193. Kumar, M., et al., *Let-7 microRNA-mediated regulation of IL-13 and allergic airway inflammation.* J Allergy Clin Immunol, 2011. **128**(5): p. 1077-85 e1-10.